

[The cerebellothalamic pathway in skilled reaching]

by

Hillary A. Wehry

Program in Neural Computation  
Neuroscience Institute  
Carnegie Mellon University

Date: \_\_\_\_\_

Approved:

---

[Dr. Robert Turner], Co-chair

---

[Dr. Byron Yu], Co-chair

---

[Dr. Steven Chase]

---

[Dr. Gelsy Torres-Oviedo]

---

[Dr. Adam Hantman] External., UNC

Thesis submitted in partial fulfillment of  
the requirements for the degree of Doctor  
of Philosophy in the Dietrich College of  
Humanities and Social Sciences  
Carnegie Mellon University

2023

Copyright by  
Hillary A. Wehry  
2023

## Clinical Significance

Movement disorders due to pathology in any part of the cerebello-thalamocortical loop circuit, e.g. Essential Tremor, affect about 5% of the population. These conditions are considered “neural circuit disorders”, in which motor deficits arise from aberrant neuronal signaling within a network of connected brain areas. Despite this high prevalence, current treatment options are predominantly ineffective and provide modest symptomatic relief at best. Improved therapies are limited by our fundamental lack of knowledge about this pathway. To date, we do not know how either normal or pathologic signaling in the cerebellum influences direct cortical control of movement. The first step towards this aim, and the first chapter of this thesis, is to characterize the role of the cerebellar-recipient motor thalamus in motor planning and execution during non-human primate reaching. The strength of this proposal, and the goal of the second and third chapters, lies in our ability to evaluate the trial-by-trial relationships between neural activity in motor thalamus and motor cortex. In doing so we can elucidate the manner in which the thalamus conveys movement-modifying information from the cerebellum to cortex. This work addresses several fundamental gaps in knowledge hindering the development of a model of dysfunction in the CTC pathway that can be used to develop therapies for associated movement disorders. My long-term career goal is to identify how pathophysiologic changes in subcortical circuits lead to changes in neural activity and motor deficits, illuminating new therapeutic targets and interventions for the broad spectrum of movement disorders.

## **Abstract**

The cerebellothalamicocortical (CTC) pathway has been implicated in a broad array of motor functions ranging from controlling the timing of movements to online error correction. Yet each brain area in this pathway has only been studied in isolation. There is a considerable gap in knowledge concerning how one of the critical subcortical brain structures involved in movement, the cerebellum, influences cortical control of the limb via the ventrolateral (motor) thalamus. My thesis aims to clarify the manner in which cerebellar input influences cortical control of movement in primates by investigating the function of the thalamic nucleus that conveys cerebellar input to M1. I aim to address multiple outstanding questions in neural basis of motor control: Does input from the M1-projecting cerebellar thalamus to M1 drive movement initiation– or the switch between motor preparation to execution? Do neurons in M1 receiving cerebellar input have features associated with its proposed role in motor preparation, initiation, and executions? A combination of simultaneous cortical and subcortical population recordings during reaching, electrical stimulation identification, statistical modeling, and simulation-based validation approaches will be used to support our answers to these questions.

# Contents

Abstract .....	v
List of Figures.....	ix
Acknowledgements.....	Error! Bookmark not defined.
1 Introduction.....	11
2 Primate cerebellar motor thalamus could trigger movement initiation in motor cortex	14
2.1 Introduction .....	14
2.2 Results.....	17
2.2.1 Task design eliminates anticipation of the go cue .....	18
2.2.2 A small subset of VLcb precedes M1.....	21
2.2.3 VLcb does not predict movement onset as strongly as M1 .....	26
2.2.4 VLcb has complex directionality over the course of the task.....	32
2.2.5 Functional separation between movement timing and planning .....	35
2.3 Discussion .....	36
2.4 Methods.....	49
2.4.1 Experimental framework.....	49
Animal subjects.....	49
Behavioral paradigm .....	50
Surgical procedures .....	54
Localization of cerebellar and globus pallidus internus stimulation sites.....	54
Neural recordings in primary motor cortex (M1) .....	55

Neural Recordings in M1-projecting cerebellar thalamus (VLp) .....	56
EMG Recordings.....	59
2.4.2 Data Analysis .....	59
Behavior .....	59
Spike sorting and artifact subtraction .....	60
Spike density functions and response onset estimation .....	60
Directional tuning .....	61
Time-locking analysis and selectivity index.....	62
3 Cerebellar input dependent activity in primary motor cortex.....	65
3.1 Introduction .....	66
3.2 Materials and Methods .....	68
3.2.1 Data and Statistical Analysis.....	68
Cerebellar-response detection .....	68
Firing rate matching using resampling.....	71
Directional Modulation .....	73
Mutual Information .....	74
Neural decoding.....	75
3.3 Results.....	77
3.3.1 M1 sites.....	77
3.3.2 M1 response properties to cerebellar stimulation .....	79
3.3.3 Behavioral task and firing rate properties .....	82
3.3.4 Directional modulation.....	85

3.3.5 Mutual information.....	89
3.3.6 Neural decoding .....	90
3.4 Discussion .....	93
3.4.1 Summary.....	93
3.4.2 Advancing understanding of M1 .....	95
3.4.3 Limitations.....	95
Experimental Approach .....	95
Analysis .....	98
4 Conclusion .....	99
Appendix A. ....	103
Appendix B.....	105
B1. Simulations.....	105
References.....	110
Biography .....	<b>Error! Bookmark not defined.</b>

# List of Figures

Figure 1. Schematic of movement initiation activity in M1, which is thought to be driven by subcortical input.....	16
Figure 2.2 Experimental Paradigm.....	20
Figure 2.3 . A subset of VLcb leads M1.....	25
Figure 2.4 Event-locking captures temporal variability in neural response onset relative to task events.....	29
Figure 2.5 VLcb is more time-locked to the cue than M1.....	31
Figure 2.6 VLcb has complex directionality over the course of the task. ....	34
Figure 2.7 Temporal separation between neural population patterns.....	36
Figure 3.1 (A) Schematic of stimulation and recording sites.....	78
Figure 3.2 CUSUM algorithm applied to real data.....	79
Figure 3.3 Cb+ responses to stimulation.....	81
Figure 3.4 Memory-guided center out reach task schema and timeline.....	82
Figure 3.5 Firing rate of Cb+ and Cb- neurons relative to task events.....	83
Figure 3.6 Directional modulation for Cb+ and Cb- neurons.....	86
Figure 3.7 Directional modulation for Cb+ and Cb- neurons after controlling for firing rate differences using nonparametric bootstrap resampling with distribution matching.).....	88
Figure 3.8 Mutual information (MI) in bits between reach target direction and neural activity for Cb+ (blue) and Cb- (green) neurons.....	89
Figure 3.9 Neural decoding of target direction.....	92
Figure A.1 Behavioral performance metrics.....	103
Figure A.2 Additional timing information.....	104

**Figure B.1 Real and simulated responses to electrical stimulation .....** 106

**Figure B.2 Response characteristics and detection algorithms.....** 108

# 1 Introduction

Neurological movement disorders affect about 10 percent of the population, yet current treatment options provide only modest relief of symptoms at best. Improved therapies are limited by our fundamental lack of knowledge concerning how the two key subcortical brain structures, the cerebellum (Cb) and the basal ganglia (BG), influence cortical control of movement. Behavioral deficits associated with damage to these brain areas have been well characterized, yet the neurophysiology—what is happening in the brain to cause motor symptoms—remains enigmatic. These structures operate within a network of connected brain areas, and motor deficits are believed to arise from aberrant neuronal signaling within these circuits. However, we do not know how normal signaling in the Cb and BG influences direct cortical control of movement, let alone how pathophysiologic processes in these structures precipitate severe motor deficits. These brain structures must act in concert with the motor cortex to shape the learning and execution of skilled movements, yet an integrated model of their respective contributions and influence on the cortex remains out of reach. The goal of this thesis is to investigate the activity of neural populations along the cerebellothalamicocortical pathway in light of its proposed function in the control of skilled movements.

There are several challenges involved in this task, which the work in this thesis aims to address. The first is conceptual: the cerebello-thalamocortical (CTC) pathway has been implicated in an exceptionally broad yet seemingly conflicting array of motor functions. These functions range from motor planning (Gao et al. 2018; Chabrol, Blot, and Mrsic-Flogel 2019), to directly controlling movement initiation (Dacre et al. 2021; Sauerbrei et al. 2020; Nashef et al. 2021; 2018; Tanaka et al. 2020),

to coordination of multi-joint movements (Cooper, Martin, and Ghez 2000; Bastian and Thach 1995; Bastian et al. 1996), online error correction (Shimansky et al. 2004; Sun et al. 2016; Becker and Person 2019; Guo et al. 2021), and motor skill learning but not execution itself (Butler, Bourke, and Horne 2000; Jeljeli et al. 2003). The diversity in hypothesized functional roles for cerebellar input to the cortex is associated with a similarly diverse set of modeling perspectives and frameworks. Our large gaps in knowledge and lack of a unifying framework for these functions greatly limits the granularity of the predictions for neural activity. Throughout this thesis, special concern is taken to integrate across perspectives.

The second major challenge is experimental, which this thesis demonstrates and proposes novel advances for in the macaque monkey. The diversity in perspectives outlined above can be partially accounted for by the difficulty in recording activity from the deep cerebellar nuclei and the cerebellar thalamus in awake, behaving animals. Recording from subcortical structures requires laminar probes, and it remains technically challenging to record from many neurons at once in the primate. Furthermore, the motor thalamus is a tightly compact area, such that additional methods like microstimulation and electrophysiology are needed to reliably identify the appropriate thalamic nuclei. Because of their proximity, perturbations of the thalamus without genetic tools are often difficult to interpret. On top of this, the behavior needs to be tightly controlled to tease apart highly related functions.

In this work we investigated the contributions cerebellar thalamus to normal motor control. We conducted a series of experiments in which we recorded populations of neurons in the motor thalamus

and motor cortex during skilled arm reaching in rhesus macaque monkeys, using multi-area electrophysiologic to identify the cerebellar thalamus.

The contributions of this thesis are organized as follows:

- In **Chapter 1**, we contextualize the study of the cerebellothalamic pathway within a broader research framework
- In **Chapter 2**, we examine cerebellar thalamic involvement in movement initiation
- In **Chapter 3**, we propose an approach for identifying primary motor cortical neurons that receive disynaptic input from the cerebellum and investigate their activity during motor planning, initiation, and execution

The experiments here bridge these gaps by establishing relationships between the neuronal activity of the cerebellar thalamus and primary motor cortex. The information gained will enable us to generate more insightful hypotheses about motor dysfunction by refining our ability to map theoretical constructs of motor control onto specific brain regions.

## **2 Primate cerebellar motor thalamus could trigger movement initiation in motor cortex**

### **2.1 Introduction**

Volitional movements can be decomposed into three phases: motor preparation, initiation, and execution. These processes involve a series of distinct neural computations within, and between, cortical and subcortical neural circuits. Neural activity in the primary motor cortex (M1) has been well characterized during the preparation and execution of practiced movements (Georgopoulos, Schwartz, and Kettner 1986; Moran and Schwartz 1999; Kakei, Hoffman, and Strick 1999), but the emergence of initiation activity— how M1 knows *when* to begin a movement— is not fully understood (Kaufman et al. 2014; Elsayed et al. 2016; Lara et al. 2018). Several recent studies have implicated the cerebellar thalamus as the instigator of initiation activity in a mouse model of visually cued reaching (Heiney et al. 2014; Dacre et al. 2021b; Lee et al. 2015). However, there has been conflicting support at the level of neural population activity, and it is difficult to reconcile the simplicity of the cerebellum’s hypothesized role in movement initiation with its involvement in more complex functions like online error correction and motor learning (Wolpert, Miall, and Kawato 1998; Shadmehr, Smith, and Krakauer 2010). In this study, we recorded neural activity within the primate cerebellar thalamus and M1 during reaching and evaluate its role in movement initiation.

There are several lines of reasoning supporting cerebellar involvement in movement initiation. Loss of cerebellar function in humans results in delayed movement initiation (e.g. prolonged reaction times) and uncoordinated movements, which are characterized by poorly timed activations of different muscle groups (A. J. Bastian et al. 1996; A. J. Bastian and Thach 1995; Ivry et al. 2002; Ivry and Keele

1989; Timmann, Watts, and Hore 1999; Zackowski, Thach, and Bastian 2002). These behavioral features were also observed in cerebellar cooling (Meyer-Lohmann, Hore, and Brooks 1977), ablation (Spidalieri, Busby, and Lamarre 1983), and electrical silencing (Nashef et al. 2019) experiments in primates. In the mouse, pharmacologic silencing of the cerebellothalamic pathway almost entirely prevents movement initiation (Dacre et al. 2021b), while cell-type specific silencing disrupts timing (Heiney et al. 2014). In addition to these loss of function experiments, excitation of this pathway drives the production of both single- and multi-joint movements across species (Dacre et al. 2021a; Lee et al. 2015).

The output of the cerebellum is hypothesized to have a simple form in initiating movement: a coordinated pulse of increased firing rate that drives changes in M1. The simplicity of this “trigger” hypothesis was first motivated by theoretical work in M1, which suggested that a reach condition-independent pulse of activity is sufficient to drive the transition in M1 between activity patterns that support a motor plan to those that execute it (Kaufman et al. 2016; Sussillo et al. 2015; for full review and citations within see Vyas et al. 2020). Across these theoretical works, changes in external inputs are only needed at the beginning of a reach to switch M1 dynamics at the right time, and movements unfold via network-level mechanisms without additional timing information. This framework is supported by the observation that nonspecific, synchronized stimulation of mouse cerebellar thalamus drives initiation of movements in a context-dependent manner, as if this perturbation mimicked the timing cue telling the animal when to begin moving (Dacre et al. 2021a).

The form of this initiation signal is likely more complex than what is suggested, especially considering that the cerebellum is thought to achieve online error correction and motor learning by

operating as a feedback controller (Shadmehr and Krakauer 2008; Wolpert, Miall, and Kawato 1998). Nevertheless, the simple trigger hypothesis can be useful to structure a principled investigation of the neural activity in this pathway during the reaction interval. In the ensuing study we test the following hypothesis: if cerebellar input is driving initiation activity in the normal animal, we expect activity in the cerebellar thalamus, the intervening node between the cerebellum and M1, to precede that of M1 on average. We also expect that, on any given trial, activity changes in the cerebellar thalamus are tightly locked to subsequent changes in M1 and the ensuing movement. The timing of neural activity in the cerebellar pathway relative to M1 has been examined in the context of externally timed movements in a few previous studies, but evidence of timing differences between areas has been equivocal thus far, with just as many studies reporting changes after M1 (Anderson and Turner 1991; Butler, Horne, and Hawkins 1992) as there are reporting changes before M1 (W. T. Thach 1975).

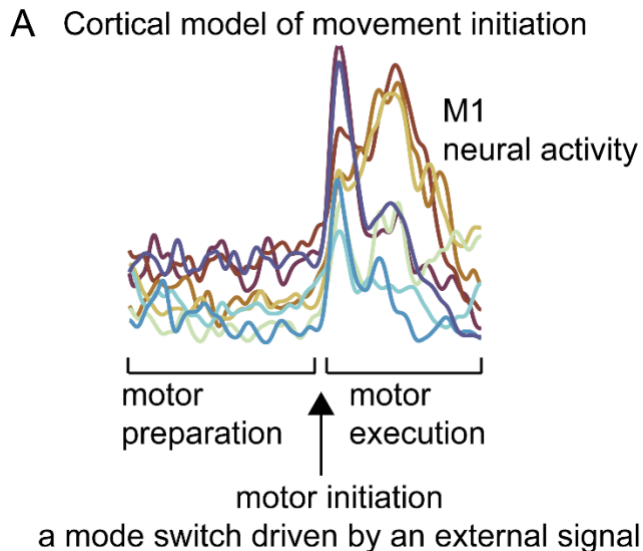


**Figure 1.** Schematic of movement initiation activity in M1, which is thought to be driven by subcortical input.

We interrogated the activity of the cerebellar motor thalamus and M1 at the time of movement initiation during nonhuman primate reaching. Our task revealed novel aspects of activity in the cerebellar thalamocortical circuit that are broadly consistent with the idea that drive to the primary motor cortex via the cerebellar-thalamocortical pathway begins the process of initiating volitional reaching. However, the simple “trigger” hypothesis fails to capture nuances in response timing observed in our data. Rather than simply preceding the activity in M1 at a fixed delay across trials, and therefore predicting the time of movement onset on each trial, the timing of responses across trials in many units seems to be distributed. Many units have responses that are instead time-locked to the cue to move. We therefore advocate for an alternative model of the cerebellothalamic involvement in movement initiation in which a component of cerebellar output reflects a stage of sensorimotor processing earlier than motor cortex. We also offer a framework for how the cerebellum may be supporting multiple functions concurrently.

## 2.2 Results

To test whether peri-movement activity in the macaque cerebellar motor thalamus is consistent with its hypothesized role in visually cued movement initiation, we recorded neural activity in M1 and the motor thalamus simultaneously while two monkeys performed a reaching task. We designed a variation of a memory-guided instructed delay, center out reaching task that dissociates motor planning from movement initiation by decoupling information about *when* to move from information about *where* to move (Crammond and Kalaska 2000). The task features two key modifications to the

classic center out paradigm: (1) a target instruction that is briefly flashed on the screen (500ms) and must be remembered throughout the delay period; and (2) a separate, nonspatial cue to begin moving, or ‘go cue’, with arrival times that are maximally unpredictable (Figure 2.2A). We used a combination of methods including MRI-guided stereotactic planning, electrophysiology, deep-structure stimulation, and thalamic stimulation to ensure our thalamic recordings were localized in the cerebellar-recipient, arm territory of the motor thalamus (VLcb) (Figure 2.2B-C; see Methods and Supplementary Figure X).

### 2.2.1 Task design eliminates anticipation of the go cue

We first assessed whether the monkeys were performing the task as designed, responding to the visual cue rather than anticipating its arrival. We began by investigating the relationship between reaction time (RT) and the length of the delay period. The uniform distribution is the classic randomization scheme for delay periods and has an exponential hazard function, meaning that the arrival time of the cue becomes more predictable over time. This structure in event timing is reflected in decreasing reaction times as a function of delay length (Churchland and Shenoy 2007; Tsunoda and Kakei 2008), and is reflected in the activity of dopamine neurons (Pasquereau and Turner 2015). Activity in the cerebellum has also been shown to time the occurrence of predictable task events (Tanaka et al. 2021; Okada, Takeya, and Tanaka 2022), which further suggests that movement initiation signals should be dissociated from predictive timing signals.

In our task, there is a negligible relationship between reaction time (RT) and length of the delay period for the two monkeys (J,K), as expected (Figure 2.2B). Since long delay periods were observed at a lower frequency than short delay periods, all successful trials in which neural activity was recorded

were first ordered by delay length and grouped into equal width bins (10ms) for each animal. The median RT is plotted for the trials within each bin, and the 2.5- and 97.5-percentiles for each bin are shown to give an estimate of delay period dependent variability. Simple linear regression using the binned values was used to test if delay period length predicted RT in each animal. The fitted regression model for monkey J was not statistically significant (RT, seconds =  $0.292 + 0^*(\text{Delay, seconds})$ ;  $R^2 = 1.24e-04$ ,  $F(1,22) = 2.05$ ,  $p > 0.05$ ), while there was a statistically significant but extremely small positive association for monkey K (RT =  $0.3056 + 0.0008^*\text{Delay}$ ;  $R^2 = 0.0012$ ,  $F(1,22) = 20.3$ ,  $< 0.0001$ ,  $\beta_1 = [0.0005, 0.0012]$ ). We then confirmed that the dependence of reaction time variance on the length of the delay period is similarly negligible in the two animals (Supplemental Figure XC).

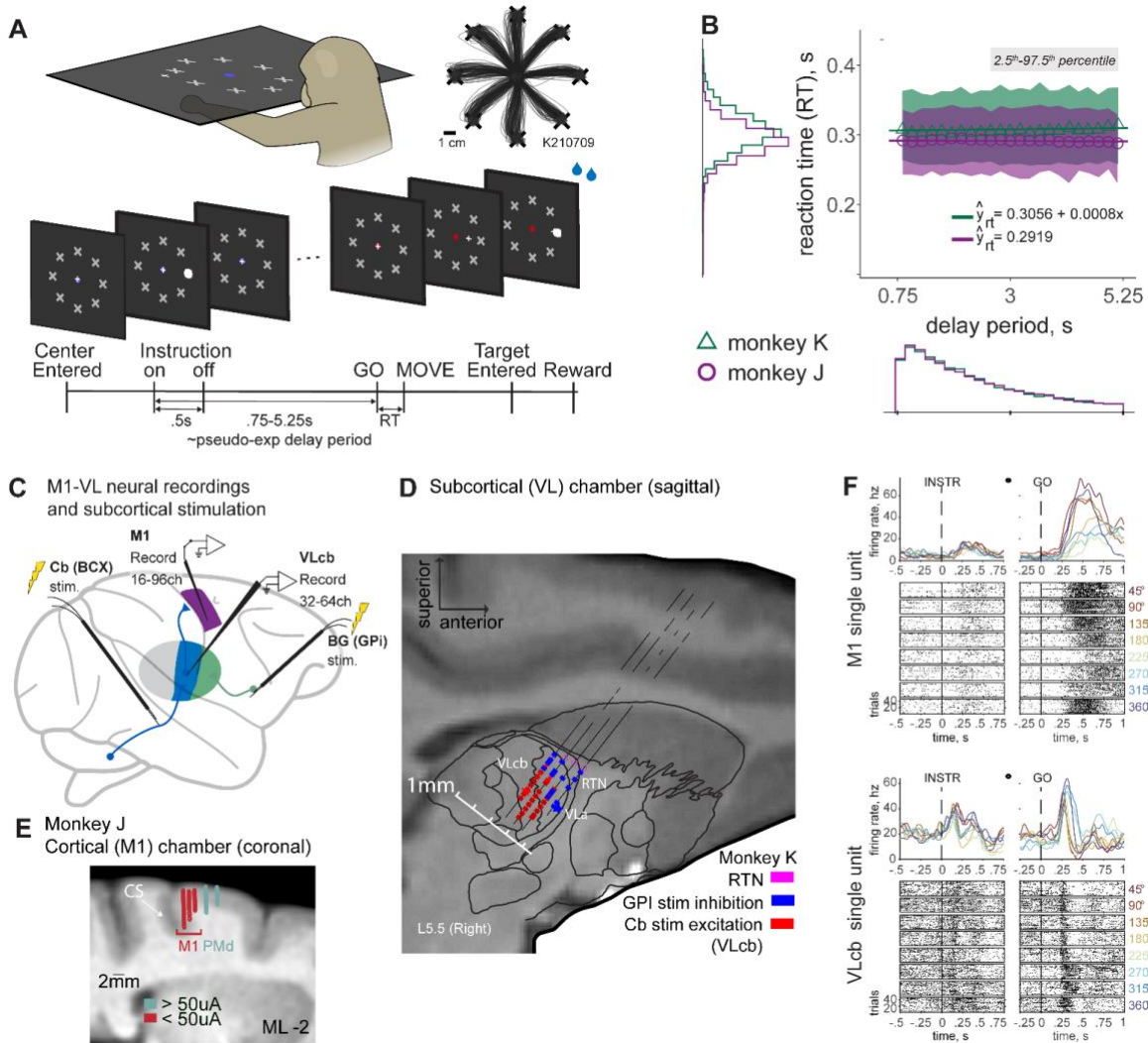


**Figure 2.2 Experimental Paradigm.** (A) Memory-guided center out reach task and timeline. Cursor trajectories during a single session performed by monkey K are shown in the inset. (B) Scatter plot and marginal histograms of reaction time and length of the delay period for all rewarded trials performed by monkey J (purple) and K (green). (C) Schematic of M1-VL neural recordings and deep brain stimulation probes used in identifying the cerebellar thalamus. (D) MRI of monkey K's motor thalamus in the sagittal plane with atlas section (L5.5) overlay. Electrophysiology (black ticks) and excitation following cerebellar stimulation (red) were used to label the cerebellar-receiving territory of the motor thalamus. (E) MRI of Monkey J's motor cortex, focusing on the pre-central gyrus (central sulcus, CS) in the coronal plane and aligned to the recording chamber coordinates. M1 is identified as having a low threshold for evoked movements ( $< 50\mu A$ ). (F) Example single-unit neural activity recorded from M1 (top) and VLcb (bottom) aligned to target instruction (left) and go cue (right).

The consistency in RT distribution across delay lengths implies the animals are not able to glean timing structure from the task and anticipate when to move. This observation was corroborated by high task performance. Success rates were high (J: 91% of total 10416 trials; K: 88% of 7715 total trials), and exceptionally few (J: 0.19%; K: 0%) anticipatory reaches (RT<100ms) were observed. Cursor trajectories (**Figure 2.2A**, inset) were consistent across trials and had bell-shaped velocity profiles that were clearly initiated well after the go cue (Supplemental Figure XB). There were some micro-movements (<1cm/s) within the 0.45cm radius center hold during the delay period in monkey J that were marginally larger for long delays ( $R^2= 0.0243$ ,  $\beta_1 = [ 0.029, \ 0.038]$ ; Supplemental Figure XD), but these were not reflective of a prediction of go cue arrival. Of the failed trials in which the monkeys could not remain within the center hold before the go cue arrived (J: 4% of total; K: 2% of total), the center hold breaktime was often before the minimum possible cue arrival, indicating a general level of attention or frustration. Furthermore, we observed no deviation of the breaktime distribution from the delay period distribution in ways consistent with temporal evidence accumulation or attempts to predict the mean (Supplemental Figure XE-F). Together, these behavioral observations imply the animals respond to the visual go cue before initiating movement, which means that the reaction interval and estimated neural response latencies accurately reflect internal processes following the cue arrival.

### **2.2.2 A small subset of VLcb precedes M1**

If the cerebellothalamic pathway is driving movement initiation activity in M1, we expect movement-related changes in VLcb activity to precede that of M1. The simplest form of the

trigger hypothesis predicts that responses in all VLcb neurons will lead M1 by the time delay imposed by a single synapse (1-3ms). We tested this prediction by estimating the response onset time (response latency, relative to movement onset) of the average peri-movement activity for each unit recorded from VLcb and M1, as well as from a validation set of muscles, in two monkeys.

We analyzed a total of 487 VLcb units, 862 M1 units, and 80 muscles with peri-movement responses between the two monkeys. Neural activity recorded from example units in M1 and VLcb is shown in **Figure 2.2F**. The activity is aligned to the times of the target instruction and the go cue, highlighting that both VLcb and M1 have preparatory activity and arm movement-related activity. Most single units recorded from the VLcb (90%) were responsive to movement, of which 90% were also responsive to the target instruction (Supplemental X). The movement-related responses are brisk and modulated by reach direction, as expected from arm-related motor territories. Responses were typically complex, multiphasic, and were heterogeneous across the recorded populations. Supplementary Table X describes other basic properties of task-related unit activity like task epoch-dependent firing rates, response type (increase, decrease, polyphasic), and trial-to-trial variability which are not the primary focus of this paper.

We found that a small subset of VLcb units does lead M1 across our recorded populations, yet the distribution of response latencies in VLcb was more heterogeneous than what was predicted for VLcb activity or observed in M1 (Figure 2.3). For each neuron we computed the average firing rate across all trials and estimated the time at which the standardized peri-movement response changed relative to the pre-go cue baseline (Figure 2.3A) using two different thresholds for detecting a response:

3-standard deviations above baseline and half the maximum firing rate (half-max) (Figure 2.3B). A leftward shift in the VLcb response onset cumulative distribution function relative to M1 is apparent for each choice of threshold in Figure 3C and Figure 3E. Seventeen percent (17.25%; 84/487 units) of the recorded VLcb population have response latencies earlier than -151.4ms relative to movement onset, the 5<sup>th</sup> percentile of M1 onset times. The VLcb population had a slightly earlier average response latency (rate-change: mu=-76ms, sigma = 90ms; halfmax: mu=-43ms, sigma = 92ms) relative to M1 (rate-change: mu=-62ms, sigma = 79ms; halfmax: mu=-16ms, sigma=86ms) regardless of the response onset estimation approach chosen (unpaired t-test; rate-change: p<0.01, halfmax: p<10<sup>-4</sup>). The median also differed significantly (ranksum; rate-change: p<10<sup>-4</sup>, halfmax: p<10<sup>-7</sup>), as reflected by the difference in the population CDFs at y=0.5 (Figure 2.3D, 2.2F). Bootstrap sampling was used to estimate the difference between population means (rate-change: -14ms, SD 4.8ms; halfmax: -27ms, SD 6.4ms) and medians (rate-change -17ms, SD 6.9 ms; halfmax: -18, SD 6.4ms). Both populations have substantially earlier average latencies than EMG (rate-change: -42ms, SD 40ms; halfmax: 10ms, SD 62ms).

The other prominent feature of the response latencies in VLcb is heterogeneity, as reflected by the high variability across the neural population (bootstrapped 95% confidence intervals for the standard deviation using the rate-change approach: VLcb, [82.6,96.3] ms; M1, [72.9, 84.8] ms; EMG, [12.8, 22] ms) and inter-quartile range (bootstrapped 95% confidence intervals: VLcb, [88,112] ms; M1, [69, 86] ms; EMG, [15,36] ms), especially relative to EMG (Supplemental Figure X). The estimated dispersion metric is always greater for VLcb than for M1 at the 90% confidence level, though the 95% confidence intervals do slightly overlap depending on the choice of metric. We then wished to know

whether the increased variability in onset times was due to a greater proportion of units that only became active during movement execution. However, number of units responsive after movement onset was no different between the two brain areas (VLcb, 17%; M1, 15%; chi-square  $p=0.25$ ), suggesting that an alternative explanation. When we examined only units with onsets earlier than movement onset ( $t=0$ ), there is a far greater difference in variance between M1 and VLcb. It is as if the average responses of individual VLcb units tile in time before movement is initiated. We also found that the average unit activity in VLcb is slightly weaker and shorter in duration than M1 (Supplemental Figure X).

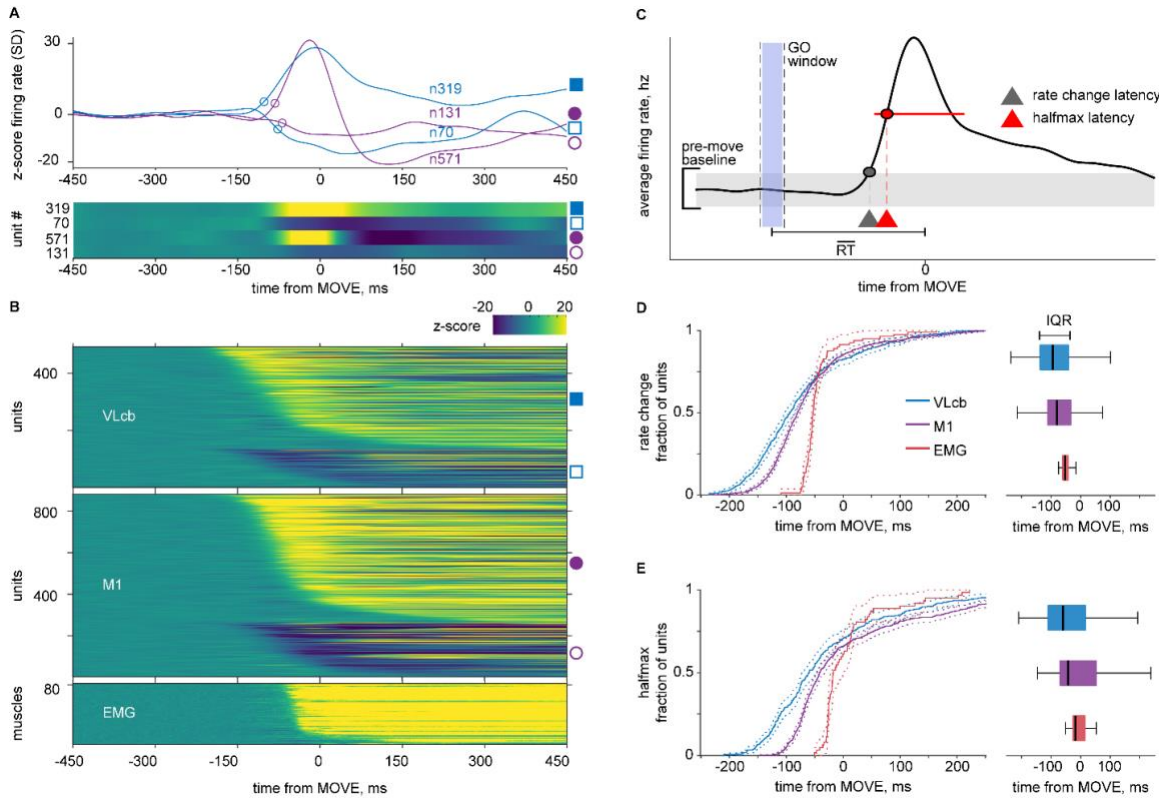


**Figure 2.3 . A subset of VLcb leads M1.** (A) Four example peri-movement responses recorded in the the cerebellar-recipient motor thalamus (VLcb, blue) and primary motor cortex (M1, purple). The firing rates are z-scored relative to the pre-go cue delay activity and converted to a color scale for visualization. (B) Heatmap of the peri-movement responses across the neural populations and muscles. (C) Schematic illustrating two estimation approaches for detecting neural response latency, “rate change” and “halfmax”. (D) Cumulative distribution function of response latencies in the VLcb (blue), M1 (purple), and muscles (EMG, red) estimated using the rate change approach (left panel). Median (bold line), IQR (shaded rectangle), and 99.7 percentile distribution limits (brackets) are shown in the right panel. (E) Same as in D for the halfmax estimation procedure.

To summarize, a subset of VLcb units is consistent with simple trigger model because their

activity changes in advance of M1 around the time of movement. Their earlier onsets led to a median difference in onset latency of  $-17 \pm 6.9$  ms between VLcb and M1. The distribution of population response latencies are also quite broad, likely broader than the M1 distribution, which suggests that the mechanism of triggering is more complex than originally conceived.

### **2.2.3 VLcb does not predict movement onset as strongly as M1**

The first prediction of the simple trigger hypothesis concerned the across-trial average timing of units. The second prediction concerns trial-to-trial variability in the neural response: On a given trial, does the timing of the response predict when movement will begin? The functional role that an area plays in movement initiation can be inferred from how tightly linked the responses are to the timing of behavioral events (Hanes, Thompson, and Schall 1995; DiCarlo and Maunsell 2005), namely the go cue and the movement onset. It is well established that the time of the peri-movement response in M1 on any given trial consistently falls at a fixed interval before movement onset, regardless of reaction time (RT). In other words, the timing of the neural response in M1 predicts when the movement begins. M1 is “time-locked” to movement onset, *not* to the go cue, while primary sensory areas are known to have the opposite relationship. The simplest model of movement initiation predicts that the VLcb must also be time-locked to movement onset: on any given trial, a change in VLcb causes a change in M1 at a small, fixed delay, which in turn results in movement onset following a second fixed delay. Motor areas are widely assumed to have a fixed relationship in time to movement onset, as reflected in the simplicity of the trigger hypothesis.

In contrast to this strong expectation, we found that VLcb is significantly less time-locked to movement onset than M1. To our knowledge, this is the first instance go cue-locking has been observed in a conventionally “motor” area. The concept of differential time-locking to the go cue and movement onset is apparent in the annotated spike rasters given for two example units in **Figure 2.4A** and **Figure 2.4B**. The unit recorded from M1 has a response that falls 75ms *before movement onset* in each trial—

there is a straight line visible in the raster when the unit activity is aligned to movement onset. In contrast, the unit recorded from VLcb has a response that falls 150ms *after the go cue* in every trial. Two different alignments of the neural activity are shown for each unit to illustrate how the simplified description of time-locking given above maps to variance in temporal intervals: there is less trial-to-trial variability in the interval between the response onset time and the time-locked event.

Our eyes can pick up on this relative variability for the example cases, but it must be quantified to assess time locking across neural populations. Previous work computed trial-to-trial variability in temporal intervals between task events and single-trial estimates of neural response onset latencies (DiCarlo and Maunsell 2005; Pasquereau and Turner 2015). Using only a single, noisy spike train to estimate neural onset is challenging, particularly when the single-to-noise ratio is lower. Here we apply a procedure that offers a middle ground: trials with similar neural responses are grouped, and response latency is estimated for each group of similar trials. Similarity in reaction time is used as a proxy for similarity in neural onset time since both types of event locking would be preserved under this grouping.

**Figure 2.4C-F** describes the event-locking quantification procedure in detail. The RT distribution is partitioned by 20-quantiles, and trials with RTs within each partition ( $Q_1, \dots, Q_{20}$ ) are summed and smoothed (**Figure 2.4C**). The neural response onset is estimated for the single smoothed neural response in each partition ( $Q_1, \dots, Q_{20}$ ) using the rate change approach shown in **Figure 2.3B** (**Figure 2.4D**). The neural response onset is regressed against reaction time for each alignment, giving an estimate for variability in the interval between the neural response and the aligning event. A

selectivity index for the locked event is found as the difference-sum ratio between the two variability estimates. A selectivity close to +1 represents a unit perfectly locked to the movement onset, while a selectivity close to -1 represents a unit perfectly locked to the go cue.

We applied this procedure to the two units in **Figure 2.4A** (**Figure 2.4D-E**) and **2.3B** (**Figure 2.4F-G**). Two alignments are shown for each unit. Consider the movement-locked M1 unit in **Figure 2.4D-E**. Since the unit's spiking activity has a close temporal relation to movement onset, the time between the go cue and the initial change in activity covaries with RT (**Figure 2.4D**). Note that there is no variability in response onset when aligned to the time-locked event RT (**Figure 2.4E**). Conversely, the unit in **Figure 2.4F-G** has a tight relationship with the go cue regardless of the RT. Thus we see covariation between the interval between the neural response and the movement onset with RT.

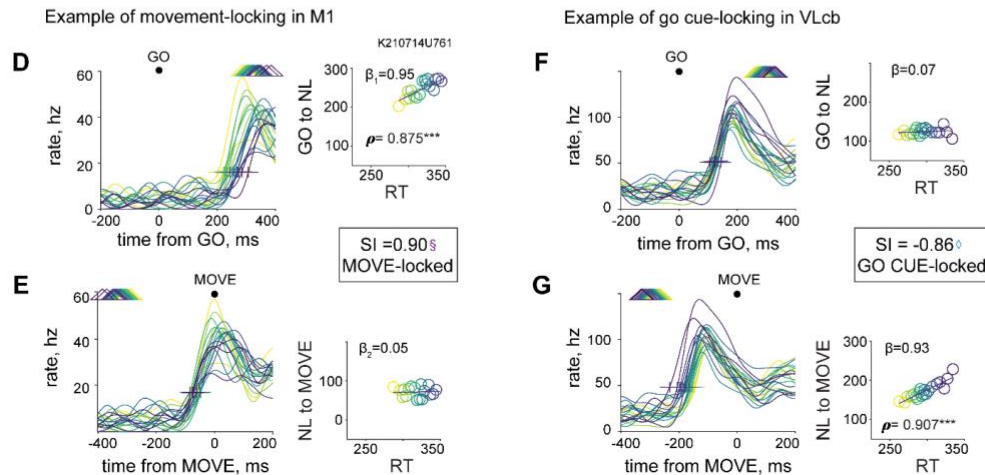
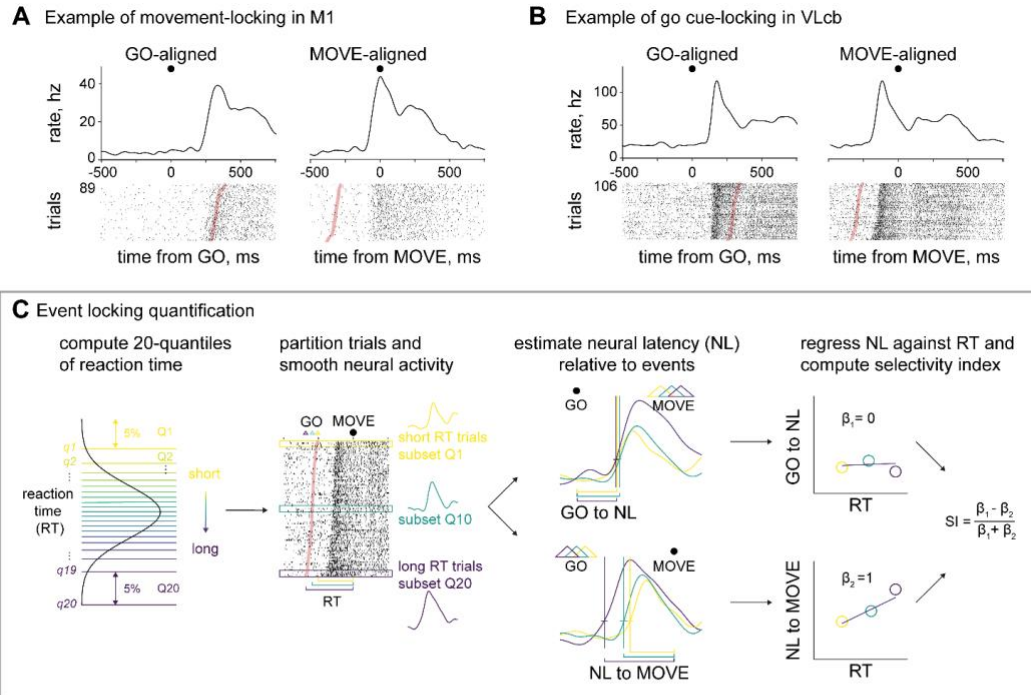


**Figure 2.4 Event-locking captures temporal variability in neural response onset relative to task events.** (A) Example unit recorded in M1 that is tightly locked to movement onset. The spike rasters ordered by RT (bottom) and smoothed spike density function (top) are shown for two event alignments (left: go cue; right: movement onset). The event not used for alignment is shown in a red triangle. (B) Example unit recorded in VLcb that is tightly locked to the go cue. (C) Event locking quantification procedure. (D-E) Application of event-locking approach to unit in A. There is a strong correlation between the Go - Neural Latency (NL) interval and RT because the unit is locked to movement onset. (F-G) Application of event-locking approach to unit in B. There is a strong correlation between the NL-movement onset interval and RT because the unit is locked to movement onset.

We applied this procedure to all units in VLcb and M1 that had an average response earlier than movement onset and found that VLcb is more time-locked to the go cue than M1 (**Figure 2.5**). **Figure 2.5A** reveals the distribution of selectivity index (SI) across the neural populations and muscles. The distribution of EMG deviates from perfect movement locking (+1), which we attribute to the inherent difficulty in estimating both movement onset and EMG response onset on the scale of milliseconds using a limited number of trials. Relative to EMG, both M1 and VLcb are marked by a pronounced leftward shift in the cumulative distributions. The cumulative distributions shown here represent a smaller fraction of units than in Figure 3. Since the RT distribution is strongly dependent on reach target, event locking was computed separately for each. Units with an insufficient number of trials (<20) or equivocal selectivity for both events were also excluded. Considering only the units with average latencies prior to movement onset, 23% of the VLcb population (46 units) were strongly locked to the cue, while 18% of the population was strongly locked to the movement onset in contrast to M1 (10% locked to cue, 20% locked to move). However, most units had mixed selectivity for task events, reflecting explanatory variance in timing related to both events.

We then assessed whether there was a relationship between the timing of the trial-average response and the preference for the event. One might assume that any unit strongly selective for the

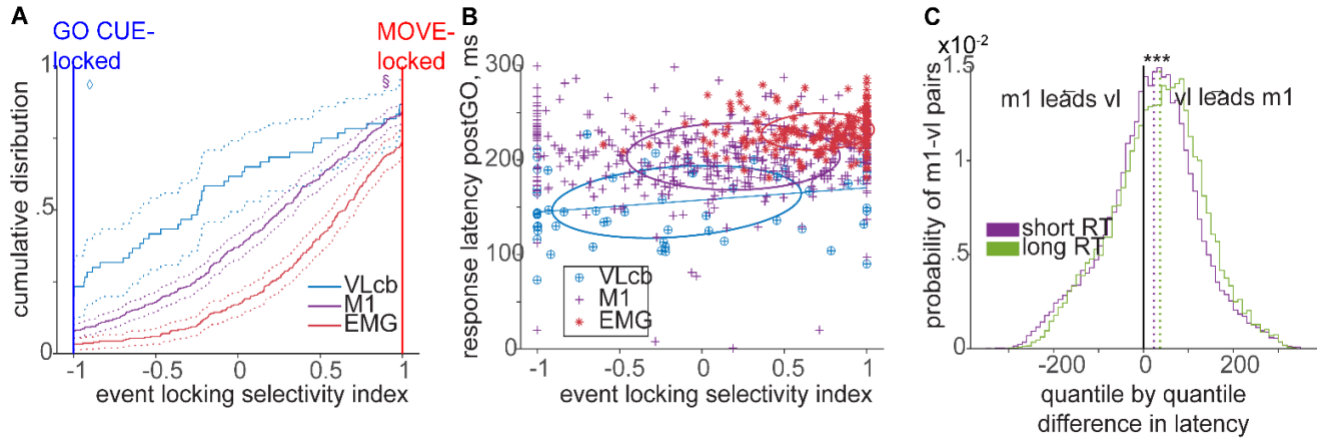


**Figure 2.5 VLcb is more time-locked to the cue than M1. (A)** Cumulative distribution of event selectivity index (SI) across neural populations. **(B)** Relationship between SI and response latency. **(C)** Difference in latencies between M1 and VLcb and its dependence on RT.

cue (-1) would have an average response latency closer in time to the cue. **Figure 2.5B** reveals that there is an association, but this is not necessarily true on a unit-by-unit basis. Additional examples of individual unit locking to task events are shown in Supplementary Figure X. We also wanted to confirm that the event-selectivity index is consistent pairwise timing differences across RT. If the population of VLcb neurons is more time-locked to the go cue, the timing difference between VLcb → M1 will be dependent on the RT. **Figure 2.5C** agrees with this prediction: on average, a single unit in VLcb leads a single unit in M1 (for neurons that are active in advance of movement onset), but this timing difference is greater when the RT is longer.

We also that it is appropriate to group the behavioral data by RT. One concern is that RT could be correlated with other features of behavioral performance, and the response timing differences we observe at the level of single neurons may reflect these other features rather than RT. Thus we returned to the behavioral data and confirmed that reaches to a given target grouped by *when* they were initiated

did not have remarkably different features. Cursor trajectories had bell-shaped velocity profiles that were highly similar regardless of reaction time (Supplemental Figure 2X). We did observe a slight negative correlation between RT and peak velocity (J:  $R^2 = 0.012$ ; K:  $R^2 = 0.039$ , average per target); and RT and rise time (J:  $R^2 = 0.096$ ; K:  $R^2 = 0.035$ , average per target), but these associations are slight in comparison to the range over which RT varies (Supplemental Figure 2X)..

In short, the trial-by-trial timing relationships found in VLcb contrasted with the predictions generated by the simple trigger hypothesis. Activity in the VLcb is not only changing earlier than M1, it is also likely reflecting an earlier but not strictly sequential stage of sensorimotor processing. The presence of go cue related activity in the cerebellar thalamus—and even, to a lesser extent, in M1—suggests that variability in reaction time may be a product of the interaction of these brain areas.

#### **2.2.4 VLcb has complex directionality over the course of the task**

The simple trigger hypothesis is the most consistent framework adopted in recent work, but there is substantial debate over whether timing input to M1 from the cerebellum also conveys directional information. On one hand, the simplest notion of a “trigger” is that the cerebellar pathway conveys the same signal to begin any planned, visual cue dependent movement regardless of which muscles are used. This idea has been adopted by theoretical work in M1 since ballistic type reaches could be executed through dynamics within M1 without externally provided directional information (Sussillo et al. 2015; Churchland et al. 2010). On the other hand, it is well understood that cerebellar damage results in ataxia, which is characterized by muscle group-specific delays in the timing of contractions (A. J. Bastian et al. 1996). The initial components of reaches to different directions require

coordination between different groups of muscles, which implies there should be directional encoding in coordination signal at the onset of the movement. The feedback control framework of cerebellar function maintains there should be signaling of sensorimotor errors or compensatory motor commands, which are similarly muscle- or movement-dependent (Shadmehr, Smith, and Krakauer 2010).

We therefore investigated the directional tuning of the cerebellar thalamus compared to M1 and found a surprisingly complex relationship over the course of the task (**Figure 2.6**). **Figure 2.6A** shows the strength of directional tuning in 250ms bins corresponding to important task epochs. The strength of directional tuning in VLcb varies substantially over the course of the task but is weaker relative to M1 at the time of movement initiation. To examine the time at which directional information becomes available in these neural populations, we computed a tuning timecourse and estimated the time at which the tuning changed around the time of movement. **Figure 2.6B** illustrates that the time of directional information around movement onset in VLcb is delayed relative to M1, regardless of the choice of method to detect onset, and even for the “earliest” units that have average responses in advance of the movement. The strength of tuning has long known to be weaker in the cerebellar thalamus than in M1 (Nashef et al. 2021), but here we show that the directional information is arriving

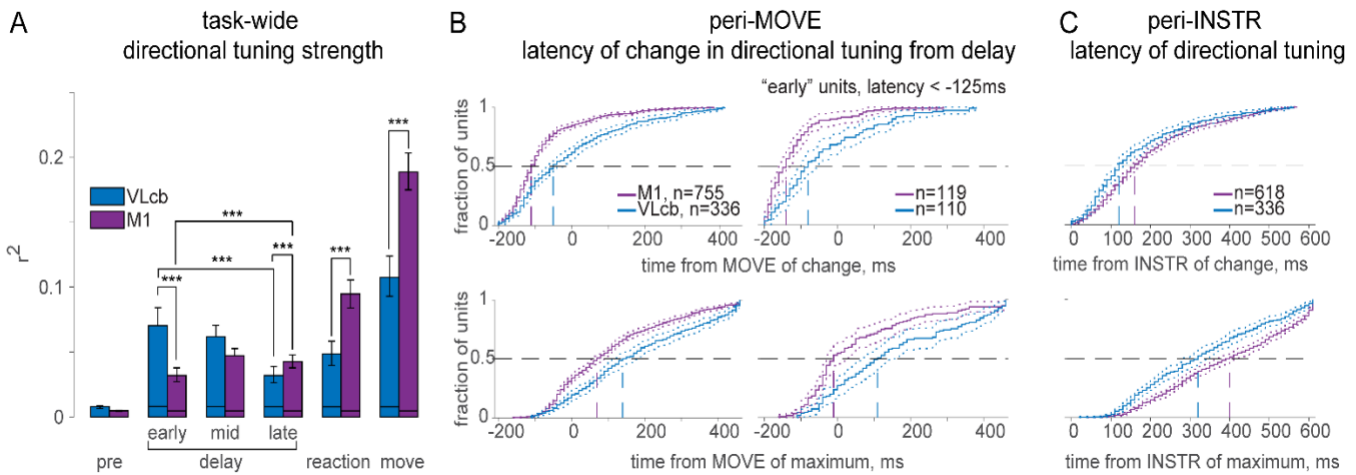


**Figure 2.6 VLcb has complex directionality over the course of the task.** (A) Directional tuning strength in 200ms bins. (B) Time of directional information appearance in timecourse of tuning around the time of the movement. (Top) Uses rate-change approach to detect deviation from pre-cue baseline. (Bottom) Uses time of maximum tuning. (C) Same as in B but around the time of the target instruction, which begins the early delay.

with or after M1. It seems unlikely that the strong directionality in M1 is a product of cerebellar input at this time in the task.

We then performed the same analyses during the delay period, beginning with the time of target instruction. In contrast to the relationship observed at the time of movement, the strength of directional tuning in VLcb is stronger and earlier relative to M1 at the time of target instruction (**Figure 2.6C**). This directional information decays over the course of the delay period, such that the average tuning strength is very close to zero by the end of the delay period.

These findings are surprising because they are consistent with the idea that cerebellum has context-specific tuning. Our task design has allowed us to see functional separation of cerebellar input to M1 over the course of the task.

## **2.2.5 Functional separation between movement timing and planning**

We observed that there are many VLcb units with an average latency earlier than M1, yet directional information arrives following that of M1. We can conceptualize the function of cerebellar input to M1 by way of the thalamus in terms of neural population activity patterns that are active at different times in the task. Movement initiation-related population activity in VLcb can be explained by two modes of firing: an earlier non-directional component followed by a directional component (**Figure 2.7**). We applied demixed principal components analysis to our condition averaged neural data in our two monkeys, viewing activity along a direction independent mode that only captures variation in time (**Figure 2.7A**), and a direction dependent mode that captures variation across reach directions (**Figure 2.7B**). We applied a bootstrap sampling approach to estimate when neural activity changes along these two modes in our two brain areas. This analysis revealed that only the direction-independent component of VLp leads M1. Activity in VLcb first changed along the direction-independent mode and later along the direction-dependent mode in both animals.

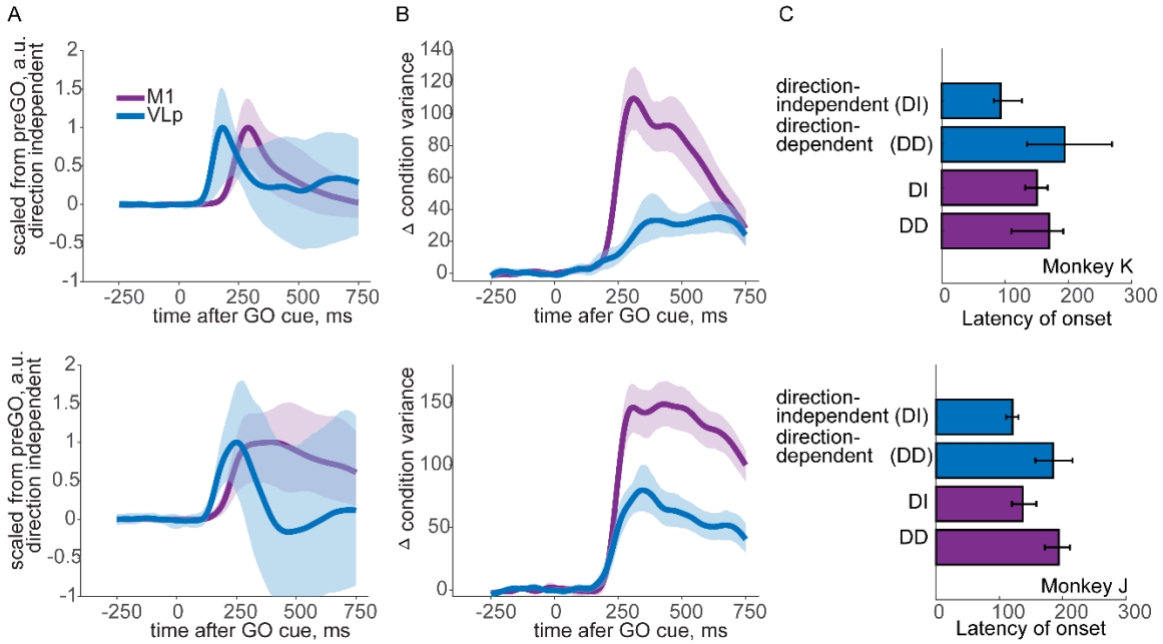


**Figure 2.7 Temporal separation between neural population patterns.** (A) Direction-independent mode. (B) Direction-dependent mode (change in target-related variance). (C) Latency of changes along modes relative to pre-cue baseline.

Figure 2.7 reveals how information about the visual cue information may be distinctly represented from signaling necessary during movement execution. Taken together with the results above, these findings suggest that the cerebellum may be multiplexing task-relevant information via different neural activity patterns.

## 2.3 Discussion

Our results are broadly consistent with the idea that drive to the motor cortex via the macaque cerebellar-thalamocortical pathway begins the process of initiating visually cued movements. Each of the findings reported in this study can be interpreted from multiple perspectives and lend insight into the proposed functional role of cerebellar input to the motor cortex.

### *Interpreting neural latency differences across studies*

This is not the first study to examine peri-movement neural onset latencies in the cerebellothalamocortical pathway and consider its involvement in movement initiation. There has been substantial conflict concerning the relative timing of the dentate nucleus and cerebellar thalamus compared to M1 in the primate. Some studies claim that average firing in the dentate precedes M1 (Nashef et al. 2021; W. T. Thach 1975), while others have suggested that activity in the dentate follows M1 (Anderson and Turner 1991; Butler, Horne, and Hawkins 1992). Many studies in the mouse did not directly compare timing between brain areas (Dacre et al. 2021b; Gaidica et al. 2018), though one recent study did report go-cue related signaling in the deep cerebellar nuclei within 15ms of the cue delivery that was available in ALM after about 20ms (Inagaki et al. 2022). Across all these studies, there is striking variability in response latencies at the level of individual brain areas, even in the setting of large sample sizes. Distributions of response latencies thus overlap substantially between areas. Yet we still hope to infer a hierarchical or sequential propagation of activity between brain areas from even slight mean differences in latencies and ignore overlap in these distributions. Our study is no exception, though we have attempted to be faithful to the broad distribution of peri-movement responses and qualify our interpretations accordingly. To add to the difficulty of contextualizing our work, previous studies all incorporate some aspect of predictive timing in their tasks. Even delayed reaching tasks with random delay periods have an element of predictive timing because the usual choices for a delay period distribution (e.g. the uniform) all have non-flat hazard rates. Many studies

do not reliably exclude the possibility of anticipatory movement, obscuring interpretation of neural onsets.

We attribute our simple yet novel findings to a relatively high sample size and controlled behavioral tasks. We found that there is a difference in timing distributions consistent with the conclusions of some of the earliest work (W. T. Thach 1975), that VLcb leads M1, though each area's distribution is quite broad and overlapping. We do show that a significant fraction of units in VLcb changes their activity before any firing changes in M1, which supports the idea that this pathway drives initiation activity in M1.

#### *The "trigger signal" as a sensorimotor transformation*

We explicitly studied externally timed movement initiation in this paper. In such a task, the sensory cue to begin moving must be transduced and ascribed meaning before the behavioral response is produced. This sensory to motor transformation is thought to be distributed across brain areas in different stages. The timing of a neuron's response during the reaction interval, i.e. between the sensory cue and the movement, is thought to be related to its involvement in, and position along, a sensorimotor processing pathway supporting a particular behavior. Short-latency changes in activity following presentation of a visual stimulus are available in visual cortex, while traditionally "motor" areas have average response latencies closer in time to movement. The role that an area plays in movement initiation, like sensory processing, can be inferred from the timing of the activity relative to these two events.

The average neural response latency is one way of evaluating the functional role of a brain area, but another way is by considering how reliably a task event can be predicted from the neural activity considering trial-to-trial variability. Since the time between cue and movement varies across trials, covariation between the time of the neural response and reaction time across trials tells us whether the activity changes are locked in time to the stimulus or the movement. Such a quantification allows the activity in different brain areas to be placed along a sensorimotor continuum. This sensorimotor transformation is not necessarily distributed into discrete stages of information transfer. For example, dynamical interaction between brain areas may subserve this transformation. This allows for the possibility of intermediate event locking.

We observed that VLcb is more locked to the stimulus than M1. A fraction of those VLcb units were very tightly locked to the go cue, while the rest had some degree of both cue and movement locking. Some component of the intermediate locking we observed is most likely due to uncertainty in the estimation process. This is most evident in the EMG responses since they are tightly locked to the movement by definition. The absence of perfect movement-locking in the EMG is a product of the process of estimating both the timing of movement onset from changes in arm velocity as well as the noise inherent to EMG and neural activity. Even with the statistical limitation of our estimation methods, we see a leftward shift towards cue-selectivity between M1 and muscles, and an even larger shift in the locking distribution between VLcb and M1.

The cue-locked changes in neural activity are unlikely to represent visual responses, as they are far later (>100ms) than stimulus evoked responses in sensory areas. Given that such signals have been

shown to be context-dependent in GO/NOGO tasks (Romo and Schultz 1987), we conceive of them as a learned association between the cue and action, or a signal of motor intention. This shift towards go cue selectivity places VLcb earlier in the sensorimotor pipeline, but also suggests that those circuits or the connection between VLcb to M1 is driving the transition between stimulus and action. From these data we infer that the cerebellum is providing a link between sensory information and the behavioral response driven by motor cortex that was previously considered a function of the parietal cortex (Snyder, Batista, and Andersen 2000). On anatomical study suggested the cerebellar pathway could be propagating such information to the parietal cortex (Gharbawie, Stepniewska, and Kaas 2016a), but this remains to be shown.

Future work should entail developing a computational model of movement initiation that explains variability in reaction time by delays required for computing the sensorimotor transformation. Synaptic variability between the cerebellar thalamus and M1 provides some degree of explanation, but it is insufficient to fully explain the distribution of response latencies and event locking reported here. Modeling will allow us to have a greater sensitivity to the different conceptual components that are incorporated in the term movement initiation. More complicated models can be developed to account for the influence of reward expectation on improving the likelihood that a behavior will be acted on quickly or at all, or that accommodate predictive timing, or improve biological plausibility. An interplay between modeling and experimental can be used to make and test more precise predictions or how cue processing and reward motivations interact at the level of the motor cortex.

### *Control theory predictions of movement initiation*

There is a long history of using control theory to conceptualize the role of the cerebellum, and it is challenging to reconcile these notions with the simple trigger model of movement initiation discussed in this paper. The cerebellum is thought to achieve precise behaviors by learning the physics of our movements, predicting the expected future state of our body (e.g. the position of the arm in space) given a motor command, and using the discrepancy between the predicted future state of the body and the intended or goal state to provide early corrective feedback to the motor cortex (Shadmehr and Krakauer 2008; Wolpert, Miall, and Kawato 1998). Although there is broad consensus at the normative level— the cerebellum uses internal models of the world to provide feedback to M1— how exactly these solutions are achieved at the level of population activity of neurons in the cerebellar output nuclei and cerebellar thalamus remains to be clarified (Amy J Bastian 2006).

Perhaps surprisingly, the simple “trigger” signal proposed to drive the transition between movement preparation and execution can be thought of as the simplest instantiation of the internal model output computed by the cerebellum. The time at which the cue arrives results in the single largest discrepancy between the state of the arm (baseline) and the goal state (target)— exactly the discrepancy computed by the cerebellum.

The data in the present study provide a foothold for thinking about how these processes are achieved by the activity of neurons along this pathway. The timing of neural activity in this study is more complicated than the simplest predictions but is not in direct conflict with the internal model framework. However, this model does predict that the signaling from VLcb → Cb is related to the

movement of the arm, whether the signal is a sensorimotor error or a corrective motor command. In contrast to this, we see a marked very weak directional information in the activity of the cerebellar thalamus during the reaction interval. The internal model output hypothesis would not predict that the directional encoding appears after M1. Additional work is needed to clarify this discrepancy and generate granular predictions.

#### *Reconciling coordination and initiation signals*

Ataxia, or “uncoordinated movement,” is characterized by inappropriate interaction torques, which result from a mismatch in the timing of muscle contractions at different joints (A. J. Bastian et al. 1996). Coordination itself can thus be broadly conceived as appropriate temporal sequencing of muscle groups. How can we reconcile this idea of coordination with visually cued movement initiation? We can think of a reach, or any dexterous movement, as a well-timed sequence of muscle contractions, where the concept of “initiation” examined in this study simply represents the first change in activity of many to come. The heterogeneity in onset times observed in VLp could, for example, reflect the need for temporal tiling of muscle commands, such that these onset times follow the somatotopy of the sequence of muscle activations. However, such tiling in response onsets is not reflected at the level of M1, which suggests the behavior of this circuit at the beginning of a movement is uniquely different from its behavior during the execution of the reach. As yet it remains unclear how to achieve full reconciliation of these ideas.

#### *Directional flow between brain areas and multiplexing in the CTC*

In our study we found there is a complex timecourse of directional encoding represented in the activity of the cerebellar thalamus. There is strong encoding of the upcoming reach target immediately following the target instruction, but this decays over time to virtually zero by the end of the delay period. The opposite relationship appears true in M1. The rise in directional encoding is delayed relative to VLcb, and the strength of encoding increases to a stable point by the end of the delay period. Although our study is correlational, striking differences between brain areas suggests there is a flow of directional information from VLcb to M1 at this point in the task. The idea of distinct subcortical planning inputs has precedent, but these data differ substantially from predictions for this circuit. Multiple studies in the mouse have used a broad array of perturbations to show that the cerebellar thalamic loop circuit with the mouse ALM is required for maintaining a motor plan (Gao et al. 2018; Guo et al. 2017; Li et al. 2016). In our data, directional information is not maintained in the activity of the cerebellar thalamus throughout the delay period as it is in these studies, or in the primate PMd/M1. It remains unclear whether this reflects a true functional difference in circuit behavior between the mouse and primate. Recent theoretical work used principles of control theory to provide a normative justification for why, and how, transient subcortical inputs could efficiently stabilize the motor plan in PMd/M1 during preparation (Kao, Sadabadi, and Hennequin 2021),

In contrast to its behavior following the target instruction, the initial response in VLcb following the go cue is surprisingly non-directional, especially relative to M1. Directionality lags the initial response of the activity of single units, meaning the earliest units do have substantial information about the reach during execution. This means there are different signals being sent by the same group of

neurons over the course of the task, all from the dentate nucleus. The cerebellum has been implicated in a diverse array of functions, and here at the single unit level, we observe how a single unit may be involved in a general, non-directional process of reach initiation, followed by highly reach-dependent activity during execution. This suggests that there must be a mechanism by which these different types of activity patterns have different functional patterns and remains a topic of future study.

One explanation for the apparent absence of directional information in VLcb at movement initiation is the idea of cortical amplification of thalamic activity. It is possible that there could be small degree of tuning that is amplified in motor cortex via convergent inputs, a mechanism that has been shown in the sensory system (Bruno and Sakmann 2006). One argument against this idea is that there are very few recorded units with directional information at this time. Only a single unit was found to have an  $r^2$  as high as in M1 during this interval, which suggests that weakly tuned by convergent inputs cannot justify a behaviorally relevance for this degree of tuning.

#### *Cortical spread of movement initiation signals*

Throughout this paper we referred to the reach-related macaque cerebellum-recipient ventrolateral thalamus as one unit, the VLcb. In primates, however, this territory encompasses two distinct nuclei, VLp and VLx (Macchi and Jones 1997; Stepniewska, Preuss, and Kaas 1994), formerly VPLo and Area X, respectively (Olszewski, Assistant Professor Of Neuro-anatomy, and Neuro-surgery 1952), which have been speculated to be involved in different functional roles. These nuclei are contiguous structures with cytoarchitectural similarities that both receive strong glutamatergic input from the dentate nucleus of the cerebellum (Asanuma, Thach, and Jones 1983b; 1983a; Hoover and

Strick 1999). VLp and VLx differ primarily by the targets of their efferent projections. The common thread across studies is that VLp is thought to primarily project to M1, while VLx primarily projects to premotor areas like PMd/v and SMA, though the purity of this division ranges substantially across studies and animals. Some studies report virtually zero projections from VLx to M1 (Holsapple, Preston, and Strick 1991; Schell and Strick 1984; Strick 1976), others show small but definitive projections (Asanuma, Thach, and Jones 1983c; Stepniewska, Preuss, and Kaas 1994), while a more recent study found half as many projections to M1 from VLx as observed from VLp to M1 (Gharbawie, Stepniewska, and Kaas 2016b). Similarly, the degree to which VLp projects to premotor areas has ranged from minimal (Schell and Strick 1984) to substantial (Matelli and Luppino 1996). What remains constant is that premotor cortical areas may provide a major route by which the cerebellum influences motor cortex output in addition to its disynaptic projection to M1.

It thus remains an open possibility that the early, cue-locked signaling in the cerebellar thalamus reported here is predominantly relayed to premotor areas. This would result in M1 initiation activity emerging as part of a cascade of changes across motor cortical areas, or perhaps within one integrated network. In agreement with this idea, go-cue-locked activity has been reported in both SMA and PMd (Romo and Schultz 1987), and both areas have been shown to have average peri-movement onset latencies that slightly precede M1 (Crutcher and Alexander 1990; Kakei, Hoffman, and Strick 2001). Furthermore, electrical disruption of the PMd significantly delays reaction time in the setting of visually cued reaching (Churchland and Shenoy 2007), though inactivation of the SMA and pre-SMA does not (Shima and Tanji 1998). An even broader literature has SMA and PMd has considered the role

of SMA and PMd in more complex contexts than visually cued movements, such as in tasks that involve predicting the timing of events (Deecke et al. 1985; Halsband et al. 1993; Mauritz and Wise 1986; Perez et al. 2008; Shima and Tanji 1998), variable decision-dependent movements (Thura and Cisek 2014), and what are referred to as self-initiated or “internally guided” movements, in which the animal moves in the absence of external timing cues (Brinkman and Porter 1979; Eccles 1982; Romo and Schultz 1987). Even the study that reported stimulating PMd delayed RT can be thought of as a disruption of predictive timing function of PMd, as opposed to impairment of movement initiation itself. The task in this study featured a short, uniformly distributed delay period (0-400ms), and there was no effect of stimulation on trials in which the delay period arrival time was unpredictable (delay < 100ms) (Churchland and Shenoy 2007). It remains to be shown how these higher order areas interact with M1 in different behavioral contexts to support the emergence of movement initiation activity.

The present study does not resolve whether VLp and VLx have different functional roles. We observed more early, cue-locked responses in the VLp compared to VLx in one animal, and the opposite relationship in the other. It is possible that this conflict is due to a combination of sampling bias and *in vivo* identification of the territories, but if there were a clear division of labor between the two nuclei, we would see clustering of the early activity along the anteromedial axis. We observed early, cue-locked signals in both the anteromedial aspect and posterolateral aspect of VLcb. We do show that such early signals propagate directly to M1, even if we cannot directly show the impact of such signals on M1 relative to input from premotor areas. Future work is necessary to distinguish the

function of cerebellothalamic pathways and the way they may operate in concert to support movement initiation across contexts.

#### *Parallel and convergent initiation circuits*

The process of volitional movement initiation likely involves multiple parallel circuits. Inactivation experiments of the basal ganglia loop circuit prolong reaction time (Catanese and Jaeger 2021; Franco and Turner 2012; Takahashi et al. 2021), impair the ability to actively suppress an action (Cruz et al. 2022), or increase the likelihood of immobility (da Silva et al. 2018; Mastro et al. 2017), depending on the site of inactivation and animal species. Inagaki and others showed that go cue signaling in the ALM-projecting thalamus was available earlier in multiple brain including the deep cerebellar nuclei and the pedunculopontine nucleus (PPN) in the midbrain, and stimulating the PPN could promote the directional licking typically evoked by the go cue (Inagaki et al. 2022). Given the variability across studies due to different experimental manipulations, behavior and behavioral context, and animal model, none of these results directly contradict the interpretation of the present study. There are significant anatomical differences in the basal ganglia output and thalamocortical projection patterns between the mouse and the primate (Bosch-Bouju, Hyland, and Parr-Brownlie 2013), which further complicates the process of interpretation. It is very apparent from these previous studies that the term “movement initiation” encompasses highly related yet conceptually distinct aspects of behavior, and we do not yet know how different neural circuits may jointly contribute to reaction time variability. One can speculate that some neural circuits relay transient go signals in a

modality- and behavior-dependent manner, such as the cerebellothalamicocortical pathway under study here, while others influence the overall likelihood of acting in response to such signals.

### *Interpreting perturbation studies*

One key limitation of this study is that the work is correlational in nature. The monkeys' reaching behavior is tightly controlled, and we attribute the relatively simple, yet novel, findings of this work to the task design. Yet, we do not directly disrupt or facilitate neural activity in this study. There are fewer tools available to precisely manipulate these circuits in primate models compared to mice, but there is another more biologically motivated reason to consider normal neurophysiology alongside direct perturbations, especially in the context of movement initiation. The motor thalamus operates within a tightly controlled loop circuit, conveying tonic excitation to M1 even in the absence of context-specific signaling. Inhibiting any part of the thalamus dampens M1 excitability, and therefore sensitivity within M1 and the supplementary motor areas, simply because it is embedded within a network. Interpretation of stimulation-evoked movements experiments is equally challenging. It is perhaps not surprising that the large, synchronous bursts of activity following stimulation of a pathway that excites the motor cortex can evoke movements. What is more surprising is that this is one of the primary pieces of evidence used in conceptualizing and justifying the simple triggering model of movement initiation. Just because the physical hardware can serve this purpose in the setting of a large, nonphysiological "push", it does not dictate the normal behavior of the circuit. In short, perturbation studies must be interpreted in the context of correlational studies, just as observation alone is insufficient.

## *Summary*

Our results are broadly consistent with the idea that drive to the motor cortex via the macaque cerebellar-thalamocortical pathway begins the process of initiating visually cued movements. Our behavioral task dramatically reduced predictive behavior and neural activity, and in this context, we found a subset of units in the cerebellar thalamus with movement-related responses that precede changes in primary motor cortex, resolving disagreement across studies for many years. We further identified that the cerebellar thalamus has a substantial proportion of unit activity with a strong temporal relationship to the timing of the go cue, rather than movement onset, placing this motor area at a junction of sensorimotor processing. Our task fully dissociated motor planning from movement initiation and revealed a timecourse of directionality in the cerebellar thalamus consistent with its proposed roles in multiple functions. Overall these data suggest that the mechanism of movement initiation is more complex than originally conceived, and subsequent modeling studies are needed to capture the nuances of inter-area timing.

## **2.4 Methods**

### **2.4.1 Experimental framework**

#### **Animal subjects**

All animal procedures were performed in the laboratory of Dr. Robert Turner and approved by the University of Pittsburgh Institutional Animal Care and Use Committee. Care and handling of animals follows recommendations in the NIH Guide for the Care and Use of Laboratory Animals. Two male rhesus macaque monkeys (*Macaca mulatta*), 9–11kg, were used for the described experiments.

Nonhuman primates are the appropriate animal model for this study due to significant differences in the functional organization of the motor system and behavioral repertoires between primates and other mammals.

## **Behavioral paradigm**

The animals were trained to perform a reach task for food reward. While performing the task, each monkey was seated in a customized primate chair and head-restrained via 3-point surgical implants. The monkeys were trained to place their left arms into an exoskeleton robot (NHP Kinarm Exoskeleton Lab, BKIN Technologies, Kingston, Canada; (Scott, 1999)). The exoskeleton includes two troughs that support the forearm/hand and upper arm segments, and the animal's upper limb is restrained within the troughs with velcro. The linkage lengths were adjusted to align the robot's axes of rotation with the monkey's shoulder and elbow joints.

Movement of the robotic exoskeleton was mapped to a virtual cursor that the monkeys could move through a 2D virtual environment displayed by a video monitor. The exoskeleton arm was hidden from view by an opaque sheet, such that the monkeys could only see the virtual environment and cursor. Animal behavior was controlled and recorded using the associated BKIN Technologies Dexterit-E software. Timing of task events was transmitted to our neural recording system via the digital output bus of the KINARM to synchronize kinematic data and neural recordings. Two rotary encoders within the KINARM reported position with a feedback resolution of 0.0006 (3 microns at the hand), and all behavioral data were sampled at a rate of 1kHz. The wrist and elbow joint positions were used by the real-time system to deliver force commands and generate a rapid rotational

perturbation (a “torque bump”) at the start of 10% of the trials, on average. Food smoothie reward was delivered via a task-controlled peristaltic pump and sipper tube.

We designed a novel behavioral task to movement initiation must be experimentally dissociated from the formation and maintenance of the motor plan to cleanly distinguish cerebellar involvement in movement initiation. To do so we designed a variation of an instructed delay, center out reaching task (Crammond and Kalaska 2000) that decouples information about when to move from information about where to move. The arrival time of the cue directing the animal to start the reach, the ‘go cue’, should also be maximally unpredictable. Some of the variability in timing estimates of neural activity along the cerebellothalamic pathway in previous studies can be explained by anticipation, such that the animals do not merely react to the external timing cue but actively predict its arrival. Moreover, the cerebellum itself may also predict the occurrence of external events (Tanaka et al. 2021), and the goal of the present study is to specifically consider visual cue driven movement initiation.

Data were collected while the monkeys performed an instructed-delay, memory-guided center out reach task. The animal initiates each trial by moving a virtual cursor (.1cm white crosshair) into a stationary virtual target, a 0.5cm circle in the center of workspace. The target instruction is cued by flashing a white 0.5cm circle on one of 8 peripheral targets, denoted by stationary white crosses for 500ms. The instruction cue is then removed, and the animal must maintain the cursor in the center hold target before being given a cue to begin the reach, an isoluminant color change of the center target, referred to throughout the text as the “go cue.” Since the reach instruction is only briefly flashed on the

screen, the animal must remember where to reach throughout the delay period yet is still making a visually-guided reach due to the presence of the stationary white crosses. The delay period between the removal of the instruction cue and the appearance of the go cue is pseudo-exponentially distributed over a range of 1 – 4.5s such that animals cannot predict the appearance of the go cue (i.e. the hazard function is approximately flat). The radial distance between the center circle and each peripheral target is 4.5cm in all sessions. After hitting the target, the animal must hold the cursor within the target for a period of 500ms before the trial can be successfully completed. The animals are given a time-out penalty if they attempt to leave the center prematurely, within 150ms of the go cue, or if they fail to leave the center before 500ms. The longest allowed response time, the sum of the reaction and movement time, was 1s. Food slurry was delivered to the animal 1s after successfully maintaining the cursor within the target. The total amount of food delivered each day ranged from 500 – 750mL of slurry, such that the animals were given a full food ration if they completed approximately 800 correct trials per day. Monkeys were highly trained on this task before experiments began, ensuring behavioral performance was consistent across sessions. Kinematic and neural data are recorded simultaneously.

We designed a novel behavioral task to address whether peri-movement activity in the macaque cerebellar motor thalamus is consistent with its hypothesized role in movement initiation. First, the time of movement initiation must be experimentally dissociated from the formation and maintenance of the motor plan to cleanly distinguish cerebellar involvement in movement initiation. To do so we designed a variation of an instructed delay, center out reaching task (Crammond and Kalaska 2000) that decouples information about when to move from information about where to move. The

arrival time of the cue directing the animal to start the reach, the ‘go cue’, should also be maximally unpredictable. Some of the variability in timing estimates of neural activity along the cerebellothalamic pathway in previous studies can be explained by anticipation, such that the animals do not merely react to the external timing cue but actively predict its arrival. Moreover, the cerebellum itself may also predict the occurrence of external events (Tanaka et al. 2021), and the goal of the present study is to specifically consider visual cue driven movement initiation.

The task features two key modifications to the classic center out paradigm: (1) a target instruction that is only briefly flashed on the screen (500ms) must be remembered throughout the delay period and (2) a separate, nonspatial cue to begin moving, or ‘go cue’, with arrival times that are maximally unpredictable (**Figure 2.2**). The instructed target is only briefly flashed on the screen (500ms), thus requiring the monkeys to remember the identity of the instructed target and maintain a stable motor plan until they are visually cued to move. This design differs from typical memory-guided tasks because visual guides for all eight peripheral targets (X’s) remain visible throughout the session to help the monkeys plan and execute precise reaches (**Figure 2.2A**). After a long, pseudo-exponentially distributed delay period, the go cue is presented in the center of the workspace. The go cue arrival time distribution was chosen to have a flat hazard function so that the monkeys cannot better predict when the cue will arrive as time elapses. The minimum delay period, 750ms, was chosen so that they are sufficiently prepared for all trials (Ames, Ryu, and Shenoy 2014; Churchland and Shenoy 2007).

## **Surgical procedures**

General surgical procedures were performed at the University of Pittsburgh under the direction of Dr. Robert Turner and have been described previously (Desmurget & Turner, 2008; Zimnik et al., 2015). The chamber implantation surgery was performed under sterile conditions with ketamine induction followed by Isoflurane anesthesia. Vital signs (i.e. pulse rate, blood pressure, respiration, end-tidal pCO<sub>2</sub>, and EKG) were monitored continuously to ensure proper adequate anesthesia. Two cylindrical titanium recording chambers were attached to the skull: (1) at stereotaxic coordinates to allow access to the decussation of the left superior cerebellar brachium conjunctivum (BCX) in the midbrain via a parasagittal approach, and (2) at stereotaxic coordinates over the right hemisphere in the coronal plane to allow access to the right M1. The chambers and head stabilization implants were fastened to the skull via bone screws and methyl methacrylate polymer. Prophylactic antibiotics and analgesics were administered post-surgically. The monkeys were habituated to head-fixed conditions for several months. The monkeys were then anesthetized with isoflurane to perform a craniotomy for M1 electrophysiological recordings in the coronal chamber. Only microcraniotomies (radius ≤ 0.8mm) were necessary to access deep structures in the sagittal chamber and were performed under ketamine sedation.

## **Localization of cerebellar and globus pallidus internus stimulation sites**

To allow electrical stimulation-based identification of cerebellar-thalamus recipient M1 neurons, we chronically implanted two stimulation macroelectrodes: one into in the arm-related left superior cerebellar brachium conjunctivum (BCX), which contains ascending projections of the cerebellum that

will synapse in the right motor thalamus, and one into the right globus pallidus internus (GPi), the output nucleus of the basal ganglia (Turner & DeLong, 2000). The anatomic locations of sites for implantation were estimated initially from structural MRI scans (Siemens 3T Allegra Scanner, voxel size of 0.6mm) using an interactive 3D software system (MonkeyCicerone) to visualize MR images and predict trajectories for microelectrode penetrations (Miocinovic et al. 2007). Single-unit microelectrode recording was then performed in combination with electrical stimulation (single biphasic pulses 200 $\mu$ A, 0.2ms-duration at 2Hz max.; Model 2100, A-M Systems) to obtain precise coordinates for the target. Custom-built stimulating electrodes were then implanted at this site using methods described previously (Turner & DeLong, 2000). The custom macroelectrodes consisted of two Teflon-insulated Pt-Ir microwires (50 $\mu$ m) glued inside a short stainless steel cannula with 0.5mm separation between the distal ends of the microwires. Insulation was stripped from 0.2mm of the distal ends of the microwire to achieve an impedance of 10k $\Omega$ . The electrode assembly was implanted transdurally via the parasagittal chamber using a protective guide cannula and stylus mounted in the microdrive. In the months following implantation, the location and integrity of macroelectrodes were monitored by comparing the muscle contractions evoked by stimulation through the electrode against what was observed during microelectrode mapping.

### **Neural recordings in primary motor cortex (M1)**

M1 sites were localized by identification of the principal arm territory along the anterior bank and gyrus of the pre-central sulcus. As reported extensively, typical neuronal discharge responded to active and/or passive movement of the arm, and microstimulation at low current ( $\leq 50\mu$ A, 10 biphasic

pulses at 300 Hz) evoked contraction of forelimb muscles (Turner and DeLong 2000; Pasquereau and Turner 2011; 2013; McCairn and Turner 2015).

The extracellular spiking activity of neurons in M1 was recorded using multiple 16, 32, or 64contact laminar depth probes (0.5–1.0MΩ, V-probe, Plexon Inc.). The vast majority of the data were collected with the 64-contact probe, which has a 50micron inter-contact spacing. These voltage potentials were recorded with different amplifiers (Tucker Davis Technologies or the RHD2000 Intan USB Board running under Open ephys), and were thus either amplified, band-pass filtered (4×, 2Hz–7.5kHz), and digitized at 24kHz (16-bit resolution; Tucker Davis Technologies).

After the laminar depth probes were lowered into M1, the probes were allowed to stabilize for ~ 1hr before beginning the cerebellar stimulation sessions. The neural data was recorded for 30s prior to initiating cerebellar stimulation. A minimum of 500 200μs pulse-width, 600μA current, biphasic pulses at 1Hz or 1.5Hz were delivered while the animal began to perform the task. After the stimulation session, the neural data and behavioral events were collected while the animal performed the behavioral task for approximately 1.5hr, 800 correct trials per animal. A second cerebellar stimulation session was performed after the behavioral session was completed to ensure that we could categorize any neurons that were not present at the beginning of the recording session.

### **Neural Recordings in M1-projecting cerebellar thalamus (VLp)**

The Turner lab has long-established expertise in studying VL thalamus (Anderson & Turner, 1991) and M1 (McCairn & Turner, 2015; Pasquereau & Turner, 2011, 2013, 2015; Turner & DeLong, 2000). Two separate recording chambers and microdrives enables simultaneous access to both VL

thalamus and M1 while the animal performs the behavioral tasks described below. Raw extracellular voltage signals conveying the discharge of multiple single neurons was sampled simultaneously using one laminar probe in the subcortical thalamus (Plexon V-probe, 16, 32, or 64 channels), and up to two laminar probes in M1 (Plexon v-probe, 16, 32, or 64 channels). Precise control over the location of the neural recordings is enabled through a combination of MR imaging, stereotactic placement of the recording chambers, and precision depth control using the Narishige Microdrive. The initial recording sessions located boundaries of proximal arm-related VL thalamus and M1 as well as the general locations where cells are responsive during performance of the tasks. Preliminary localization was performed using sensory and motor responsiveness of neurons and the effects of microstim at the threshold of evoking movement. Connectivity between sites in M1 and VL thalamus will be verified by stimulating through each cortical microelectrode in turn while recording from thalamic electrodes. This approach, used previously the Turner lab, cannot test connectivity between the specific neurons being studied but can indicate that recordings were from connected regions of M1 and VL thalamus.

Recently, we have recorded from antidromically-identified VL->M1 neurons in a non-human primate NHP during performance of a choice reaction time reaching task (Franco & Turner, 2012). A microstimulation (microstim) approach developed by the Turner lab is used to distinguish VLp from VL<sub>a</sub> in vivo and thereby address the cerebellum->VLp-> M1 circuit. Along individual recording tracks, we distinguished VLp from the adjacent thalamic nucleus VL<sub>a</sub> preliminarily according to the effects of microstim (**Figure 2.2**). The two adjacent nuclei of VL thalamus, VLp and VL<sub>a</sub>, were differentiated through a combination of microstim and evoked responses. See **Figure 2.2** for preliminary results

illustrating the use of in vivo microstim to localize recordings in VLp and VLa. VLa was distinguished from adjacent nuclei by: the presence of stimulus-evoked depressions in firing in response to microstim in GPi, the absence of stimulus-evoked excitations in firing in response to microstim in BCX, inability to elicit movement by microstim, and absence of proprioceptive responses to rapid rotational perturbations of the arm. VLp was distinguished from adjacent nuclei by: the absence of stimulus-evoked depressions in firing in response to microstim in GPi, the presence of stimulus-evoked excitations in firing in response to microstim in BCX, low thresholds for eliciting movement by microstim, and presence of moderate-latency proprioceptive responses to rapid rotational perturbations of the arm.

We adopted a dual recording chamber approach to record from M1 and the primate motor thalamus simultaneously. We achieved in vivo identification of the cerebellar-recipient, arm territory of the motor thalamus (VLcb) using a combination of MRI-guided stereotactic localization, electrophysiology, and deep-structure and thalamic electrical stimulation (**Figure 2.2C**; see Methods). We distinguished the VLcb from the basal ganglia-recipient motor territory VLa by electrically stimulating the cerebellum and the output nucleus of the basal ganglia, the internal pallidum (GPi): the cerebellar recipient territory receives excitatory projections from the dentate nucleus but no inhibitory projections from the basal ganglia (GPi) (**Figure 2.2D**; Supplementary Figure X). VLcb is in fact an umbrella term for two cerebellar-recipient territories that on average send projections to different motor cortical areas, the VLp and VLx (also referred to as Area X), respectively. While VLx is thought to project to premotor areas, VLp is the histologically identified subnucleus that predominantly

projects to M1. Previous work showed some consistency between microexcitability, or the tendency to evoke movements with lower current electrical stimulation relative to adjacent areas, and the histologically identified VLp territory [citation needed]. We combine data from the putative VLx and VLp into the umbrella term VLcb throughout this work unless explicitly noted.

## **EMG Recordings**

We recorded electromyographic (EMG) activity using acutely placed intramuscular electrodes. EMG signals were bandpass filtered (10–500 Hz), digitized at 1 kHz, rectified, smoothed with a Gaussian kernel with standard deviation of 20 ms, and averaged across trials to produce peri-stimulus time histograms.

### **2.4.2 Data Analysis**

No statistical methods were used to predetermine sample size. The experiments were not randomized. The investigators were not blinded to allocation during experiments and outcome assessment.

## **Behavior**

Kinematic signals were filtered using a 4th order low-pass Woltring (cubic spline) filter with a cutoff frequency of 20 Hz. All error trials were excluded from further analysis. Types of errors include leaving the center hold target too early ( $\leq 150\text{ms}$ ) or too late ( $\geq 500\text{ms}$ ), not reaching the peripheral target within the acceptable response time (1s), or not holding at the peripheral target after acquisition. Movement onset was the time at which the animal's radial velocity exceeded 1cm/s. This occurred well

before the animal left the center target. Reaction time is defined as the interval between the go cue and this detected onset of movement. Target acquisition is the time at which the cursor hits the target.

### **Spike sorting and artifact subtraction**

Single units in M1 and VL were isolated using Kilosort 2 with drift correction (<https://github.com/MouseLand/Kilosort2>) (Pachitariu et al., 2016). The recommended 30micron spatial constant and thresholds on spike detection were used in the optimization, but the timebins were not sorted by similarity due to the presence of probe shifts in each recording. Manual curation was performed on candidate Kilosort2 clusters using Phy. Only neurons with a clear refractory period (< .5% candidate action potentials within 1ms), a canonical depolarization, and a consistent waveform over time were accepted. In this work we combined all the neurons across all sessions for two monkeys, thus treating all neurons as independent samples.

### **Spike density functions and response onset estimation**

A minimum of 80 valid behavioral trials (minimum of 10 in each direction) was required to include a neuron in single-unit, task-based analyses. Single-trial spike density functions (SDFs) were constructed by convolving each unit's spike time stamps (1 kHz resolution) with a Gaussian kernel  $\sigma = 25$  ms). SDFs were aligned to different task events (target instruction, go cue, and movement onset) for each trial, and across-trial mean SDFs were constructed separately for reaches to each target. We adopted a 'Rate Change" approach for detecting neural response onsets relative to key task events. The PSTH is first smoothed with a Gaussian kernel of small bandwidth (25ms shown throughout), and boundaries given by the mean firing rate +/- 3 standard deviations during the baseline is constructed.

Binwise statistical outlier detection, which refers to determining whether it would have been unlikely to draw test spike count sample from the distribution defined during the baseline period, was applied such that if a point exceeded the bands defined above a response was detected and the time at which a response was first detected was reported as the best estimate for onset latency(Baker & Gerstein, 2001; Barnett & Lewis, 1984).

## **Directional tuning**

Two approaches were used to determine the strength and timecourse directional tuning of all units with a peri-movement response. First a cosine tuning regression analysis was performed using large, 200ms bins of single-unit spiking activity around key task epochs. Statistical significance testing was performed hierarchically. A permutation (shuffle) test with 10000 randomizations of trial labels was used to define the null distribution of coefficient of determination values for each unit. We determined a p value for kinematic encoding to be the fraction of null regression values that were larger than the single regression fit determined from the non-shuffled data. We then used bootstrap sampling across the population of single units to define the population variability in r<sup>2</sup> for each epoch of interest. Statistical comparisons between neural populations were performed by comparing the bootstrapped confidence intervals for average r<sup>2</sup> in each epoch. Since all windows were significant, we performed a two-way ANOVA using neural population, i.e. M1 and VLp, and epoch as the two factors. A two-way ANOVA revealed there was a statistically significant interaction between the neural population and task epoch under study ( $F(3,2333)=31.22, p<0.01$ .

We then applied a cosine tuning regression analysis over the course of the task using sliding windows. Spiking data was binned in sliding windows of 100ms each, and the overlap was 10ms. These smoothed tuning functions had some variability during stable periods of the task, which was used to define an effective baseline period from which the tuning smoothly deviated following the go cue or the target instruction. Bonferroni type test in which we divide by the effective number of independent bins was used to adjust the significance level. For the latency tests, fewer VLp units had a large change in R<sup>2</sup>. As such the latency curves shift depending on how strong of an impact is required for a statistically significant change. The latency curves become closer together for more stringent tests, for which fewer VLp unit pass the threshold criteria. Currently, an alpha of 0.001 and 20 consecutive bins (200ms) are required. Lowering the threshold widens the curve. Making it more stringent (alpha 0.001 and 30 consecutive bins) selects for fewer units.

### **Time-locking analysis and selectivity index**

For unit responses that occurred during the reaction interval, i.e. before movement onset, we tested whether the onset of the response was better time-locked to the go cue or to the time of movement onset across trials. A version of this analysis in which single-trial response onsets were estimated was reported previously (Pasquereau & Turner, 2015). First, all trials for a given reach direction in a single session are sorted by reaction time (RT) and grouped into ventiles (20-quantiles), such that each group represents approximately 5% of trials. Units with fewer than 15 trials to a given target are excluded. Post-go cue spiking activity over time from trials in each group are averaged and smoothed with a 20ms Gaussian kernel, and the onset of the responses relative to the go cue is

estimated per the response estimation method described above. Each ventile is also associated with a single RT, the median RT in each group. Next, the onset times of each ventile were tested for significant temporal relationships (i.e. time locking) with the two task events (the go cue, and the movement onset detected from the arm velocity). If a unit's peri-movement response has a tight temporal relationship to the movement onset, i.e. there is a fixed delay between the neural response and the movement onset, then the time interval between the go cue and the neural response would vary with RT. Conversely, if a unit's response is tightly locked to the go cue (i.e. there is a fixed delay between the go cue and the neural response across all trials), you would expect the interval between the neural response and the movement onset to covary with RT. Spearman's rank correlations were calculated for each interval duration (go-to-response and response-to-movement) and RT. We used the Spearman correlation because it is less sensitive to strong outliers than the Pearson correlation, since outliers are limited to the value of their rank. Significance of this correlation was found with using a trial shuffle control. Some units were clearly either cue-locked or movement-locked using this analysis, but many of the units had some degree of intermediate locking in which the correlation between both intervals and RT was significant, but one captured less variation in RT. To address this, if either interval duration covaried significantly with RT, the selectivity for the locking was determined. This was computed using a difference to sum ratio was found between the unnormalized slopes obtained using robust linear regression with a bisquare weighting function (MATLAB default).



### **3 Cerebellar input dependent activity in primary motor cortex**

The neural signaling pathway that links the cerebellum to motor cortex by way of the thalamus is referred to as the cerebello-thalamocortical (CTC) circuit. It is still unclear how normal signaling in the cerebellum influences cortical control of movement, nor is there a consistent framework to understand how pathophysiological processes in this structure precipitate severe motor deficits. The proposed roles for cerebellar input are myriad, ranging from adapting motor commands in response to sensory feedback, triggering of movement initiation, and predictive, online control of movement. We approach this open question by studying the activity of M1 neurons that receive the most direct input from the cerebellum in the context of its proposed computational roles. In this work, we used electrical stimulation and a cumulative sum response detection algorithm to identify the subgroup of M1 neurons that receive disynaptic excitatory input from the cerebellum and study the activity in a non-human primate model of reaching. We motivate the performance of our identification approach through simulation and demonstrate a novel difference in firing rates between subtypes of neurons that is not due to bias of our detection algorithm. We found that neurons that receive excitatory cerebellar input have greater movement-related responsiveness and directional modulation that cannot be explained by a difference in baseline firing rates. These neurons, however, do not carry more mutual information about reach direction than the remaining M1 neurons, which motivates a more refined hypothesis regarding the role of cerebellar input to M1.

### **3.1 Introduction**

A movement as simple as reaching for a cup, though typically performed with ease in daily life, requires high spatial precision and dynamic coordination of muscle activity. In mammals, this ability is thought to be primarily mediated by cerebellar input to cortical motor areas, namely primary motor cortex (M1) and premotor cortex (PMv), by way of motor thalamus (W Thomas Thach, Goodkin, and Keating 1992; Middleton and Strick 1998; Jones 2007; Sherman 2005; Guillery and Sherman 2002). This pathway is referred to as the cerebello-thalamocortical circuit (CTC). In dysfunction of this pathway, the strength of muscle contraction is unaffected, yet the spatial accuracy and timing of movement components are disrupted (Kandel et al. 2000). Multi-joint limb movements, including those required for normal gait, are especially impaired (ataxic) (Mason et al. 1998; Goodkin and Thach 2003). This is thought to be a consequence of the greater temporal precision of motor commands needed to adequately control time-varying interaction torques across muscle distributions (Topka et al. 1998; Kandel et al. 2000).

The cerebellum is now widely thought to mediate the coordination and accurate timing of movements by constructing internal models of the limbs as part of an optimal feedback control loop with M1 and reconciling disparities between motor intention and action. The cerebellum is hypothesized to aid both online control and adaptation in response to feedback using a combination of forward models, which predict the sensory outcome of motor commands, and inverse models, which translate deviations in motor intention into the appropriate motor commands (Shadmehr and Krakauer 2008; Todorov and Jordan 2002; Scott 2012; Laurens, Meng, and Angelaki 2013). These control-theoretic

predictions for cerebellar activity have been most clearly grounded in the neural control of eye movements. Output signals from the cerebellum have been shown to predict both the real-time motion of the eye during saccades as well as the timing of saccade onset via the combined inputs of Purkinje cells onto individual neurons within the deep cerebellar nuclei (Herzfeld et al. 2015; Tanaka et al. 2020; Shadmehr, Smith, and Krakauer 2010). At least part of the output of the cerebellum was shown to represent a motor correction that could be added to the ongoing motor commands (Herzfeld et al. 2018; Sun et al. 2016).

The neural mechanism by which cerebellar output shapes motor commands in cortex, however, remains unclear. In rodents, there is significant experimental support for the idea that feedforward cerebellar excitation of M1 is required for motor planning (Gao et al. 2018; Chabrol, Blot, and Mrsic-Flogel 2019; Li and Mrsic-Flogel 2020; Sauerbrei et al. 2020). It was also shown in rodents that stimulation of cerebellar output disproportionately affects end-movement kinematics and can bidirectionally control reach extent, suggesting a stronger ability to directly influence motor commands during the movement than previously shown (Becker and Person 2019). Far less work has been done in the non-human primate. (Nashef, Cohen, Harel, et al.) proposed to address this question by *electrically inhibiting* the output pathway of the macaque cerebellum and studying the consequences on reaching and neural activity in M1. The authors found that cerebellar inhibition disrupts coordinated reaches, i.e. induces ataxia-like behavior, and significantly decreased the peri-movement responses of M1 neurons as well as the depth of their directional modulation across targets (Nashef et al. 2018;

2019). Pharmacological inhibition of the macaque cerebellar-recipient motor thalamus was also shown to decrease movement-related firing rate in M1.

These lines of evidence suggest two important points. The first is that cerebellar input to M1 directly influences reach direction over time, perhaps to improve precision. The second is that the M1 neurons that receive excitatory disynaptic input from the cerebellum, here we call them Cb+, may play a specific functional role within the larger M1 network during both the planning and execution of reaching movements. In this work, we propose to further elucidate the nature of cerebellar input to M1 by studying the activity of these neurons in the context of the proposed computational role of the cerebellum. As our first step to this end, we tested the prediction that Cb+ neurons are more related to reach direction than other neurons in M1. If our prediction is true, this would support the idea that cerebellar input is indeed directly shaping multi-joint motor commands by exciting a subset of the M1 network.

## 3.2 Materials and Methods

See Methods in 2.4 for experimental paradigm.

### 3.2.1 Data and Statistical Analysis

#### Cerebellar-response detection

We adopted an orthodromic electrical activation approach to excite the disynaptic excitatory pathway between the cerebellum and primary motor cortex. We delivered 500 electrical pulses to the fiber bundle of the superior cerebellar peduncle (see 2.4) while recording activity in M1. Electrical artifacts were observed in the analog data at the time of electrical stimulation and were largely

removed using median filtering across channels. A maximum period of [0 – 0.5]ms around the onset of stimulation was also “blanked” and replaced with pre-stimulation data to improve spike sorting with Kilosort2 and eliminate the appearance of stimulation induced electrical artifacts in the sorted data.

After spike sorting with Kilosort2, we constructed peri-stimulation time histograms of M1 unit activity in a [-300,200]ms window about the time of electrical stimulation and binned neural spike counts using 0.5ms windows of uniform width. Other choices of bin sizes were evaluated (0.25ms and 1ms), but the 0.5ms was chosen because it offered an appropriate trade-off between time resolution and noise reduction (data not shown). Based on the biological constraints of a disynaptic excitatory connection, we expected to see an excitation in M1, or an increase in firing rate, between 1 – 10ms following the delivery of electrical stimulation. Our algorithms were designed to detect a change in firing rate during this test interval. We also aimed to estimate the latency of response onset to support our claim that the responses we see in M1 are in fact disynaptic.

We apply three detection methods to this problem. The first method, termed the “Mean Change” approach, evaluates whether the mean of the set of samples in the test interval (spike counts across bins) was unlikely to have been drawn from the distribution of mean spike counts during the baseline using a z-test. We are able to use the z-test because the sample size of the pre-stimulation baseline period is quite large, and we can adequately estimate the variance of spike counts across bins. The second method, termed the “Rate Change” approach, first smooths the PSTH with a Gaussian kernel of small bandwidth (2ms shown throughout), and boundaries given by the mean firing rate +/- 3 standard deviations during the baseline is constructed . Then binwise statistical outlier detection,

which refers to determining whether it would have been unlikely to draw test spike count sample from the distribution defined during the baseline period, was applied such that if a point exceeded the bands defined above a response was detected and the time at which a response was first detected was reported as the best estimate for onset latency (Baker and Gerstein [2001]; Barnett and Lewis [1984]).

The third method that was applied to our experimental data is the CUSUM algorithm, which is based upon repeated use of the sequential probability ratio test (SPRT) (see derivation in Appendix \ref{appendix:sprt}), under an assumption of Gaussian distribution of counts, a minimum expected change in firing rate  $\sqrt{\lambda_0}$  where  $\lambda_0$  is the firing rate during the baseline, and a detection threshold of 6 std (Wald 1945; Ellaway 1978). Although differences in underlying distributions (i.e. Poisson spiking as opposed to Gaussian) may theoretically affect the performance of the CUSUM method, previous work has shown that the CUSUM method under an assumption of Gaussian-distributed spike counts performs just as well as the method for the Poisson assumption for neural data (Koepcke, Ashida, and Kretzberg 2016). These choices are fully explored in the Appendix \ref{appendix:sims}.

The direct relationship between the SPRT and the CUSUM algorithm is given in the Appendix C. However, we can write out the form of the CUSUM residual  $\Lambda_n$  or sufficient statistic under the Gaussian assumption. Given a stream of neural spike counts  $X_1, \dots, X_n$  where  $X \sim N(\mu, \sigma^2)$ , constant variance  $\sigma^2$ , suppose we want to test a null hypothesis  $H_0: \mu = \mu_0$  against an alternative hypothesis  $H_1: \mu$

$$\begin{aligned}\Lambda_n &= \max \left( 0, \Lambda_{n-1} + \left( x_n - \mu_0 - \frac{\nu}{2} \right) \right) \\ T &= \min\{k : \Lambda_k \geq \log(B) \frac{\sigma^2}{\nu}\} \\ &= \min\{k : \Lambda_k \geq \log(B)\sigma\}\end{aligned}$$

$= \mu_0 + \nu$ , where  $\nu$  is the minimum expected response magnitude and is typically taken to be some multiple  $k$  of  $\sigma$ . The CUSUM residual  $\Lambda_n$  and decision time  $T$  is given by:

where  $B$  is the factor that governs the detection threshold and was chosen to be 6 in this study (Appendix A). If there is a  $\Lambda_k$  that exceeds the threshold within the first 10ms following stimulation, the unit was classified as cerebellar-recipient or Cb+.

So far, in this methods summary, we have discussed the response magnitudes of simulated data, which are known and intentionally manipulated. The real data, however, do not have known response magnitudes, and the response magnitudes must be estimated using very few bins (response duration << test interval) of noisy spike counts. For cells in which no response was detected, response magnitude was quantified as the mean firing rate in the 2ms window following the maximum bin count detected in under 10ms. For cells in which a response was detected (candidate Cb+ units) in the first 10ms, response magnitude was quantified as the mean firing rate in the 2ms window following the detected response onset.

### Firing rate matching using resampling

A nonparametric bootstrap resampling approach with distribution matching was adopted to control for differences in firing rate between our two neural populations during some matching epoch, e.g. during the pre-instruction baseline. Since there are many more Cb- samples, the idea behind this approach is to sample higher firing rate neurons in the Cb- group more often so that the distribution of firing rates during the matching epoch is more similar to the Cb+ group. When performing a nonparametric bootstrap approximate 95%CI for an unknown quantity  $\varphi$  (e.g. the median) from a

sample  $x_1, \dots, x_n$ , one typically generates a new sample (also of size  $n$ ) by resampling the observations, with replacement, for  $G$  repetitions and computing an estimate of  $\varphi$  using each new sample. In this classic bootstrapping scenario, each observation has an equal probability of being drawn during the procedure ( $1/n$ ). Intuitively, we might like to re-weight the observations in the Cb- group such that observations that are under-represented in Cb- (relative to Cb+) are assigned a higher weight, whereas over-represented cases are downweighted and less likely to be sampled. These new weights can be found by taking a density ratio between our Cb+ and Cb- firing rate distributions. A kernel density approach is first used to estimate the firing rate distributions for both the Cb+ neurons  $\hat{p}^{Cb+}(x)$  and the Cb- neurons  $\hat{p}^{Cb-}(x)$  during the matching epoch, where  $x$  is the firing rate Silverman [1986]. The

$$\hat{\beta}(x) = \frac{\hat{p}^{Cb+}(x)}{\hat{p}^{Cb-}(x)}$$

resampling weights is inferred by the ratio of our estimated densities (Sugiyama, Suzuki, and Kanamori 2012):

The firing rate observations in the Cb- group are then resampled according to our ratio, where each observation  $x_i$  now has  $\hat{\beta}(x_i)$  probability of being sampled. Since each of the observations during the matching epoch in fact corresponds to a single neuron that has spiking activity recorded throughout the trial, we can then compute the test statistic of interest (like modulation depth) of the Cb- group during the *test epoch*, e.g. during movement. This procedure is repeated  $G = 10,000$  times, and a bootstrap approximate 95%CI for our unknown quantity of interest  $\varphi$ , e.g. median modulation depth, is constructed. This distribution represents the null distribution of our test statistic, under the null hypothesis  $H_0$  that  $\varphi_{Cb-}$  and  $\varphi_{Cb+}$  are not different given that the firing rate distributions are

equivalent during the matching epoch. To perform a statistical comparison between our two groups, we found the approximate p-value for observing the actual test statistic of the Cb+ group,  $t_{obs}$ , under the null distribution. This is found by determining the number of times the  $|t^{(g)} \geq t_{obs}|$  in the bootstrap samples and dividing by G. In all figures, the following notation is used for denoting significance:  $p < .05,*$ ;  $p < .01,**$ ;  $p < .001,***$ ;  $p < .0001, \diamond$ .

## Directional Modulation

The reach direction for which firing rate is highest is termed the preferred direction (PD), and the reach direction for which firing rate is lowest is termed the anti-preferred direction (anti-PD). We studied directional tuning by computing the maximum firing rate difference across reach conditions ( $FR_{PD} - FR_{anti-PD}$ ), i.e. the depth of directional modulation in firing rate, at different points in the behavioral task. The task epochs chosen for this were: "postcue", 0–500ms after the instruction appears on the screen; "delay", -750 – 0ms before the go cue; "reaction", 0 – 150ms after the go cue; "mvt", 0 – 300ms after the time of movement onset; and "targacq", -150 – 450ms around the target has been touched. Spike counts were summed over this interval and scaled by the width of the window to determine the firing rate. Only neurons with an average firing rate above 1hz across conditions per test epoch were considered for this analysis, so fewer units were compared following the target instruction, i.e. during the "postcue" period, than during the movement period.

The population averages for each neural subtype in **Figure 2.6** were computed by selecting the SDFs for the preferred direction and the anti-preferred direction and averaging them separately across the population. Standard error across each population was computed separately for each 1ms time bin.

The bootstrap resampling approach above (see 0) was adopted to control for firing rate differences during a matching epoch and test for differences in modulation depth in a test epoch. The nonparametric bootstrap approximate 95%CI for the median directional modulation during the test epoch was constructed for the Cb- group, and the approximate p-value for observing the actual median modulation depth of the Cb+ group under the null distribution was also computed and reported. This sampling approach was also used to find the the Cb- population average activity to the PD and anti-PD as a function of time, where the bootstrap samples (in neurons) were used to select the SDFs.

To quantify variability in our estimate of the median modulation depth in the Cb+ group, we also computed the nonparametric bootstrap approximate 95%CI for the median modulation depth using the typical sampling approach, in which each sample has an equal probability of being drawn ( $1/N_{Cb+}$ ). This sampling approach was also used to find the Cb+ population average activity to the PD and anti-PD as a function of time, where the bootstrap samples (in neurons) were used to select the SDFs.

## Mutual Information

Mutual information was used to capture model-free interactions between neural activity and reach condition (i.e. target direction). Mutual information was computed between neural activity,  $X$ , and reach condition,  $Y \in \{1, \dots, 8\}$ :

$$I(X, Y) = H(X) - H(X|Y) = \sum_{x \in X, y \in Y} p(x, y) \log_2 \left( \frac{p(x, y)}{p(x)p(y)} \right) \quad (1)$$

To compute the joint probability distribution over neural activity and reach condition, given by  $p(x, y)$ , neural spiking was first binned using non-overlapping, “uniform width” windows of widths

50, 150, or 250ms (Timme and Lapish [2018]). We computed mutual information separately for each time bin and considered reach trials independent observations. This means that we assumed that a neuron's relationship to reach direction was not changing throughout each session. The value of each state  $P(x = x_1, y = y_1) = N(x_1, y_1)/N_{\text{trials}}$ , where  $N(x_1, y_1)$  is the number of experimental observations in which the spike count in the bin of interest was 1 and the reach direction was 1, or 45deg. Once this joint distribution has been constructed, the MI can be computed directly from Equation 1.

A crucial part of computing MI is ensuring that we have adequately sampled the space of possible joint states. We excluded possible neurons that were not stably isolated for at least 10 trials to each direction, though the median number of trials per direction was far greater. We chose to limit our analysis to reach condition, which is a discrete and small set, rather than a finer estimate of actual reach angle, which is a continuous variable, to limit the total possible joint space.

This procedure resulted in an estimate of MI per unit over time. To obtain the estimates across the recorded neural population in 8, we obtained a nonparametric bootstrap estimate of the mean and 95% confidence intervals by sampling our MI distributions across neurons with replacement for each timebin. These confidence intervals are overlapping at all points in time, so no further statistical tests were necessary.

## **Neural decoding**

A Gaussian Naïve Bayes (GNB) Classifier was used to predict reach target,  $c_k \in \{1, 2, \dots, 8\}$  from neural activity. Neural activity was first binned using non-overlapping windows of width 50, 100, 150, or 300ms, such that the spike counts on trial  $j$  for a given time bin are represented by the vector  $x^j =$

$(x_1, \dots, x_N)$ , where  $N$  is the number of neurons simultaneously Cb+ or Cbneurons recorded during a given experimental session. Reach trials were considered independent samples to construct a separate cross-validated GNB classifier for each point in time.

A GNB classifier computes a posterior probability for each test sample  $\mathbf{x}^j$  and estimates the class, i.e. reach direction, by choosing the one with the maximum posterior probability:

$$\text{class}(\mathbf{x}^j) = c_{\hat{k}} = \underset{k \in \{1, \dots, 8\}}{\operatorname{argmax}} p(c_k | \mathbf{x}^j) \quad (2)$$

$$= \underset{k \in \{1, \dots, 8\}}{\operatorname{argmax}} p(c_k) \prod_{i=1}^N p(x_i^j | c_k) \quad (3)$$

where the posterior probability can be calculated from the data likelihoods and prior probabilities by Bayes theorem. The Naive Bayes assumption decouples the distributions of neural activity given the class ( $p(x_m^j, x_p^j | c_k) = p(x_m^j | c_k)p(x_p^j | c_k)$ ), meaning that each distribution can be independently estimated, and the joint distribution is the product of the marginals (or the sum of the logs if computing the log likelihood). With our choice of a Gaussian NB classifier, we postulated that that the class conditional likelihood function for each neuron is a Gaussian with mean  $\mu_k$  and standard deviation  $\sigma_k$  for a given time point in each trial  $j$ :

where  $S$  is the number of trials in per class (reach target). Here, the number of trials per class is

$$p(x_i^j | c_k) = \frac{1}{\sqrt{2\pi}\sigma_i^k} \exp\left(-\frac{(x_i^j - \mu_i^k)^2}{2(\sigma_i^k)^2}\right) \text{ where} \quad (4)$$

$$\mu_i^k = \frac{1}{S} \sum_{j=1}^S x_i^j \quad \text{and} \quad \sigma_i^k = \frac{1}{S} \sum_{j=1}^S (x_i^j - \mu_i^k)^2 \quad (5)$$

approximately equal, so we take the prior probability for an unknown sample for each class to be equal,  $p(c_k) = 1/8$ . This procedure yielded a time-varying estimate of decoding accuracy for each dataset. To summarize accuracy across either Cb+ or Cb- datasets, we then computed a nonparametric

bootstrap approximate 95%CI for the sample mean, shown in 9. Given a neural population (either Cb+ or Cb-) and a timepoint in the trial, decoding accuracies for the datasets were bootstrap resampled  $G = 10,000$  times with replacement, and the test statistic  $T^g$  was computed for each sample. The test statistic was ordered to create  $O^1, \dots, O^G$ , so that the approximate 95%CI for  $T$  was  $(O^{0.025G}, O^{0.975G})$ , and the mean was given by  $\hat{T} = \frac{1}{G} \sum_{i=1}^G T^i$  (Efron [1982]; Kass et al. [2014]).

In **Figure 3.9** the best fit lines were computed using least squares regression, where the estimates for the 95%CI of the regression coefficients  $\beta_i$  (only slopes  $\beta_1$  are shown) are determined analytically using the Wald method. The  $100 * (1 - \alpha)\%$ CI for regression coefficients are:

where  $\beta_i$  is the coefficient estimate,  $SE(\beta_i)$  is the standard error of the coefficient estimate, and

$$\beta_i \pm t_{1-\alpha/2, n-p} SE(\beta_i), \quad (6)$$

$$SE = \frac{1}{\sqrt{n-2}} \sqrt{\frac{\sum(y_i - \bar{y})^2}{\sum(x_i - \bar{x})^2}} \quad (7)$$

$t_{1-\alpha/2, n-p}$  is the  $100(1 - \alpha/2)$  percentile of the  $t$ -distribution with  $n - p$  degrees of freedom,  $n$  being the number of observations and  $p$  being the number of regression coefficients.

We can compare the regression coefficients between our two neural populations to test the null hypothesis  $H_0: \beta_i(Cb+) = \beta_i(Cb-)$ , i.e.  $\beta_i(Cb+) - \beta_i(Cb-) = 0$ . The test statistic for this comparison is:

$$t = \frac{\beta_i(Cb+) - \beta_i(Cb-)}{\sqrt{SE(\beta_i(Cb+))^2 + SE(\beta_i(Cb-))^2}} \sim T(n_{Cb+} + n_{Cb-} - 4) \quad (8)$$

### 3.3 Results

#### 3.3.1 M1 sites

**Figure 3.1A** illustrates a schematic of our recording sites in M1 and implanted macroelectrode in the cerebellar output fibers. We first aimed to identify primary motor cortex (M1). M1 receives

cerebellar input via motor thalamus and is identified by microstimulation. **Figure 3.1B** depicts the result of microstimulating tracks in M1 and checking for evoked activity in the arm muscles. Low-current electrical stimulation of the posterior tracks (in red) can evoke muscle activity, but higher current ( $> 50\mu\text{A}$ ) is required to evoke muscle activity in the more anterior tracks.

A total of 13 recording locations in arm-M1 were identified in Monkey J, and 8 recording locations in arm-M1 were identified in Monkey J, and 8 recording locations in arm-M1 were identified

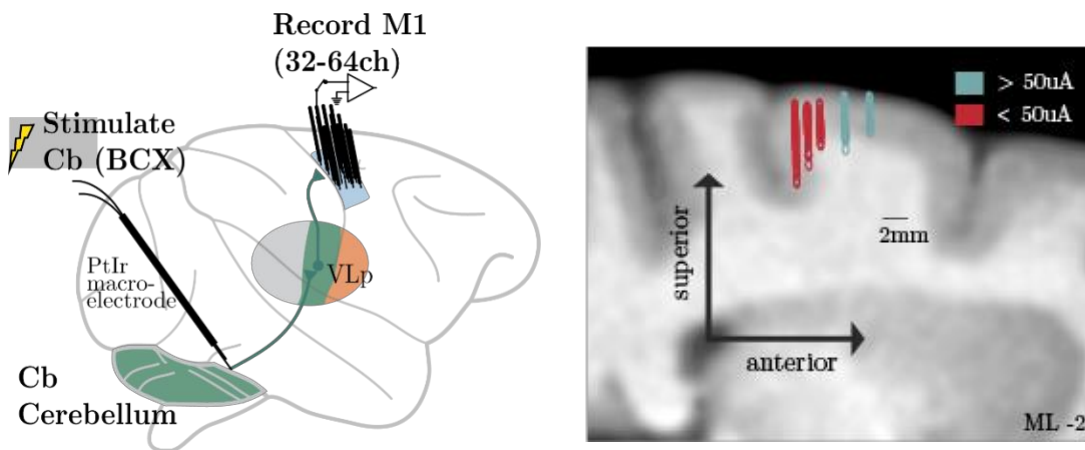
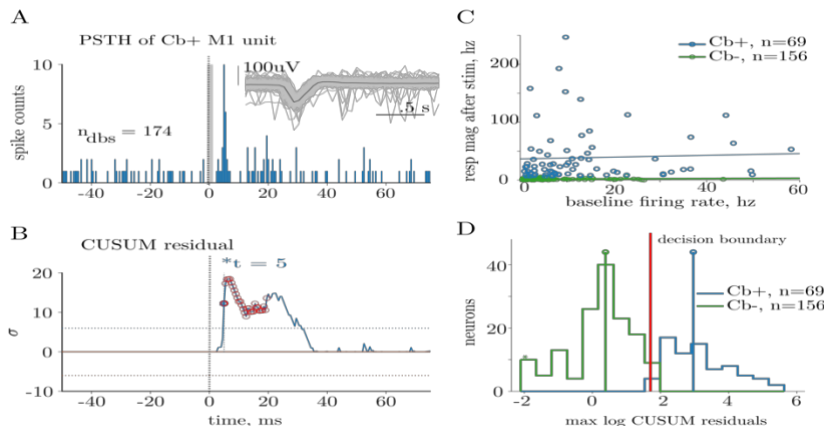


**Figure 3.1 (A)** Schematic of stimulation and recording sites. **(B)** M1 recording sites, Monkey J, chamber ML-2 plane: imagine taking a slice of the M1 territory shown in A. Electrical stimulation of sites indicated with red circles evoked muscle activity in the arm with current  $\leq 50\mu\text{A}$ . Green-blue sites indicate premotor areas because larger currents were required to evoke muscle activity.

in Monkey K (see Appendix B). Once we obtained stable isolation of M1 neurons, we began the stimulating the output of the cerebellum and recording the neural responses in M1.

### 3.3.2 M1 response properties to cerebellar stimulation

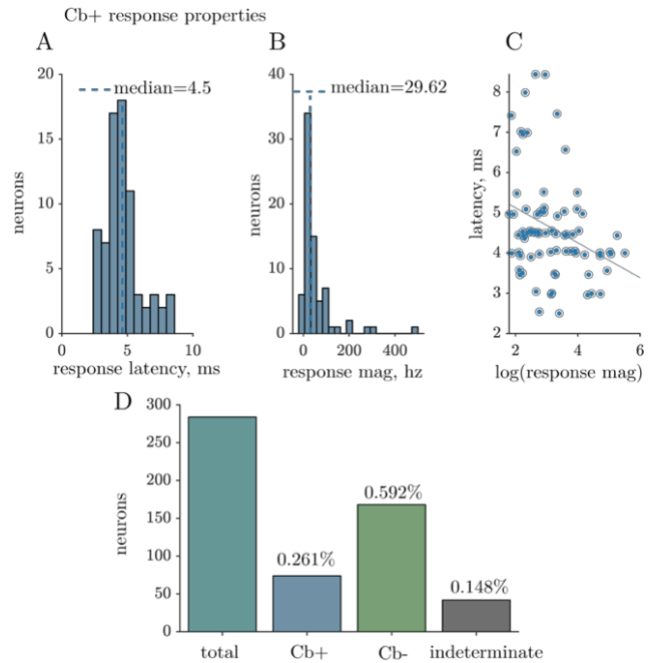
We chose the cumulative sum (CUSUM) algorithm for detecting M1 responses to cerebellar stimulation based on detection performance of simulated data in Appendix A, Figure 12. The hyperparameters associated with the detection approach include spike count bin size (0.5ms), the minimum expected response size (1 baseline standard deviation), and detection threshold. Simulation was used to choose these aspects of the detection approach, but only the study of detection threshold is shown in Appendix A. We chose a threshold of 6 (in units of baseline standard deviation) because this ensured the false positive rate would remain under 5% for different response magnitudes.



**Figure 3.2 CUSUM algorithm applied to real data.** (A) Example PSTH of a Cb+ M1 unit across 174 electrical pulses (typically 500). Inset: consistency in the spike waveform snippets reflects that the unit is well-isolated from noise. (B) The CUSUM residual over time, where  $t = 5$  is the time of the first detected response (see 2.6.3). (C) Response magnitude quantified by the maximum CUSUM residual during the test period across baseline firing rates. (D) Log of max CUSUM residuals during the test intervals reveals separation in the population densities. Red line indicates the decision boundary of  $\log(6)$ .

We applied the CUSUM method (see 0) on the real M1 neural activity collected during cerebellar stimulation and sought to characterize the response properties of the neural activity. **Figure 3.2A** depicts an example of a strong response to cerebellar stimulation in M1 after only a couple

hundred pulses. **Figure 3.2B** illustrates the accumulation of the CUSUM residual over time, where the response is first detected at  $T = 5\text{ms}$ . **Figure 3.2C** reflects how the response magnitude, here quantified by the max CUSUM residual during the test period, for the real data varies with the baseline firing rate. The CUSUM residuals are extremely heavy tailed, so it is easiest to visualize how the residuals compare between our  $\text{Cb}+$  and  $\text{Cb}-$  groups in the log scale shown in **Figure 3.2D**. The population densities are well separated from the decision boundary ( $\log(6)$ ), which suggests that it is appropriate to categorically label these responses as either  $\text{Cb}+$  or  $\text{Cb}-$ .



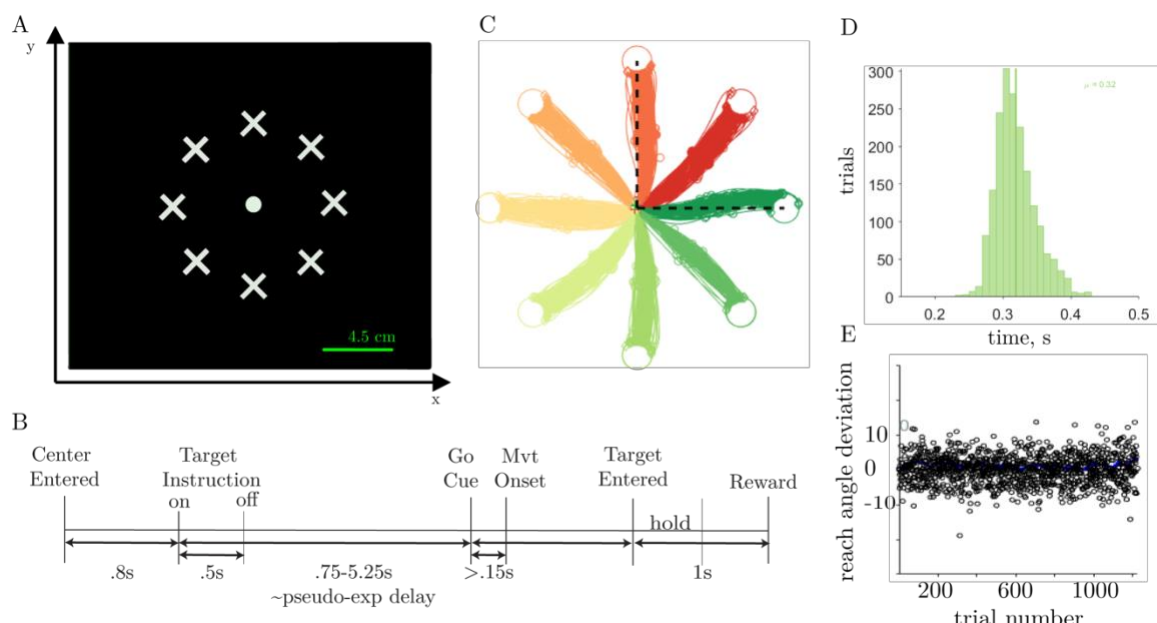
**Figure 3.3 Cb+ responses to stimulation.** **(A)** Histogram of response latencies, median is 4.5ms.**(B)** Histogram of response magnitudes (computed using firing rate), median is 29.62hz. **(C)** Relationship between latency, ms, and the log response magnitude. **(D)** The fraction of recorded neurons classified as Cb+ (blue), Cb- (green), or indeterminate (grey). If the firing rates were less than 1hz during the stimulation session we did not categorize that neuron.

Figure 3.3A reveals a distribution of response latencies that has a median consistent with a disynaptic excitatory pathway, and the vast majority of the samples are short latency (< 6ms). We assumed based on these findings that our detection approach is returning response onsets that are biologically plausible. There is a significant negative correlation between the latency of the detected response and the size of the response onset, which was expected because more time bins are needed to detect the weakest responses, as seen in our simulation study of latency estimation in A. About a quarter of the neurons we recorded were classified as Cb+, though there was a heterogeneous

anatomical distribution across the cortical surface as well as a difference between our two animals (see B).

### 3.3.3 Behavioral task and firing rate properties

Having categorized the neurons as either Cb+ or Cb- in 3, their activity was then recorded during the behavior described as follows. The animals performed a memory-guided center out reach task in which they needed to remember the target location throughout the delay period but were given visual cues to ensure they were able to make long (4.5cm), fast, and precise reaches (**Figure 3.4AB**).



**Figure 3.4 Memory-guided center out reach task schema and timeline.** (A) The reach workspace preserved visual cues on the screen at all times. The animal needed to make a reach to one of 8 peripherally targets. (B) The task timeline reveals that the animals need to remember where to reach throughout a long, pseudo-exponentially distributed delay period. (C) Reach trajectories on a randomly selected training day for Monkey J. (D) Distribution of reaction times for Monkey K ( $\mu = 320\text{ms}$ ). (E) Distribution of reach angle deviation from the average reach (angle = 0) across trials for Monkey J (same session as in C).

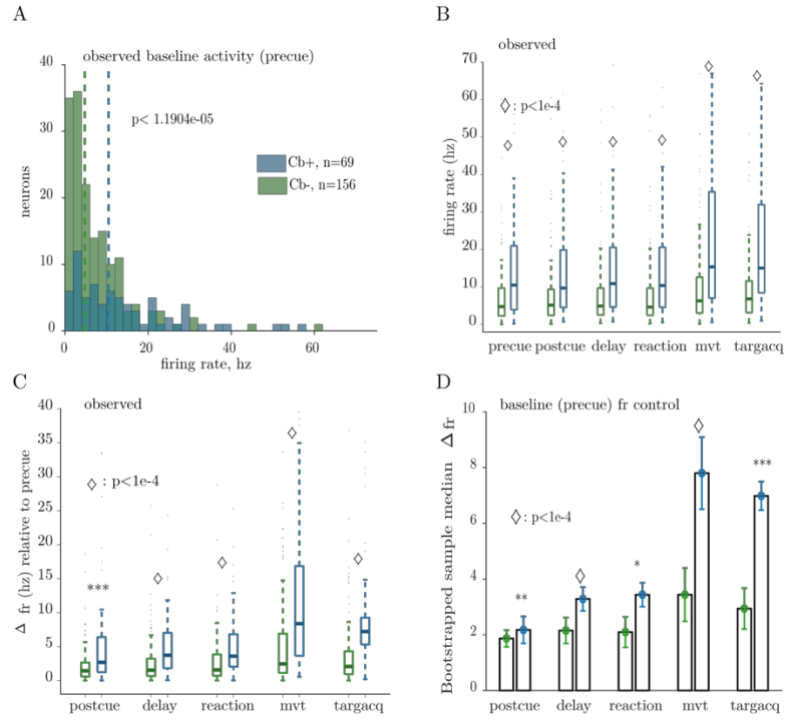


**Figure 3.5 Firing rate of Cb+ and Cb- neurons relative to task events. (A)** Histogram of the distributions of baseline (precue) activity for our two neural populations (Cb+, blue; Cb-, green). **(B)** Firing rate during different task epochs (Cb+, blue; Cb-, green). **(C)** Change in firing rate during different task epochs relative to the baseline or precue period. **(D)** The nonparametric bootstrap approximate 95% CI for the median change in firing rate was computed after controlling for the difference in baseline (precue) firing rate distributions (see 0).

In **Figure 3.4BD** we can see that the reaction times are not at the imposed boundaries of the behavioral tasks, e.g. response time cut-offs, indicating that the animal is neither preemptively reaching or executing a delayed, unprepared reach. The median reaction time was expected for an instructed delay task. The choice of delay period distribution ensured that the animals are not able to predict the appearance of the go cue, even for long trials (data not shown). **Figure 3.4CE** reveal that the reach trajectories are straight and the distribution of the animal's initial reach angles has low variance, clustered at the mean across trials.

We define a dataset as a recording of at least one well-isolated neuron during both a behavioral session and at least one cerebellar stimulation session. A total of 16 datasets from Monkey J and 9 datasets from Monkey K were recorded. We first sought to characterize basic properties of the task-related neural activity. **Figure 3.5AB** reveals that the Cb+ neurons had greater baseline firing rates as well as greater firing rates throughout the behavioral task. Cb+ neurons were also more responsive to the behavioral task, which was quantified by finding the difference in activity relative to the precue baseline in different task epochs.

We tested whether the difference in task-related firing rate changes between the Cb+ and Cb- groups is explained by the difference in the baseline activity. A nonparametric bootstrap resampling approach (see 2.6.5) was adopted to match the firing rate distributions in the baseline period (before target instruction) of the Cb+ and Cb- neurons. In **Figure 3.5D**, the Cb- neurons were resampled so that the baseline firing rates matched, and the change in firing rate relative to the resampled baseline was evaluated at different test epochs. We found that the difference in task-related change persisted even after controlling for firing rate during the baseline.

After observing these distributional differences in firing rate, we returned to simulation (see Appendix A) to address whether our detection approach was imposing a firing rate bias. In Figure 14 we observe that the detection sensitivity is not reduced for low firing rate neurons (assuming FR > 1hz) under the critical assumption that response magnitude is uncoupled from firing rate. Figure 15 reveals that the low firing rate neurons observed in the real data have high enough response magnitude for our

detection approach to reliably identify them. Thus it seems less likely that low firing rate neurons are more difficult to categorize as Cb+ (for full discussion see Appendix A).

### 3.3.4 Directional modulation

We next aimed to address whether Cb+ M1 neurons represent the direction of reaching differently than Cb- M1 neurons. M1 neurons classically have directional tuning, i.e. their firing rates are different across reach directions in **Figure 3.6A**, where the direction in which firing rate is highest is termed the preferred direction (PD) and the direction in which firing rate is lowest is termed the antipreferred direction (anti-PD). We studied directional tuning by computing the maximum magnitude of firing rate differences across reach conditions, i.e. the depth of directional modulation in firing rate. Under our guiding hypothesis, we expected Cb+ neurons to have greater directional tuning than Cb- neurons.

We observed that Cb+ neurons did in fact have greater directional modulation across targets relative to Cb- neurons in **Figure 3.6C**. The population averaged activity differed greater between the Cb+ and Cb- neurons in **Figure 3.6B**.

We then found that there is a strong correlation between firing rate during movement and modulation depth in **Figure 3.6D**. Since the distribution of firing rates for the Cb+ and Cb- units are significantly different, we were concerned that the results in **Figure 3.6** could all be predicted from the firing rate difference already reported. Similar to the procedure described in the analysis of firing rate changes, we aimed to address whether the observed difference in modulation depth could be explained

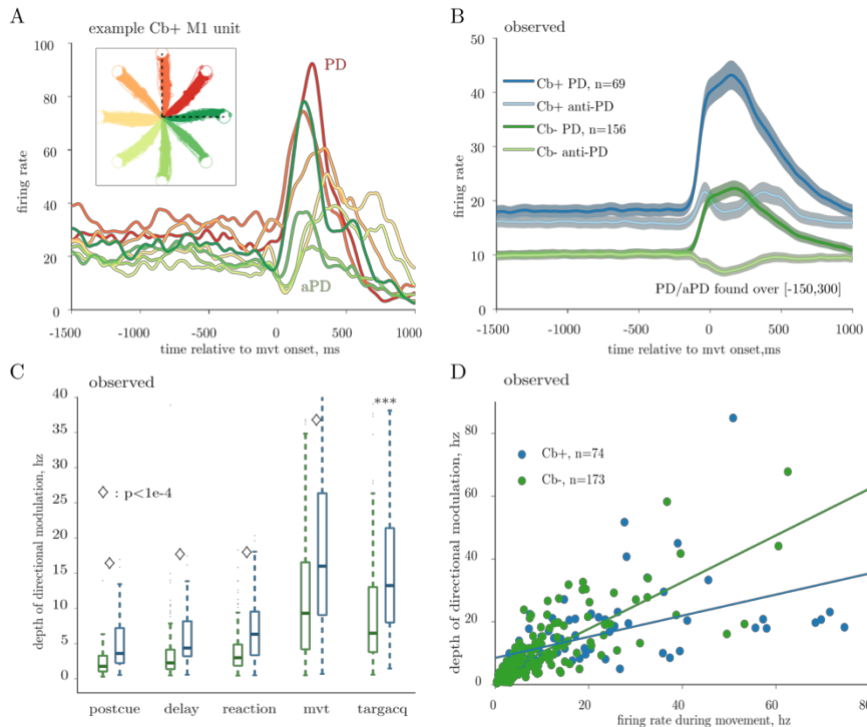


**Figure 3.6 Directional modulation for Cb+ and Cb- neurons.** **(A)** Kernel-smoothed spike density functions (SDFs) of spiking activity over time computed for each reach condition. Colors are more similar for adjacent targets in the physical workspace (inset), revealing that the SDFs of nearby targets are more similar. The referred direction (PD) is that in which firing rate is highest, and the anti-preferred direction (aPD) is the condition for which firing rate is lowest. **(B)** The SDFs for the PD and aPD for each unit are collected and averaged across the Cb+ (blue) and Cb- (green) populations. The approximate standard errors of the population means are given by the shaded area (blue, Cb+; green, Cb-). **(C)** The distributions of directional modulation (max firing across targets - min firing across targets) given for the Cb+ (blue) and Cb- (green) units using activity during different task epochs. **(D)** Scatter plot of directional modulation as a function of the firing rate during the window [-150,300] relative to movement. The regression lines for both populations are significant.

by firing rate using a series of firing rate controls. A nonparametric bootstrap resampling approach (see 2.6.5) was adopted to match the firing rate distributions in the baseline (before target instruction) of the Cb+ and Cb- neurons. In **Figure 3.7A**, the Cb- neurons were resampled so that the baseline firing rates matched, and the modulation depth was evaluated at different test epochs. The median modulation depth was computed for each bootstrap sample, and the approximate median and 95%CI indicated with the error bars for the Cb- neurons. The procedure was repeated for the Cb+ neurons, only the samples were drawn directly from the empirical CDF. **Figure 3.7A** and B reveal that the difference in modulation depths was preserved in all tested task epochs. Thus we infer that the difference in baseline firing rates does not fully account for the difference in modulation depth between the Cb+ and Cb- neurons.

Lastly we aimed to determine whether this difference in tuning was expected given the difference in movement-related change in activity shown in 5. We repeated the bootstrap resampling approach but used the firing rate distributions during the movement itself as the distributions used for matching. In other words, we primarily sampled the most movement-related Cb- neurons in order to

match the firing rate to the Cb+ neurons groups. Then, we computed the modulation depth in the different task epochs.

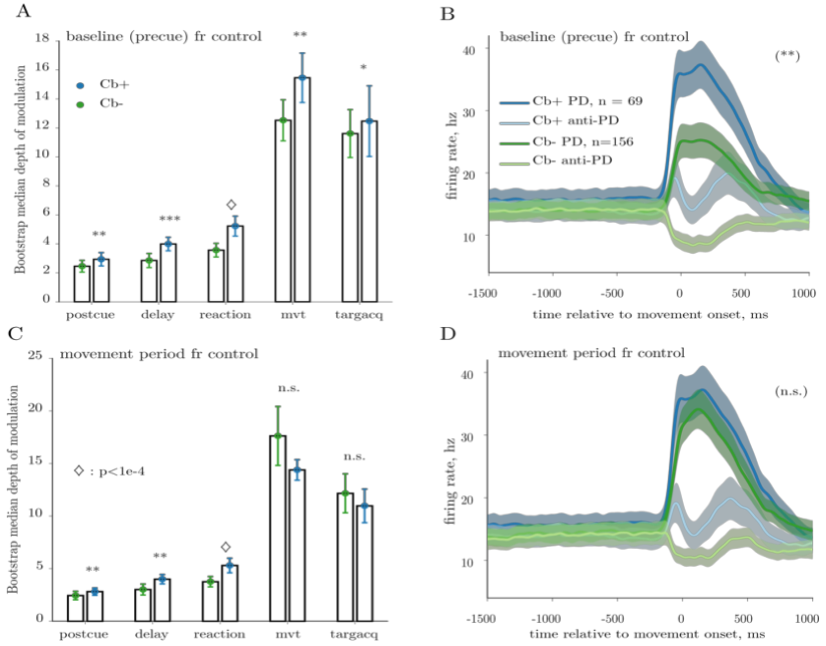


**Figure 3.7 Directional modulation for Cb+ and Cb- neurons after controlling for firing rate differences using nonparametric bootstrap resampling with distribution matching.** (A) The nonparametric bootstrap approximate 95% CIs for median directional modulation are indicated by the height of the bars and circles (Cb-, green; Cb+, blue). The Cb- neurons were resampled to match the higher firing rate distribution of the Cb+ group during the baseline (pre-instruction) epoch (see 0). (B) The bootstrap samples used in A are also used to select unit SDFs for the PD and anti-PD. The solid lines indicate the bootstrap mean across the Cb+ (blue) and Cb- (green) populations. The nonparametric bootstrap approximate  $\pm SE$  for the bootstrap population means are given by the shaded area (blue, Cb+; green, Cb-). (C) The nonparametric bootstrap approximate 95% CIs for median directional modulation are indicated by the height of the bars and circles (Cb-, green; Cb+, blue). The Cb- neurons were resampled to match the higher firing rate distribution of the Cb+ group during the movement epoch (see 0) (D) The bootstrap samples used in C are also used to select unit SDFs for the PD and anti-PD. The solid lines indicate the bootstrap mean across the Cb+ (blue) and Cb- (green) populations. The nonparametric bootstrap approximate  $\pm SE$  for the bootstrap population means are given by the shaded area (blue, Cb+; green, Cb-).

### 3.3.5 Mutual information

Given the difference in directional modulation between Cb+ and Cb- neurons, we wanted to return to our guiding hypothesis and directly ask whether individual Cb+ neurons contained more information about reach direction. To address this, we computed the mutual information between the reach target direction and the neural spike counts at different parts of the trial (see 0). **Figure 3.8A** describes the distributions of mutual information for our two neural populations of interest in the 100ms bin at the time of movement onset. In **Figure 3.8B** we see

We observe in **Figure 3.8A** that there is no significant difference in mutual information at the time of movement onset between our two groups, Cb+ and Cb-. The timecourse of mutual information in **Figure 3.8B** also reveals that the approximate confidence intervals for the population average MI for

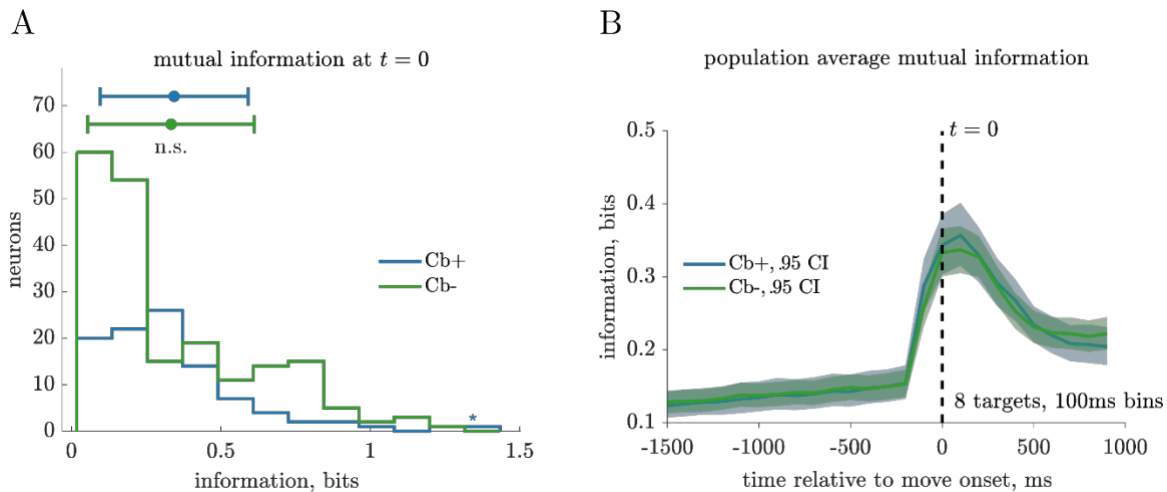


**Figure 3.8 Mutual information (MI) in bits between reach target direction and neural activity for Cb+ (blue) and Cb- (green) neurons. (A)** Histogram of MI at the time of movement onset, where the y-axis is neurons. Asterisk(\*) indicates 2 neurons with information  $> 1.4$ . **(B)** MI across the population relative to the time of movement onset,  $t = 0$  (black dashed vertical line). The approximate 95% CI for the population averages are given by the shaded area (blue, Cb+; green, Cb-).

Cb+ and Cb- neurons overlap throughout the trial, reflecting that there is not a significant difference in MI between our two groups.

### 3.3.6 Neural decoding

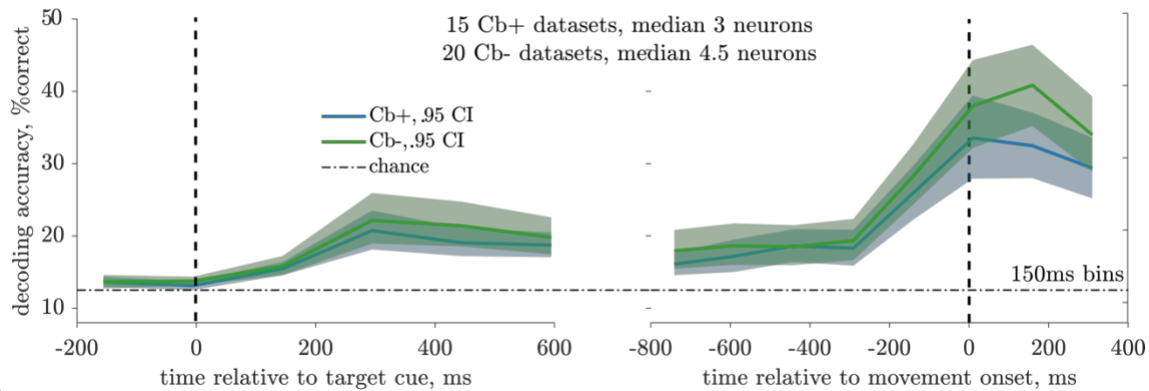
The next question we aimed to address was whether populations of Cb+ neurons have more information about reach target direction, i.e. whether or not the activity of these neurons can more robustly predict the target direction. In other words, on a given trial, can the activity of a group of Cb+ neurons tell you which direction the monkey will reach more reliably than if you only observed the activity of a group of Cb- neurons? Given the differences in modulation depths seen above Figure 3.6, we expected to see greater predictive performance of a decoder trained on the activity of Cb+ neurons, relative to that of the Cb- neurons. We trained a Gaussian Naive Bayes decoder (0) using either the activity of simultaneously recorded Cb+ neurons or the activity of simultaneously recorded Cb- neurons to predict reach direction on a trial by trial basis for a given dataset. In Figure 3.9A, we see that the cross-validated decoding accuracy across datasets only rises above chance levels for both subtypes of neural populations after the appearance of the target cue. Decoding accuracy reaches a peak at or 150ms after the time of movement onset. Here, neural spike counts are binned in chunks of 150ms, and we see that the maximum accuracy with which we can predict reach target is at most 30 – 40%. The choice of bin size greatly affects predictive performance, and the accuracy at the time of movement onset increased up to 80-90% for a binsize of 300ms.

The 95% confidence intervals for the bootstrapped population means in Figure 3.9A are overlapping throughout the trial, which reflects that there is not a discernible difference in the

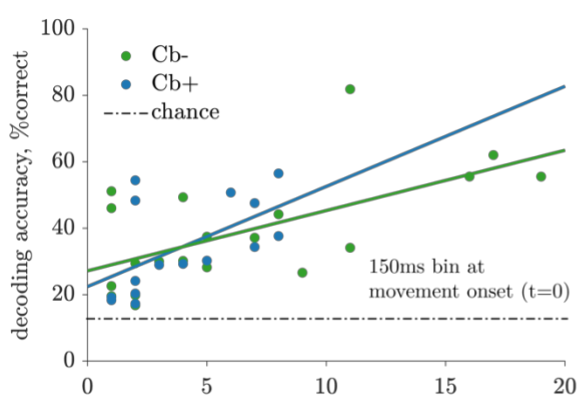
representation of target direction between our two neural populations of interest. The number of neurons recorded simultaneously was, however, significantly different between our two groups (3 neurons, Cb+; 4.5 neurons, Cb-). We expect decoding accuracy to increase as a function of number of neurons before reaching a plateau, so the absence of a difference in decoding accuracy between our two groups in **Figure 3.9A** may be a consequence of recording more Cb- neurons simultaneously on any given recording day. This motivated a study of how decoding accuracy varied as a function of the number of simultaneously recorded neurons per dataset in **Figure 3.9B**. Here it is clear that many Cb- datasets have more neurons than the Cb+ datasets, and we are operating in the regime where increasing the number of neurons does increase decoding accuracy. Thus **Figure 3.9** does not illustrate a fair comparison between our two groups, and we chose to investigate the nature of the relationship between decoding accuracy against the number of recorded neurons, either Cb+ or Cb-, at different points in time. As revealed in **Figure 3.9C**, we do not see a significant difference in the slopes (or offset,

not shown) of the regression lines computed as in **Figure 3.9B** between our two groups over the course of the trial.

**A**



**B**



**C**

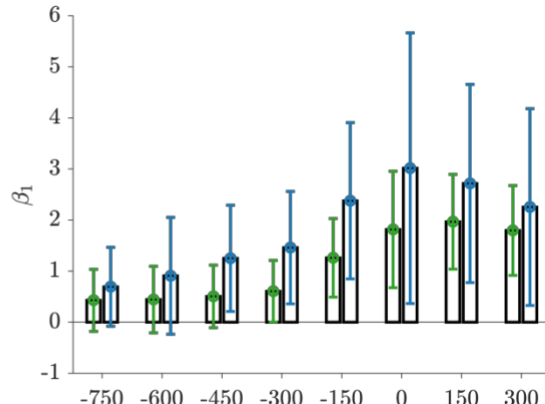


**Figure 3.9 Neural decoding of target direction.** (A) Cross-validated decoding accuracy across datasets as a function of time, relative to both the target cue (left) and the time of movement onset (right). The thick colored line indicates the bootstrapped population mean across datasets for either Cb+ neurons (blue) or Cb- neurons (green). The shaded area corresponds to the bootstrapped 95% confidence interval for each population. Prior to the onset of the target cue (black, dashed vertical line at 0 ms on the left) the decoding accuracy is at chance (black dashed horizontal line), and it rises 150 – 300ms afterwards. The maximum decoding accuracy is achieved 0 – 150ms relative to movement onset (black, dashed vertical line at 0 ms on the right) for both populations (B) Cross-validated decoding accuracy of each dataset as a function of the number of neurons simultaneously recorded. (C) Slopes of the regression lines illustrated in B at different timepoints in the trial. The slopes are not significantly different between groups at any point in time.

## **3.4 Discussion**

### **3.4.1 Summary**

In this work, we use electrical stimulation to identify the subgroup of M1 neurons that receive disynaptic excitatory input from the cerebellum (Cb+) and study their activity in a non-human primate model of reaching. We first demonstrate a high degree of sensitivity and specificity of our detection algorithm using simulation. In doing so, we illustrate that previously proposed methods in the literature suffered from reduced rates of sensitivity for low response magnitudes as well as in the setting of polyphasic response types. These prior studies also likely included false positives due to consistent underestimation of response onset times shown for their detection approach (Nashef et al. 2018; 2019).

We showed a novel difference in baseline firing rates between these subtypes of M1 neurons (Cb+ vs. Cb-). We demonstrated that this difference is not due to bias in our detection algorithm by comparing the response sizes and firing rates observed in our real data to that of our simulated data. The expected sensitivity of our detection algorithm is quite high for the vast majority of the firing rate and response magnitude combinations we observe in the real data. Very large responses to stimulation are observed even for neurons with low firing rates, which suggests that low firing rate neurons with real responses are not less likely to be classified as Cb+ units.

We find that Cb+ M1 neurons have greater movement-related responsiveness or change in firing rate relative to the precue baseline that cannot be explained by a difference in baseline firing

rates. This description of neural activity is condition *independent*, meaning that a neuron could respond in the same way to every target, but provided its firing rate has changed relative to precue it would be considered "movement-responsive." We also find that these neurons have greater directional depths of modulation even after controlling for differences in baseline firing rates. The measure of neural activity is condition *dependent*; the firing rate must vary across reach directions to have directional modulation. The difference in directional modulation between the Cb+ and Cb- is not, however, any greater than what you would expect given greater movement-related firing rates in the Cb+ group. These findings all support prior work that cerebello-thalamo input to motor cortex provides tonic excitation to the M1 network, though the greater difference between groups during the movement epoch suggests there may be an increase in excitation at the start of movement.

Contrary to expectation, individual Cb+ units do not contain more information about reach target direction than individual Cb- units despite differences in firing rate, response to movement, and directional modulation. Nor could we see enhanced target decoding accuracy given the activity of Cb+ neurons. These results offer a basic characterization of the activity of Cb+ neurons during movement and represent the most foundational step forward. Our prediction was unsupported by our data, which motivates a more refined hypothesis regarding the potential functional role for Cb+ neurons, as well as a different approach to study the role of cerebellar input to M1 (see **Error! Reference source not found.**).

### **3.4.2 Advancing understanding of M1**

Those who usually think of M1 computation in terms of neural dynamics across undifferentiated populations of M1 neurons may see this predominantly single-unit perspective as dissatisfying, instead preferring to adopt an approach that allows a study of how the M1 network collectively responds to cerebellar input. Previous work by (Nashef et al. 2018), however, showed that Cb+ neurons were specifically impacted by cerebellar inhibition, implying that there is in fact localization of the consequence of cerebellar input. In other words, there is segregation of information to specific cell subtypes in M1. In this study, we show that task-related information *does* differ between M1 subpopulations defined by whether or not they are excited by cerebellar stimulation. This finding, and its precursors, suggests that approaches examining undifferentiated M1 populations may be missing important aspects of the way in which M1 functions. One might imagine that knowledge of neural subtypes defined by their anatomical inputs can allow for targeted inspection of the M1 network as a whole. Thus we view this approach as potentially quite interesting and not antithetical to prevailing views of M1 activity.

### **3.4.3 Limitations**

#### **Experimental Approach**

Although the scope of the project is not in itself a limitation, there are specific parts of our approach that require assumptions, both conceptual and technical. This work, at its core, assumes that the mechanism of Cb+ input to M1 can be clarified by defining subtypes of M1 neurons in terms of

their inputs. M1, however, has a high degree of intracortical connectivity, meaning that neurons without excitatory disynaptic input from the cerebellum (i.e. Cb-) may still be impacted by cerebellar activity via nearby M1 neurons that do receive projections from cerebellar-thalamus. In other words, it is not obvious *a priori* that Cb+ neurons would necessarily be different than other units in M1, both in terms of information that they have access to and in terms of their contribution to movement execution.

There are also several fundamental issues with using orthodromic electrical activation to identify subsets of M1 neurons that receive cerebello-thalamic projections. Due to the absence of other reliable methods for input identification in non-human primates, in addition to the fundamental differences between rodent and primate neuroanatomy, we accept several limitations. The first is we cannot be certain that are exciting the entire bundle of cerebellar output fibers. We try to account for this by carefully designing the macroelectrode implantation approach to target the BCX and stimulating with high current ( $600\mu\text{A}$ ). Even still, we may have insufficiently excited the entire fiber bundle, meaning that there may be more M1 neurons that have real input from cerebellum but would not have a response in the peri-stimulation time histogram. Thus there may be false negatives in our sample of identified Cb- or non-responsive neurons that is not due to bias in our detection algorithm.

Second, when studying orthodromic effects there is always exists a concern that the longest disynaptic latencies could also include short trisynaptic (or higher order polysynaptic) responses. One cannot be absolutely certain which pathway mediated the response that you observe downstream of the stimulation site. We tried to mitigate this concern by selecting a detection algorithm that does not underestimate response onset latency for large magnitude responses and by removing responses in

which we could detect inhibition or decreases in firing prior to excitation. The responses we report in this study are present at sufficiently short latencies that most of the responses are due to excitatory CTC pathway, but we cannot be 100% certain using this approach.

Finally, we do not know what single-unit response magnitude in M1 following stimulation in the cerebellum actually constitutes an important connection, either anatomical or functional. Ideally the response would be truly binary (large relative to baseline rate, or zero), but the reality is more graded. Imagine a scenario in which a neuron in M1, which would typically fire at a rate of ~15Hz, receives so little input from cerebellar thalamus-- say, a single synapse at distal dendrite-- that its true response to electrical excitation of the cerebellum is an extremely small increase firing rate of 0.5Hz. Does such a small change in firing rate represent a meaningful response? In this study, we assume that there is no response if the estimated response magnitude is less than 1 standard deviation above the baseline activity (for Poisson random variables, this is  $\sqrt{\lambda_0}$  where  $\lambda_0$  is the baseline firing rate), and as a result our detection algorithm is unable to detect a change of this size or smaller. The approach in this study does accept response sizes 2-3x smaller than shown before Nashef et al. [2018]. When visualizing the max log CUSUM residual in 2, it is clear that there exists a margin between the density of labeled samples and the decision boundary. Under the assumption that very small response magnitudes are not true responses, this suggests that we actually can classify the majority of the units. There just may be a small number of units in the classification boundary area where the label may be indeterminate.

## Analysis

The analyses described in this study are limited in scope, not in justification, yet the following points may alleviate pressing concerns. Regarding the choice of detection algorithm, we showed that the cumulative sum approach is strictly superior to previous approaches in the detection of fast responses to electrical stimulation. We chose to accept the performance of this detection approach and move forward in our study of neural activity rather than evaluating this algorithm in the context of more advanced approaches. For example, we could have implemented a maximum likelihood solution to a multiple changepoint detection problem outlined in Appendix \ref{appendix:multichange}. We chose not to pursue this route due to the extremely small number of samples available during the test period since it is well understood that MLE suffers in the setting of limited observations and multiple changepoints (Inclan and Tiao 1994), but whether this approach would return meaningful improvement remains to be seen. Similarly, we could have implemented a point process approach but chose not to pursue this route in favor of studying the neural activity in relationship to behavior (Ventura 2004).

In the mutual information analysis, we chose to limit our analysis to target direction rather than a finer estimate of actual reach angle. We have a sufficient number of trials to accurately sample the joint distribution of neural activity and target direction, but this may not be the case if we were to instead relate neural activity to a much larger set of possible reach angles, even if broadly discretized. We have some ideas about how to construct a state space representation of neural activity and error, but we reserve this for future work (**Error! Reference source not found.**).

In this study we have not yet explained why modulation depth significantly differs between the Cb+ and Cb- populations, but the mutual information analysis reveals that there is no difference in directionality. We think this could be a consequence of greater trial-to-trial variability of the Cb+ neurons, because variability typically scales with firing rate.

## 4 Conclusion

In this thesis we investigated the functional role of the cerebellothalamicocortical (CTC) circuit in the context of skilled reaching. Our findings have contributed to a growing body of knowledge regarding how this circuit supports multiple functional roles, including movement initiation and motor planning. The experimental paradigm employed in this thesis has proven invaluable in demonstrating that tightly controlled behavior and *in vivo* electrophysiological identification of sub-regions of the motor thalamus allow us to tease apart previously unresolved questions concerning the role of cerebellar input to the primary motor cortex (M1).

This thesis work was introduced by contextualizing the work within the broader study of motor control. We began by discussing the relevant neuroanatomy, which is complex and dependent on the animal model under study. We then highlighted a combination of behavioral, neurophysiological, and computational modeling studies and provided the overarching framework for studying the CTC pathway.

In Chapter 2, we specifically examined the contribution of the macaque cerebellar thalamus to movement initiation. Our findings are broadly consistent with the idea that cerebellar input to the

motor cortex drives initiation activity in M1. We found further evidence that the cerebellar thalamus may be acting as a critical junction in the sensorimotor transformation between stimulus and action, which has not been reported in motor areas. Our task was designed to fully dissociate motor planning and initiation, and it revealed a complex timecourse of directional encoding in the cerebellar thalamus. In general, the strength of directional encoding during movement execution is weaker in the cerebellar thalamus than it is in M1, which has been observed in previous work. However, the dynamics of encoding in the cerebellar thalamus during the delay period and reaction interval suggested a time-varying flow of directional information from the cerebellar thalamus to M1 following the instruction. The cerebellum may be relaying the task instruction to M1 at the beginning of the trial but does not maintain a representation of the motor plan throughout the delay, and the component of activity that is consistent with the role of movement initiation is not directional. Together these findings suggest that the cerebellar thalamus may be performing different functional roles like motor planning and initiation via different patterns of activity.

In Chapter 3, we adopted an approach to identify M1 neurons that receive excitatory disynaptic input from the cerebellum, denoted M1-Cb+, and compared their activity to that of the larger M1 network recording during the planning, initiation, and execution of reaches. In general, we found that cerebellar input to these units raises their baseline and task-dependent firing rates. We examined how the upcoming reach was encoded in the activity of these neurons and observed substantially larger directional encoding in these neurons throughout the task relative to M1 neurons that were not labeled

as receiving cerebellar input. We validated our Cb-input identification approach to ensure that these findings were not a byproduct of our selection approach.

The findings we report in Chapter 2 and 3 are surprising because the directional encoding observed in the cerebellar thalamus during reach execution is far weaker than in M1, yet cerebellar input appears to drive directionality and higher firing rates within M1 itself. Though it remains speculative, there are several ways in which disparity could arise. The simplest concern is that we may have under sampled parts of the cerebellar thalamus with the most directional encoding and thus underreported the true strength of directional encoding. Given the high neuron count and spread of recordings used in our analysis, this seems less likely. The primary concern is that the degree of cerebellar input may be associated with other factors that drive directionality, leading us to incorrectly presume the role of cerebellar input. M1-cb units are unlikely to be characterized just by their Cb-recipient nature. For example, it may be that layer 5 pyramidal tract neurons are the type of M1 neuron most likely to receive Cb input and those PT neurons receive directional information from some other source (e.g. PMd). The network of M1 neurons could be composed of non-PT neurons, which have low directionality and tend to not receive Cb input, and PT neurons, which have high directionality and tend to receive Cb input. There are two other network-level explanations that make it biologically plausible. The CTC pathway provides excitatory feedback to the motor cortex even at rest or baseline conditions. Even if the cerebellar input to M1 plays no functional role, the additional e4xcitoatyr input and resulting higher firing rates in the M1-Cb+ neurons may be increasing the sensitivity of those neurons to other inputs. The other idea concerns the cerebellar thalamus. Weakly tuned inputs may

converge in cortex to amplify their effect, such that directional information is more strongly represented at the single neuron in M1. We reasoned that very few neurons in the cerebellar thalamus actually have directional information at the epochs where this mattered (end of delay, reaction interval). Additional work is needed to address the questions posed by this thesis.

As we move forward, the findings from this thesis will serve as a foundation for future research on the cerebellothalamic circuit. We hope that this work, including the posed conceptual frameworks, will spur additional discussion and insights into the behavior and functional role of cerebellar inputs to cortex. We aim to understand how cerebellar input shapes cortical firing so that we can understand the neurophysiological consequences of cerebellar dysfunction and motivate neuromodulatory strategies.

## Appendix A.

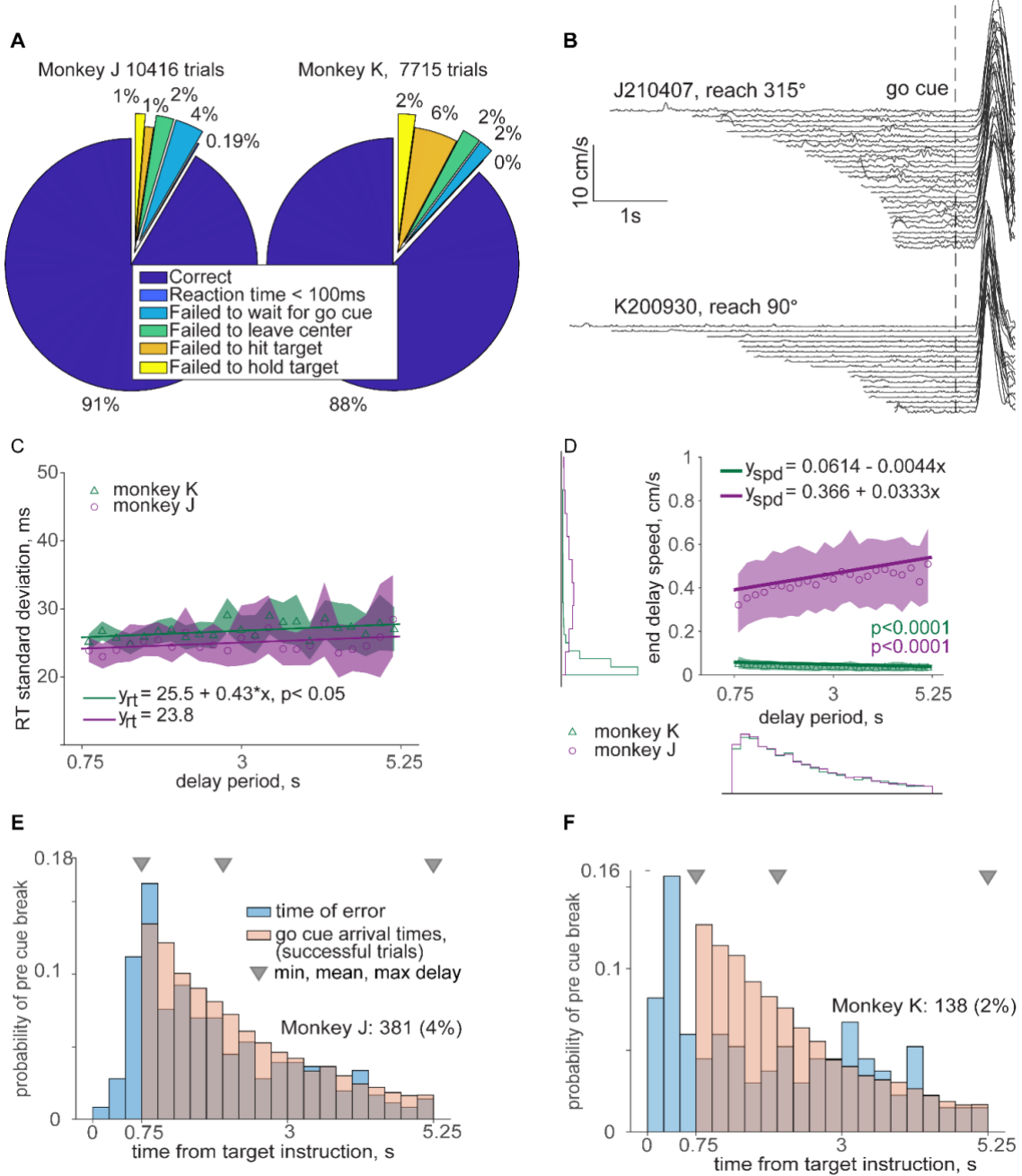


**Figure A.1 Behavioral performance metrics.** **(A)** Performance of the task. **(B)** Speed profiles of cursor trajectories, ordered by length of the delay period. **(C)** Standard deviation of reaction times, dependent on delay period. **(D)** End delay period speed, binned by del

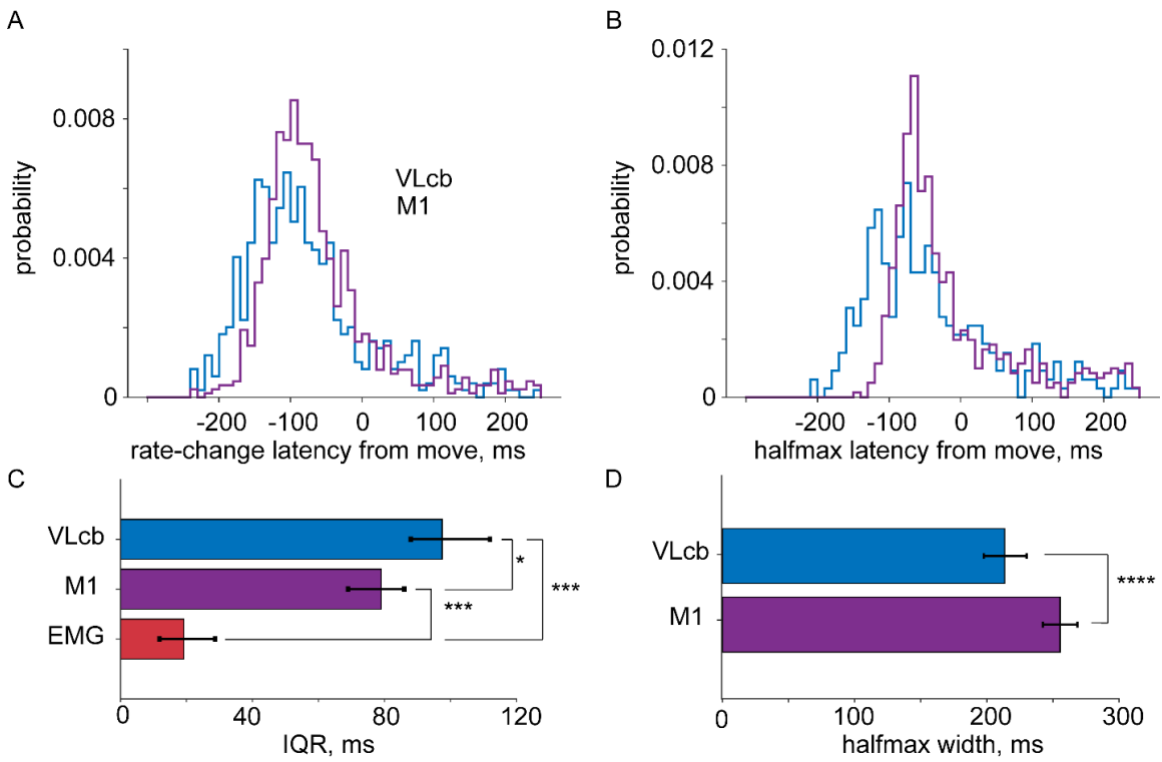


**Figure A.2 Additional timing information.** (A) Probability distribution of neural response latencies relative to movement onset, rate-change method. (B) Same as in A, but the latencies are estimated using the halfmax approach. (C) Bootstrapped inter-quartile range

## **Appendix B.**

### **B1. Simulations**

After peri-stimulation time histograms are constructed, a method to detect responses to stimulation as well as the latency of response onset must be applied. There are numerous challenges that must be taken into consideration when choosing a detection approach.

The spiking data are Poisson distributed (data not shown). This means that the pre-electrical stimulation baseline variability scales linearly with firing rate. There are very few time points (10ms), and the responses can be quite fast. Neural activity can be excited and then inhibited within the first 10ms or even inhibited, then excited, then inhibited once more. Additionally, the response is most related to the density of spiking, not just the peak response. Lastly, we briefly note that the scale of temporal change in firing rate is on the same order as the noise. Biologically speaking, current injection of the Cb output fibers abruptly changes the firing rate of any target neuron in MI. In other words, if we are to model the change in firing rate over time in response to stimulation, the change in firing rate would not be smooth. This makes it difficult to apply methods reliably used to smooth peri-stimulus time histograms because they assume slower changes in underlying firing rate. For this data, we tried to improve our estimate of the stimulation response by smoothing using bayesian adaptive regression splines (BARS) and locally adaptive kernel optimization, but neither approach provided reliable fits across neurons with different response profiles (DiMatteo et al. [2001]; Shi-mazaki and Shinomoto [2010]). These properties of the real data are illustrated in Fig AA and B. Only a few examples of M1

units have very strong, time-locked responses as in Fig AA. The vast majority exhibit an increase in spiking spread out in time, as in Fig AB, and fast polyphasic responses. These two examples have very clear responses, i.e. one can say that the activity following stimulation is strikingly different than the activity preceding it. In fact in both cases there are several bins in which the activity is so high that it

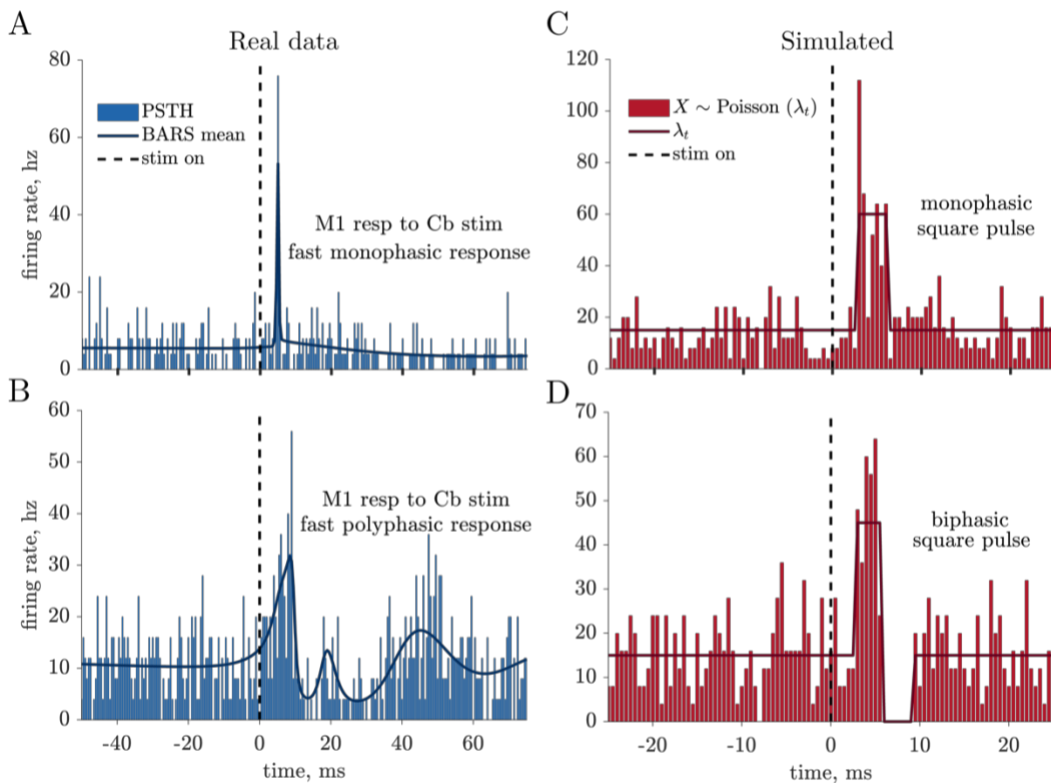


**Figure B.1 Real and simulated responses to electrical stimulation at  $t = 0\text{ ms}$**  (dashed black vertical line throughout). **A.** Example real M1 neuron (blue PSTH) with a strong excitatory response to cerebellar (Cb) stimulation. The BARS mean (bold line) is computed according to DiMatteo et al. [2001]. In this example, the response is strong, fast, and monophasic. The data is binned into  $0.5\text{ ms}$  spike counts, and the vertical axis has been scaled to accommodate both the number of stimulation pulses delivered (i.e. the number of trials or shocks) as well as the bin width. **B.** Example real M1 neuron with a strong excitatory response to cerebellar (Cb) stimulation. In this example, the response is strong but less time-locked than in A and polyphasic, i.e. the neuron is inhibited shortly after being excited and so on. **C.** Example simulated unit with a strong monophasic response. This response profile was designed to model units like in A. **D.** Example simulated unit with a strong biphasic response. This response profile was designed to model units similar to B.

would have been exceedingly unlikely to have observed those spike counts during the baseline, given the rate and variability we see in the figure.

We would, however, like to be able to detect responses that are weaker than what is shown in these examples, but we do not have access to the "ground truth responses in the real data to evaluate our detection approaches. We need to use simulation to evaluate detection approaches and address concretely questions about detection accuracy, detectable response magnitudes, and estimation of response onset latencies.

Figure C and D depict the simple simulation framework used throughout this work. The simulated data are distributed according to Poisson process with rate parameter  $\lambda_t$ , and the shape of response profiles is either a monophasic square pulse or a biphasic square pulse, where the excitatory part has a width of 3ms for each. These simple reductions capture many important features of the response profiles in the real data.

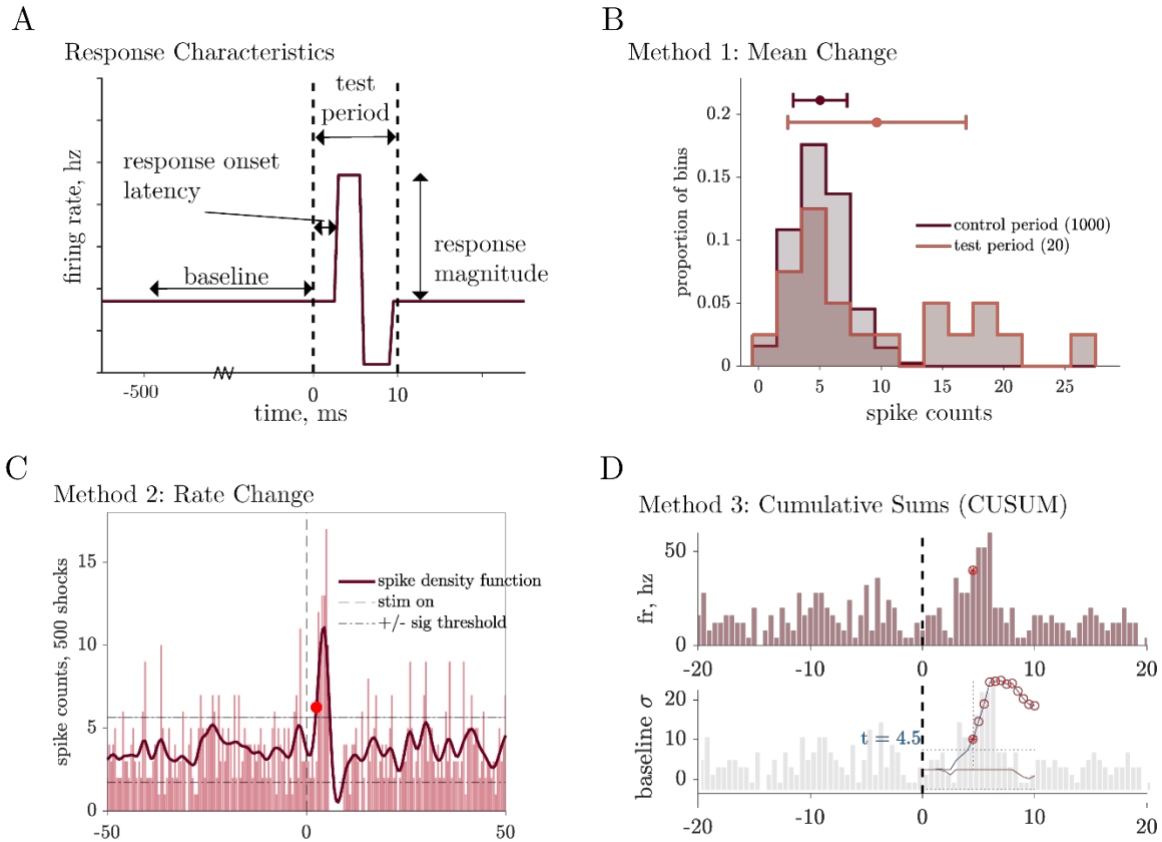


**Figure B.2 Response characteristics and detection algorithms.** **A.** Schematic of the responses in the real data and the simulated data. The 500ms period prior to the time of stimulation is referred to as the baseline, and our test period is defined over the window 1, 10 ms relative to the time of stimulation due to biological constraints. For the simulated data, the response magnitude is the difference in the true response height and the true baseline height. Here the y-axis has been rescaled in terms of firing rate, but all detection is performed in the unscaled, binned spike count space. **B.** Schematic of the Mean Change detection method, in which the mean over the set of bins in the test period is compared to the baseline activity. **C.** Schematic of the Rate Change detection method. The PSTH is first kernel smoothed, and then each bin in the test period is given a z-score under the distribution of baseline activity. Points that exceed  $\pm 3\text{std}$  from the baseline mean are considered "significantly" different, and the time of the first threshold crossing is the latency of onset. **D.** Schematic of the CUSUM detection method. The bottom panel depicts the accumulation of the CUSUM residual as the spike counts during the test interval are very different relative to the baseline activity.

Three different detection methods are depicted in Figure 11: Method 1, Mean Change; Method 2, Rate Change, and Method 3, the cumulative sum (CUSUM) algorithm. These methods are described in detail in Methods 2.6.3. In order to compare these approaches, we first simulated responses given a constant baseline firing rate ( $\lambda_0 = 15\text{hz}$ ) and different response magnitudes (5hz, 10hz, 15hz, and 30hz) for the two different types of response profiles. Then we systematically varied the detection threshold for each method to attain Receiver-Operator Characteristic (ROC) curves, which depict the true positive rate or sensitivity of a detection method as a function of the false positive rate. The ROC curves and summary AUC and TPR are given in 12.

## References

- Anderson, M. E., and R. S. Turner. 1991. "Activity of Neurons in Cerebellar-Receiving and Pallidal-Receiving Areas of the Thalamus of the Behaving Monkey." *Journal of Neurophysiology* 66 (3): 879–93. <https://doi.org/10.1152/jn.1991.66.3.879>.
- Asanuma, C., W. T. Thach, and E. G. Jones. 1983a. "Anatomical Evidence for Segregated Focal Groupings of Efferent Cells and Their Terminal Ramifications in the Cerebellothalamic Pathway of the Monkey." *Brain Research Reviews* 5 (3): 267–97. [https://doi.org/10.1016/0165-0173\(83\)90016-4](https://doi.org/10.1016/0165-0173(83)90016-4).
- . 1983b. "Cytoarchitectonic Delineation of the Ventral Lateral Thalamic Region in the Monkey." *Brain Research Reviews* 5 (3): 219–35. [https://doi.org/10.1016/0165-0173\(83\)90014-0](https://doi.org/10.1016/0165-0173(83)90014-0).
- . 1983c. "Distribution of Cerebellar Terminations and Their Relation to Other Afferent Terminations in the Ventral Lateral Thalamic Region of the Monkey." *Brain Research Reviews* 5 (3): 237–65. [https://doi.org/10.1016/0165-0173\(83\)90015-2](https://doi.org/10.1016/0165-0173(83)90015-2).
- Bastian, A. J., T. A. Martin, J. G. Keating, and W. T. Thach. 1996. "Cerebellar Ataxia: Abnormal Control of Interaction Torques across Multiple Joints." *Journal of Neurophysiology* 76 (1): 492–509. <https://doi.org/10.1152/jn.1996.76.1.492>.
- Bastian, A. J., and W. T. Thach. 1995. "Cerebellar Outflow Lesions: A Comparison of Movement Deficits Resulting from Lesions at the Levels of the Cerebellum and Thalamus." *Annals of Neurology* 38 (6): 881–92. <https://doi.org/10.1002/ana.410380608>.
- Bastian, Amy J. 2006. "Learning to Predict the Future: The Cerebellum Adapts Feedforward Movement Control." *Current Opinion in Neurobiology*, Motor systems / Neurobiology of behaviour, 16 (6): 645–49. <https://doi.org/10.1016/j.conb.2006.08.016>.
- Becker, Matthew I, and Abigail L Person. 2019. "Cerebellar Control of Reach Kinematics for Endpoint Precision." *Neuron* 103 (2): 335–48.
- Bosch-Bouju, Clémentine, Brian Hyland, and Louise Parr-Brownlie. 2013. "Motor Thalamus Integration of Cortical, Cerebellar and Basal Ganglia Information: Implications for Normal and Parkinsonian Conditions." *Frontiers in Computational Neuroscience* 7. <https://www.frontiersin.org/articles/10.3389/fncom.2013.00163>.
- Brinkman, C., and R. Porter. 1979. "Supplementary Motor Area in the Monkey: Activity of Neurons during Performance of a Learned Motor Task." *Journal of Neurophysiology* 42 (3): 681–709. <https://doi.org/10.1152/jn.1979.42.3.681>.
- Bruno, Randy M., and Bert Sakmann. 2006. "Cortex Is Driven by Weak but Synchronously Active Thalamocortical Synapses." *Science* 312 (5780): 1622–27. <https://doi.org/10.1126/science.1124593>.
- Butler, EG, MK Horne, and NJ Hawkins. 1992. "The Activity of Monkey Thalamic and Motor Cortical Neurones in a Skilled, Ballistic Movement." *The Journal of Physiology* 445 (1): 25–48.
- Catanese, Julien, and Dieter Jaeger. 2021. "Premotor Ramping of Thalamic Neuronal Activity Is Modulated by Nigral Inputs and Contributes to Control the Timing of Action Release." *Journal of Neuroscience* 41 (9): 1878–91. <https://doi.org/10.1523/JNEUROSCI.1204-20.2020>.

- Chabrol, Francois P., Antonin Blot, and Thomas D. Mrsic-Flogel. 2019. "Cerebellar Contribution to Preparatory Activity in Motor Neocortex." *Neuron* 103 (3): 506-519.e4. <https://doi.org/10.1016/j.neuron.2019.05.022>.
- Churchland, Mark M., John P. Cunningham, Matthew T. Kaufman, Stephen I. Ryu, and Krishna V. Shenoy. 2010. "Cortical Preparatory Activity: Representation of Movement or First Cog in a Dynamical Machine?" *Neuron* 68 (3): 387–400. <https://doi.org/10.1016/j.neuron.2010.09.015>.
- Churchland, Mark M., and Krishna V. Shenoy. 2007. "Delay of Movement Caused by Disruption of Cortical Preparatory Activity." *Journal of Neurophysiology* 97 (1): 348–59. <https://doi.org/10.1152/jn.00808.2006>.
- Crammond, Donald J., and John F. Kalaska. 2000. "Prior Information in Motor and Premotor Cortex: Activity During the Delay Period and Effect on Pre-Movement Activity." *Journal of Neurophysiology* 84 (2): 986–1005. <https://doi.org/10.1152/jn.2000.84.2.986>.
- Crutcher, M. D., and G. E. Alexander. 1990. "Movement-Related Neuronal Activity Selectively Coding Either Direction or Muscle Pattern in Three Motor Areas of the Monkey." *Journal of Neurophysiology* 64 (1): 151–63. <https://doi.org/10.1152/jn.1990.64.1.151>.
- Cruz, Bruno F., Gonçalo Guiomar, Sofia Soares, Asma Motiwala, Christian K. Machens, and Joseph J. Paton. 2022. "Action Suppression Reveals Opponent Parallel Control via Striatal Circuits." *Nature* 607 (7919): 521–26. <https://doi.org/10.1038/s41586-022-04894-9>.
- Dacre, Joshua, Matt Colligan, Thomas Clarke, Julian J. Ammer, Julia Schiemann, Victor Chamosa-Pino, Federico Claudi, et al. 2021a. "A Cerebellar-Thalamocortical Pathway Drives Behavioral Context-Dependent Movement Initiation." *Neuron* 109 (14): 2326-2338.e8. <https://doi.org/10.1016/j.neuron.2021.05.016>.
- . 2021b. "A Cerebellar-Thalamocortical Pathway Drives Behavioral Context-Dependent Movement Initiation." *Neuron* 109 (14): 2326-2338.e8. <https://doi.org/10.1016/j.neuron.2021.05.016>.
- Deecke, Lüder, H Kornhuber, W Lang, M Lang, and Herbert Schreiber. 1985. "Timing Function of the Frontal Cortex in Sequential Motor and Learning Tasks." *Human Neurobiology* 4 (February): 143–54.
- Desmurget, Michel, and Robert S Turner. 2008. "Testing Basal Ganglia Motor Functions through Reversible Inactivations in the Posterior Internal Globus Pallidus." *Journal of Neurophysiology* 99 (3): 1057–76.
- DiCarlo, James J., and John H. R. Maunsell. 2005. "Using Neuronal Latency to Determine Sensory–Motor Processing Pathways in Reaction Time Tasks." *Journal of Neurophysiology* 93 (5): 2974–86. <https://doi.org/10.1152/jn.00508.2004>.
- Eccles, John C. 1982. "The Initiation of Voluntary Movements by the Supplementary Motor Area." *Archiv Für Psychiatrie Und Nervenkrankheiten* 231 (5): 423–41. <https://doi.org/10.1007/BF00342722>.
- Ellaway, PH. 1978. "Cumulative Sum Technique and Its Application to the Analysis of Peristimulus Time Histograms." *Electroencephalography and Clinical Neurophysiology* 45 (2): 302–4.

- Elsayed, Gamaleldin F, Antonio H Lara, Matthew T Kaufman, Mark M Churchland, and John P Cunningham. 2016. "Reorganization between Preparatory and Movement Population Responses in Motor Cortex." *Nature Communications* 7 (1): 1–15.
- Franco, Vanessa, and Robert S Turner. 2012. "Testing the Contributions of Striatal Dopamine Loss to the Genesis of Parkinsonian Signs." *Neurobiology of Disease* 47 (1): 114–25.
- Gaidica, Matt, Amy Hurst, Christopher Cyr, and Daniel K Leventhal. 2018. "Distinct Populations of Motor Thalamic Neurons Encode Action Initiation, Action Selection, and Movement Vigor." *Journal of Neuroscience* 38 (29): 6563–73.
- Gao, Zhenyu, Courtney Davis, Alyse M Thomas, Michael N Economo, Amada M Abrego, Karel Svoboda, Chris I De Zeeuw, and Nuo Li. 2018. "A Cortico-Cerebellar Loop for Motor Planning." *Nature* 563 (7729): 113–16.
- Georgopoulos, Apostolos P., Andrew B. Schwartz, and Ronald E. Kettner. 1986. "Neuronal Population Coding of Movement Direction." *Science* 233 (4771): 1416–19.  
<https://doi.org/10.1126/science.3749885>.
- Gharbawie, Omar A, Iwona Stepniewska, and Jon H Kaas. 2016a. "The Origins of Thalamic Inputs to Grasp Zones in Frontal Cortex of Macaque Monkeys." *Brain Structure and Function* 221 (6): 3123–40.
- . 2016b. "The Origins of Thalamic Inputs to Grasp Zones in Frontal Cortex of Macaque Monkeys." *Brain Structure and Function* 221 (6): 3123–40.
- Goodkin, HP, and WT Thach. 2003. "Cerebellar Control of Constrained and Unconstrained Movements. I. Nuclear Inactivation." *Journal of Neurophysiology* 89 (2): 884–95.
- Guillery, RW, and S Murray Sherman. 2002. "Thalamic Relay Functions and Their Role in Corticocortical Communication: Generalizations from the Visual System." *Neuron* 33 (2): 163–75.
- Guo, Zengcai V., Hidehiko K. Inagaki, Kayvon Daie, Shaul Druckmann, Charles R. Gerfen, and Karel Svoboda. 2017. "Maintenance of Persistent Activity in a Frontal Thalamocortical Loop." *Nature* 545 (7653): 181–86. <https://doi.org/10.1038/nature22324>.
- Halsband, U., N. Ito, J. Tanji, and H.-J. Freund. 1993. "The Role of Premotor Cortex and the Supplementary Motor Area in the Temporal Control of Movement in Man." *Brain* 116 (1): 243–66. <https://doi.org/10.1093/brain/116.1.243>.
- Hanes, Doug P., Kirk G. Thompson, and Jeffrey D. Schall. 1995. "Relationship of Presaccadic Activity in Frontal Eye Field and Supplementary Eye Field to Saccade Initiation in Macaque: Poisson Spike Train Analysis." *Experimental Brain Research* 103 (1): 85–96. <https://doi.org/10.1007/BF00241967>.
- Heiney, Shane A., Jinsook Kim, George J. Augustine, and Javier F. Medina. 2014. "Precise Control of Movement Kinematics by Optogenetic Inhibition of Purkinje Cell Activity." *Journal of Neuroscience* 34 (6): 2321–30. <https://doi.org/10.1523/JNEUROSCI.4547-13.2014>.
- Herzfeld, David J, Yoshiko Kojima, Robijanto Soetedjo, and Reza Shadmehr. 2015. "Encoding of Action by the Purkinje Cells of the Cerebellum." *Nature* 526 (7573): 439–42.
- . 2018. "Encoding of Error and Learning to Correct That Error by the Purkinje Cells of the Cerebellum." *Nature Neuroscience* 21 (5): 736–43.

- Holsapple, James W, James B Preston, and Peter L Strick. 1991. "The Origin of Thalamic Inputs to the "Hand" Representation in the Primary Motor Cortex." *Journal of Neuroscience* 11 (9): 2644–54.
- Hoover, John E, and Peter L Strick. 1999. "The Organization of Cerebellar and Basal Ganglia Outputs to Primary Motor Cortex as Revealed by Retrograde Transneuronal Transport of Herpes Simplex Virus Type 1." *Journal of Neuroscience* 19 (4): 1446–63.
- Inagaki, Hidehiko K., Susu Chen, Margreet C. Ridder, Pankaj Sah, Nuo Li, Zidan Yang, Hana Hasanbegovic, Zhenyu Gao, Charles R. Gerfen, and Karel Svoboda. 2022. "A Midbrain-Thalamus-Cortex Circuit Reorganizes Cortical Dynamics to Initiate Movement." *Cell* 185 (6): 1065-1081.e23. <https://doi.org/10.1016/j.cell.2022.02.006>.
- Inclan, Carla, and George C Tiao. 1994. "Use of Cumulative Sums of Squares for Retrospective Detection of Changes of Variance." *Journal of the American Statistical Association* 89 (427): 913–23.
- Ivry, Richard B., and Steven W. Keele. 1989. "Timing Functions of The Cerebellum." *Journal of Cognitive Neuroscience* 1 (2): 136–52. <https://doi.org/10.1162/jocn.1989.1.2.136>.
- Ivry, Richard B., Rebecca M. Spencer, Howard N. Zelaznik, and Jörn Diedrichsen. 2002. "The Cerebellum and Event Timing." *Annals of the New York Academy of Sciences* 978 (1): 302–17. <https://doi.org/10.1111/j.1749-6632.2002.tb07576.x>.
- Jones, Edward G. 2007. *The Thalamus*. 2nd ed. Cambridge ; New York: Cambridge University Press.
- Kakei, Shinji, Donna S. Hoffman, and Peter L. Strick. 1999. "Muscle and Movement Representations in the Primary Motor Cortex." *Science* 285 (5436): 2136–39. <https://doi.org/10.1126/science.285.5436.2136>.
- . 2001. "Direction of Action Is Represented in the Ventral Premotor Cortex." *Nature Neuroscience* 4 (10): 1020–25. <https://doi.org/10.1038/nn726>.
- Kandel, Eric R, James H Schwartz, Thomas M Jessell, Steven Siegelbaum, A James Hudspeth, and Sarah Mack. 2000. *Principles of Neural Science*. Vol. 4. McGraw-hill New York.
- Kao, Ta-Chu, Mahdieh S Sadabadi, and Guillaume Hennequin. 2021. "Optimal Anticipatory Control as a Theory of Motor Preparation: A Thalamo-Cortical Circuit Model." *Neuron* 109 (9): 1567–81.
- Kaufman, Matthew T, Mark M Churchland, Stephen I Ryu, and Krishna V Shenoy. 2014. "Cortical Activity in the Null Space: Permitting Preparation without Movement." *Nature Neuroscience* 17 (3): 440–48.
- Kaufman, Matthew T, Jeffrey S Seely, David Sussillo, Stephen I Ryu, Krishna V Shenoy, and Mark M Churchland. 2016. "The Largest Response Component in the Motor Cortex Reflects Movement Timing but Not Movement Type." *Eneuro* 3 (4).
- Koepcke, Lena, Go Ashida, and Jutta Kretzberg. 2016. "Single and Multiple Change Point Detection in Spike Trains: Comparison of Different CUSUM Methods." *Frontiers in Systems Neuroscience* 10: 51.
- Lara, Antonio H, Gamaleldin F Elsayed, Andrew J Zimnik, John P Cunningham, and Mark M Churchland. 2018. "Conservation of Preparatory Neural Events in Monkey Motor Cortex Regardless of How Movement Is Initiated." Edited by Jennifer L Raymond and Timothy E Behrens. *eLife* 7 (August): e31826. <https://doi.org/10.7554/eLife.31826>.

- Laurens, Jean, Hui Meng, and Dora E Angelaki. 2013. "Computation of Linear Acceleration through an Internal Model in the Macaque Cerebellum." *Nature Neuroscience* 16 (11): 1701–8.
- Lee, Ka Hung, Paul J. Mathews, Alexander M. B. Reeves, Katrina Y. Choe, Shekib A. Jami, Raul E. Serrano, and Thomas S. Otis. 2015. "Circuit Mechanisms Underlying Motor Memory Formation in the Cerebellum." *Neuron* 86 (2): 529–40. <https://doi.org/10.1016/j.neuron.2015.03.010>.
- Li, Nuo, Kayvon Daie, Karel Svoboda, and Shaul Druckmann. 2016. "Robust Neuronal Dynamics in Premotor Cortex during Motor Planning." *Nature* 532 (7600): 459–64.
- Li, Nuo, and Thomas D. Mrsic-Flogel. 2020. "Cortico-Cerebellar Interactions during Goal-Directed Behavior." *Current Opinion in Neurobiology* 65: 27–37. <https://doi.org/10.1016/j.conb.2020.08.010>.
- Macchi, Giorgio, and Edward G. Jones. 1997. "Toward an Agreement on Terminology of Nuclear and Subnuclear Divisions of the Motor Thalamus." *Journal of Neurosurgery* 86 (1): 77–92. <https://doi.org/10.3171/jns.1997.86.1.0077>.
- Mason, Carolyn R, Lee E Miller, James F Baker, and James C Houk. 1998. "Organization of Reaching and Grasping Movements in the Primate Cerebellar Nuclei as Revealed by Focal Muscimol Inactivations." *Journal of Neurophysiology* 79 (2): 537–54.
- Mastro, Kevin J., Kevin T. Zitelli, Amanda M. Willard, Kimberly H. Leblanc, Alexxai V. Kravitz, and Aryn H. Gittis. 2017. "Cell-Specific Pallidal Intervention Induces Long-Lasting Motor Recovery in Dopamine-Depleted Mice." *Nature Neuroscience* 20 (6): 815–23. <https://doi.org/10.1038/nn.4559>.
- Matelli, Massimo, and Giuseppe Luppino. 1996. "Thalamic Input to Mesial and Superior Area 6 in the Macaque Monkey." *Journal of Comparative Neurology* 372 (1): 59–87.
- Mauritz, K. -H., and S. P. Wise. 1986. "Premotor Cortex of the Rhesus Monkey: Neuronal Activity in Anticipation of Predictable Environmental Events." *Experimental Brain Research* 61 (2): 229–44. <https://doi.org/10.1007/BF00239513>.
- McCairn, Kevin W, and Robert S Turner. 2015. "Pallidal Stimulation Suppresses Pathological Dysrhythmia in the Parkinsonian Motor Cortex." *Journal of Neurophysiology* 113 (7): 2537–48.
- Meyer-Lohmann, J., J. Hore, and V. B. Brooks. 1977. "Cerebellar Participation in Generation of Prompt Arm Movements." *Journal of Neurophysiology* 40 (5): 1038–50. <https://doi.org/10.1152/jn.1977.40.5.1038>.
- Middleton, Frank A., and Peter L. Strick. 1998. "Cerebellar Output: Motor and Cognitive Channels." *Trends in Cognitive Sciences* 2 (9): 348–54. [https://doi.org/10.1016/S1364-6613\(98\)01220-0](https://doi.org/10.1016/S1364-6613(98)01220-0).
- Miocinovic, Svetlana, Jianyu Zhang, Weidong Xu, Gary S Russo, Jerrold L Vitek, and Cameron C McIntyre. 2007. "Stereotactic Neurosurgical Planning, Recording, and Visualization for Deep Brain Stimulation in Non-Human Primates." *Journal of Neuroscience Methods* 162 (1–2): 32–41.
- Moran, Daniel W., and Andrew B. Schwartz. 1999. "Motor Cortical Representation of Speed and Direction During Reaching." *Journal of Neurophysiology* 82 (5): 2676–92. <https://doi.org/10.1152/jn.1999.82.5.2676>.
- Nashef, Abdulraheem, Oren Cohen, Ran Harel, Zvi Israel, and Yifat Prut. 2019. "Reversible Block of Cerebellar Outflow Reveals Cortical Circuitry for Motor Coordination." *Cell Reports* 27 (9): 2608–19.

- Nashef, Abdulraheem, Oren Cohen, Zvi Israel, Ran Harel, and Yifat Prut. 2018. "Cerebellar Shaping of Motor Cortical Firing Is Correlated with Timing of Motor Actions." *Cell Reports* 23 (5): 1275–85.
- Nashef, Abdulraheem, Rea Mitelman, Ran Harel, Mati Joshua, and Yifat Prut. 2021. "Area-Specific Thalamocortical Synchronization Underlies the Transition from Motor Planning to Execution." *Proceedings of the National Academy of Sciences* 118 (6).
- Okada, Ken-ichi, Ryuji Takeya, and Masaki Tanaka. 2022. "Neural Signals Regulating Motor Synchronization in the Primate Deep Cerebellar Nuclei." *Nature Communications* 13 (1): 2504. <https://doi.org/10.1038/s41467-022-30246-2>.
- Olszewski, J., Department Of Neurology Assistant Professor Of Neuro-anatomy, and McGill University Neuro-surgery. 1952. "The Thalamus of the Macaca, Mulatta. An Atlas for Use with the Stereotaxic Instrument." *The Thalamus of the Macaca, Mulatta. An Atlas for Use with the Stereotaxic Instrument*. <https://www.cabdirect.org/cabdirect/abstract/19522203025>.
- Pachitariu, Marius, Nick Steinmetz, Shabnam Kadir, Matteo Carandini, and Kenneth Harris. 2016. "Fast and Accurate Spike Sorting of High-Channel Count Probes with KiloSort." In *NIPS Proceedings*. Neural Information Systems Foundation, Inc.
- Pasquereau, Benjamin, and Robert S Turner. 2011. "Primary Motor Cortex of the Parkinsonian Monkey: Differential Effects on the Spontaneous Activity of Pyramidal Tract-Type Neurons." *Cerebral Cortex* 21 (6): 1362–78.
- . 2013. "Primary Motor Cortex of the Parkinsonian Monkey: Altered Neuronal Responses to Muscle Stretch." *Frontiers in Systems Neuroscience* 7: 98.
- . 2015. "Dopamine Neurons Encode Errors in Predicting Movement Trigger Occurrence." *Journal of Neurophysiology* 113 (4): 1110–23.
- Perez, Monica A., Satoshi Tanaka, Steven P. Wise, Daniel T. Willingham, and Leonardo G. Cohen. 2008. "Time-Specific Contribution of the Supplementary Motor Area to Intermanual Transfer of Procedural Knowledge." *Journal of Neuroscience* 28 (39): 9664–69. <https://doi.org/10.1523/JNEUROSCI.3416-08.2008>.
- Romo, R., and W. Schultz. 1987. "Neuronal Activity Preceding Self-Initiated or Externally Timed Arm Movements in Area 6 of Monkey Cortex." *Experimental Brain Research* 67 (3): 656–62. <https://doi.org/10.1007/BF00247297>.
- Sauerbrei, Britton A, Jian-Zhong Guo, Jeremy D Cohen, Matteo Mischiati, Wendy Guo, Mayank Kabra, Nakul Verma, Brett Mensh, Kristin Branson, and Adam W Hantman. 2020. "Cortical Pattern Generation during Dexterous Movement Is Input-Driven." *Nature* 577 (7790): 386–91.
- Schell, G. R., and P. L. Strick. 1984. "The Origin of Thalamic Inputs to the Arcuate Premotor and Supplementary Motor Areas." *Journal of Neuroscience* 4 (2): 539–60. <https://doi.org/10.1523/JNEUROSCI.04-02-00539.1984>.
- Scott, Stephen H. 1999. "Apparatus for Measuring and Perturbing Shoulder and Elbow Joint Positions and Torques during Reaching." *Journal of Neuroscience Methods* 89 (2): 119–27.
- . 2012. "The Computational and Neural Basis of Voluntary Motor Control and Planning." *Trends in Cognitive Sciences* 16 (11): 541–49.

- Shadmehr, Reza, and John W Krakauer. 2008. "A Computational Neuroanatomy for Motor Control." *Experimental Brain Research* 185 (3): 359–81.
- Shadmehr, Reza, Maurice A Smith, and John W Krakauer. 2010. "Error Correction, Sensory Prediction, and Adaptation in Motor Control." *Annual Review of Neuroscience* 33: 89–108.
- Sherman, S Murray. 2005. "Thalamic Relays and Cortical Functioning." *Progress in Brain Research* 149: 107–26.
- Shima, Keisetsu, and Jun Tanji. 1998. "Both Supplementary and Presupplementary Motor Areas Are Crucial for the Temporal Organization of Multiple Movements." *Journal of Neurophysiology* 80 (6): 3247–60. <https://doi.org/10.1152/jn.1998.80.6.3247>.
- Silva, Joaquim Alves da, Fatuel Tecuapetla, Vitor Paixão, and Rui M. Costa. 2018. "Dopamine Neuron Activity before Action Initiation Gates and Invigorates Future Movements." *Nature* 554 (7691): 244–48. <https://doi.org/10.1038/nature25457>.
- Snyder, L. H., A. P. Batista, and R. A. Andersen. 2000. "Intention-Related Activity in the Posterior Parietal Cortex: A Review." *Vision Research* 40 (10): 1433–41. [https://doi.org/10.1016/S0042-6989\(00\)00052-3](https://doi.org/10.1016/S0042-6989(00)00052-3).
- Spidalieri, G., L. Busby, and Y. Lamarre. 1983. "Fast Ballistic Arm Movements Triggered by Visual, Auditory, and Somesthetic Stimuli in the Monkey. II. Effects of Unilateral Dentate Lesion on Discharge of Precentral Cortical Neurons and Reaction Time." *Journal of Neurophysiology* 50 (6): 1359–79. <https://doi.org/10.1152/jn.1983.50.6.1359>.
- Stepniewska, Iwona, Todd M. Preuss, and Jon H. Kaas. 1994. "Thalamic Connections of the Primary Motor Cortex (M1) of Owl Monkeys." *Journal of Comparative Neurology* 349 (4): 558–82. <https://doi.org/10.1002/cne.903490405>.
- Strick, P. L. 1976. "Anatomical Analysis of Ventrolateral Thalamic Input to Primate Motor Cortex." *Journal of Neurophysiology* 39 (5): 1020–31. <https://doi.org/10.1152/jn.1976.39.5.1020>.
- Sugiyama, Masashi, Taiji Suzuki, and Takafumi Kanamori. 2012. "Density-Ratio Matching under the Bregman Divergence: A Unified Framework of Density-Ratio Estimation." *Annals of the Institute of Statistical Mathematics* 64 (5): 1009–44.
- Sun, Zongpeng, Marc Junker, Peter W Dicke, and Peter Thier. 2016. "Individual Neurons in the Caudal Fastigial Oculomotor Region Convey Information on Both Macro-and Microsaccades." *European Journal of Neuroscience* 44 (8): 2531–42.
- Sussillo, David, Mark M. Churchland, Matthew T. Kaufman, and Krishna V. Shenoy. 2015. "A Neural Network That Finds a Naturalistic Solution for the Production of Muscle Activity." *Nature Neuroscience* 18 (7): 1025–33. <https://doi.org/10.1038/nn.4042>.
- Takahashi, Naoya, Sara Moberg, Timothy A Zolnik, Julien Catanese, Robert NS Sachdev, Matthew E Larkum, and Dieter Jaeger. 2021. "Thalamic Input to Motor Cortex Facilitates Goal-Directed Action Initiation." *Current Biology* 31 (18): 4148–55.
- Tanaka, Masaki, Jun Kunimatsu, Tomoki W Suzuki, Masashi Kameda, Shogo Ohmae, Akiko Uematsu, and Ryuji Takeya. 2020. "Roles of the Cerebellum in Motor Preparation and Prediction of Timing." *Neuroscience*.

- . 2021. "Roles of the Cerebellum in Motor Preparation and Prediction of Timing." *Neuroscience* 462: 220–34.
- Thach, W. T. 1975. "Timing of Activity in Cerebellar Dentate Nucleus and Cerebral Motor Cortex during Prompt Volitional Movement." *Brain Research* 88 (2): 233–41.  
[https://doi.org/10.1016/0006-8993\(75\)90387-X](https://doi.org/10.1016/0006-8993(75)90387-X).
- Thach, W Thomas, HP Goodkin, and JG Keating. 1992. "The Cerebellum and the Adaptive Coordination of Movement." *Annual Review of Neuroscience* 15 (1): 403–42.
- Thura, David, and Paul Cisek. 2014. "Deliberation and Commitment in the Premotor and Primary Motor Cortex during Dynamic Decision Making." *Neuron* 81 (6): 1401–16.  
<https://doi.org/10.1016/j.neuron.2014.01.031>.
- Timmann, D., S. Watts, and J. Hore. 1999. "Failure of Cerebellar Patients to Time Finger Opening Precisely Causes Ball High-Low Inaccuracy in Overarm Throws." *Journal of Neurophysiology* 82 (1): 103–14. <https://doi.org/10.1152/jn.1999.82.1.103>.
- Todorov, Emanuel, and Michael I Jordan. 2002. "Optimal Feedback Control as a Theory of Motor Coordination." *Nature Neuroscience* 5 (11): 1226–35.
- Topka, Helge, Jürgen Konczak, Klaus Schneider, Andreas Boose, and Johannes Dichgans. 1998. "Multijoint Arm Movements in Cerebellar Ataxia: Abnormal Control of Movement Dynamics." *Experimental Brain Research* 119 (4): 493–503.
- Tsunoda, Yoshiaki, and Shinji Kakei. 2008. "Reaction Time Changes with the Hazard Rate for a Behaviorally Relevant Event When Monkeys Perform a Delayed Wrist Movement Task." *Neuroscience Letters* 433 (2): 152–57. <https://doi.org/10.1016/j.neulet.2007.12.063>.
- Turner, Robert S, and Mahlon R DeLong. 2000. "Corticostriatal Activity in Primary Motor Cortex of the Macaque." *Journal of Neuroscience* 20 (18): 7096–7108.
- Ventura, Valérie. 2004. "Testing for and Estimating Latency Effects for Poisson and Non-Poisson Spike Trains." *Neural Computation* 16 (11): 2323–49.
- Vyas, Saurabh, Matthew D. Golub, David Sussillo, and Krishna V. Shenoy. 2020. "Computation Through Neural Population Dynamics." *Annual Review of Neuroscience* 43 (1): 249–75.  
<https://doi.org/10.1146/annurev-neuro-092619-094115>.
- Wald, Abraham. 1945. "Sequential Tests of Statistical Hypotheses." *The Annals of Mathematical Statistics* 16 (2): 117–86.
- Wolpert, Daniel M, R.Chris Miall, and Mitsuo Kawato. 1998. "Internal Models in the Cerebellum." *Trends in Cognitive Sciences* 2 (9): 338–47. [https://doi.org/10.1016/S1364-6613\(98\)01221-2](https://doi.org/10.1016/S1364-6613(98)01221-2).
- Zackowski, K. M., W. T. Thach, and A. J. Bastian. 2002. "Cerebellar Subjects Show Impaired Coupling of Reach and Grasp Movements." *Experimental Brain Research* 146 (4): 511–22.  
<https://doi.org/10.1007/s00221-002-1191-9>.
- Zimnik, Andrew J, Gerald J Nora, Michel Desmurget, and Robert S Turner. 2015. "Movement-Related Discharge in the Macaque Globus Pallidus during High-Frequency Stimulation of the Subthalamic Nucleus." *Journal of Neuroscience* 35 (9): 3978–89.